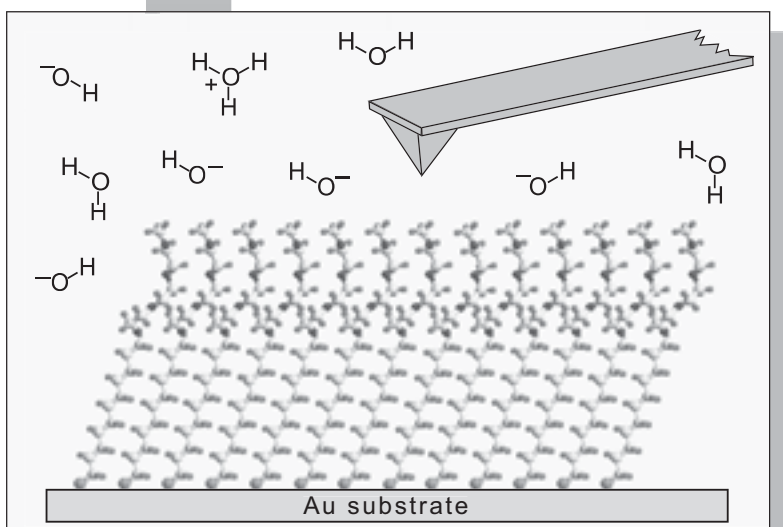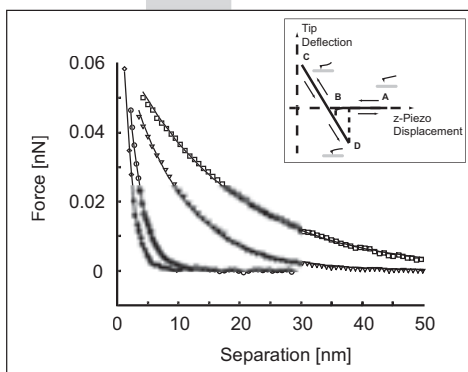# Ultrathin Organic Films as Biointerfaces:

A Chemical Force Spectroscopy Study

Christian Dicke

Diss. ETH No. 14956

Ultrathin Organic Films as Biointerfaces:

A Chemical Force Spectroscopy Study

A Dissertation submitted to the

SWISS FEDERAL INSTITUTE OF TECHNOLOGY ZÜRICH

for the degree of

DOCTOR OF NATURAL SCIENCES

presented by

CHRISTIAN DICKE
Dipl. Phys.
Westfälische Wilhelms-Universität Münster, Germany
born September 30th, 1973
citizen of Gemany

accepted on the recommendation of

Prof. Dr. N. D. Spencer, examiner
Prof. Dr. L. Gauckler, co-examiner

Zürich, 2002

"There are two sorts of curiosity - the momentary and the permanent. The momentary is concerned with the odd appearance on the surface of things. The permanent is attracted by the amazing and consecutive life that flows on beneath the surface of things."

Robert Lynd

To my family.

Table of Contents

Abstract

This thesis is concerned with the resistance to protein adsorption of synthetic biomaterial surfaces. Today, biomaterials play a vital role in everyday life and it is widely perceived that significant advances in their development and use will become the dominant focus of materials research in the near future.

One promising class of a great variety of potential technological applications is the specific recognition of proteins by biosensors. Substantial molecular understanding of the driving forces relevant for the resistance to non-specific protein adsorption is of utmost importance for the tailoring of suitable surface properties. Atomic force microscopy (AFM), employing chemically modified probes, represents a highly suitable tool in order to gain information on the underlying mechanism. On a structural level, from a reductionist point of view, proteins can be thought of as consisting of hydrophobic and charged patches. Therefore, hydrophobically and electrostatically functionalised AFM probes can be utilised to mimic the different local structures of proteins and thus to study separately the different contributions of these local structures to the overall interaction. Of particular interest is the fact that the nanometer-scale contact between probe and surface resembles the typical dimensions of the real contact area between proteins and biomaterials.

Poly(ethylene glycol) (PEG) modified surfaces have been recognised for their outstanding protein-resistant properties because of the high conformational flexibility of their solvated chains ('steric repulsion'). More recently, self-assembled monolayers (SAMs) of oligo(ethylene glycol) (OEG)-containing alkanethiols adsorbed on Au have been found to also resist the adsorption of proteins. Because the conformational freedom of the EG strands in the densely packed SAM is highly restricted, another mechanism must account for the remarkable protein-repelling properties of these self-assembled structures.

The goal of this work is to elucidate the driving forces rendering these self-assembled structures protein-resistant and thus making them so attractive for potential biotechnological applications.

Force-versus-distance measurements have been performed in aqueous electrolyte solutions while varying experimental parameters such as ionic strength, pH-value and type of dissolved ions in order to study the contributing factors to the interaction at the SAM/water interface in detail. The observed interaction force appears to be electrostatically promoted. In fact, an effective negative surface charge density can be ascribed to the SAM/water interface. Additional force measurements employing chemically functionalised (hydrophobic and charged) probes confirm the presence of a negative surface charge. The observed independence of the type of dissolved ions further suggests that the charges are most likely due to the adsorption of hydroxyl ions from solution. A model comprising a thin layer of interfacial water that is associated to the organic film via strong hydrogen bonds is proposed to support and stabilise the adsorption of hydroxyl ions.

The influence of the number of EG units terminating the synthetic organic surface has also been studied in depth in order to test for a transition in the interaction from the well-characterised polymer to the short-chain oligomers. In fact, force measurements performed on partially covered polymer films show an interaction behaviour that is similar to that of the SAM films. From this result, a conformation of the PEG chains in a two-dimensional layer similar to that of the EG tail at the top of the SAM surface is stressed.

In another approach to investigating the nature of the resistance to protein adsorption of these films in more detail, the hydrophobic character of OEG-containing SAMs has been altered by addition of terminal alkyl groups. The derivatised tri- and hexa(ethylene glycol)-containing SAMs have been found to adsorb proteins if a critical length of the hydrophobic alkyl tail is exceeded. Therefore, a simple model taking into account the charges established at the SAM/water interface as well as the degree of hydrophobicity of the SAM is proposed in order to describe the observed interaction forces in more detail.

Zusammenfassung

Diese Dissertation befasst sich mit der Resistenz von synthetischen Oberflächen gegen Proteinadsorption. Heutzutage spielen Biomaterialien eine entscheidende Rolle im täglichen Leben, und es wird allgemein anerkannt, dass sich der Fokus zukünftiger Forschung im Bereich Materialwissenschaften auf signifikante Fortschritte in ihrer Weiterentwicklung konzentrieren wird.

Eine besonders vielversprechende Klasse aus einer Vielzahl von möglichen technologischen Anwendungen stellt die spezifische Erkennung von Proteinen mittels Biosensoren dar. Hierzu ist ein grundsätzliches Verständnis der für die Proteinresistenz relevanten Kräfte auf molekularem Level von grösster Wichtigkeit, um Materialoberflächen mit geeigneten Eigenschaften zu entwickeln. Mit Hilfe der Rasterkraftmikroskopie (Atomic Force Microscopy, AFM) ist es durch den spezifischen Einsatz chemisch modifizierter Sonden möglich, Informationen über den zugrunde liegenden Mechanismus zu erlangen. Proteine können stark vereinfacht durch eine aus hydrophoben und geladenen Anteilen zusammengesetzte Struktur beschrieben werden. Aus diesem Grund können hydrophob beziehungsweise elektrostatisch funktionalisierte AFM-Sonden benutzt werden, um die unterschiedlichen lokalen Strukturen von Proteinen zu simulieren, und somit die verschiedenen Beiträge dieser lokalen Strukturen zur Gesamtwechselwirkung zu untersuchen. Von besonderem Interesse ist dabei die Tatsache, dass die Kontaktfläche zwischen Sonde und Probenoberfläche auf Nanometer-Skala sehr gut mit der typischen Grössenordnung der realen Kontaktfläche zwischen Proteinen und Biomaterialien übereinstimmt.

Materialien, deren Oberflächeneigenschaften durch die Adsorption von Poly(Ethylen Glykol) (PEG) modifiziert wurden, sind bereits seit längerer Zeit für ihre hervorragende Proteinresistenz bekannt. Diese resultiert aus der hohen Konformationsflexibilität der solvatisierten Polymerketten, welche allgemein in dem Begriff 'sterische Repulsion' zusammengefasst wird. In der letzten Zeit konnten zudem selbst-organisierende Monolagen

(Self-Assembled Monolayers, SAMs) basierend auf Alkanthiolen mit funktionellen Endgruppen bestehend aus Oligo(Ethylen Glykol) (OEG) mit ähnlichen Eigenschaften hinsichtlich ihrer Resistenz gegen Proteinadsorption nachgewiesen werden. Doch aufgrund der Einschränkung der Konformationsflexibilität der einzelnen EG-Einheiten in dem dicht gepackten Film muss ein anderer Mechanismus für die ausgezeichneten Protein-abweisenden Fähigkeiten solcher SAMs verantwortlich sein.

Das Ziel dieser Arbeit ist es, die Kraft, welche diese selbst-organisierenden Strukturen proteinresistent und damit hochinteressant für biotechnologische Anwendungen macht, zu identifizieren.

Aus diesem Grund werden in der vorliegenden Arbeit Kraft-Distanz Messungen in wässrigen Elektrolytlösungen in Abhängigkeit von verschiedenen Parametern wie der Salz-konzentration, dem pH-Wert und der Art der gelösten Ionen durchgeführt, um die verschiedenen zu der Wechselwirkung an der Film/Wasser Grenzfläche beitragenden Kräfte zu untersuchen. Die dabei beobachtete Kraft scheint grundsätzlich von elektrostatischer Natur zu sein. Zusätzliche Kraft-Distanz Messungen mit chemisch modifizierten (hydrophoben bzw. geladenen) Sonden bestätigen in diesem Zusammenhang das Vorhandensein einer negativen Oberflächenladungsdichte. Die beobachtete Unabhängigkeit von der Art der gelösten Ionen unterstützt weiter diesen Eindruck und lässt vermuten, dass die Ladungen mit hoher Wahrscheinlichkeit von der Adsorption von Hydroxyl-Ionen aus der Elektrolytlösung stammen. Dazu wird ein Modell entwickelt, welches diese Ionen-Adsorption auf der Basis einer dünnen Wasserschicht, die sich über starke Wasserstoff-Brücken Bindungen an der SAM/Wasser Grenzfläche etabliert, beschreibt.

Darüber hinaus wird der Einfluss der Anzahl der EG-Einheiten, welche den synthetisch organischen Film kennzeichnen, im Detail untersucht, um einen möglichen Übergang von dem typischen und sehr gut verstandenen Verhalten des Polymers zu dem Oligomer zu finden. Tatsächlich weisen Kraft-Distanz Messungen an Polymer-Filmen mit unvollständiger Bedeckung ein Wechselwirkungsverhalten auf, welches dem der Oligomer-Filme sehr ähnlich ist. Aufgrund dieser Ergebnisse wird eine Modellvorstellung entwickelt, nach der die Polymer-Ketten auf der Goldoberfläche eine Konformation in einem zwei-dimensionalen Netzwerk ähnlich zu dem der EG-Gruppen am Kopf der SAM-Filme annehmen.

In einer weiteren Versuchsreihe, um das Wesen der Resistenz solch synthetischer organischer Filme gegen Proteinadsorption genauer zu ergründen, ist der hydrophobe Charakter der OEG-SAMs durch Zugabe weiterer Alkylgruppen verändert worden. Es wird nachgewiesen, dass Filme, bestehend aus derivatisierten Tri- und Hexa(Ethylen Glykol) SAMs, in Abhängigkeit von einer kritischen Länge der hydrophoben Endgruppe ihre Resistenz gegen Proteinadsorption verlieren. Daher wird ein einfaches Modell vorgeschlagen, welches sowohl die an der SAM/Wasser Grenzschicht ausgebildeten Ladungen als auch den Grad der Hydrophobizität des organischen Filmes berücksichtigt, um die beobachteten Wechselwirkungskräfte im Detail zu beschreiben.

Chapter 1

Introduction

1.1 General Introduction

Due to the progressive tendency to miniaturisation of technical systems over the past decades the properties of materials surfaces have become more and more important, because the bulk/surface ratio has subsequently shifted. Thus, surface behaviour of materials is crucial to everyday life. In a large diversity of applications special surface coatings help, for instance, to reduce wear, to prevent corrosion, to improve catalytic processes, to influence optical properties or to render materials biocompatible. In order to characterise these surfaces at smaller and smaller scales an enormous number of surface analytical techniques has been developed over the years. In particular, microscopic (e.g. SEM, STM, AFM)[*] as well as spectroscopic (e.g. IRS, XPS, SIMS)[*] methods play a vital role in the ongoing process to develop an understanding of surface properties.

One promising class of versatile surface coatings with a striking variety of potential technological applications are self-assembled monolayers (SAMs). SAMs form organic interfaces with properties that are largely controlled by the end groups of the molecules comprising the film [1,2]. They represent model systems for the study of organic and biological interfaces and are of great technical interest for future technological applications,

---

[*] SEM - Scanning Electron Microscopy
STM - Scanning Tunneling Microscopy
AFM - Atomic Force Microscopy
IRS - Infrared Spectroscopy
XPS - X-ray Photoelectron Spectroscopy
SIMS - Secondary Ion Mass Spectroscopy

because they are easy to prepare while, at the same time, offering a wide range of flexibility with respect to functionalisation. Consequently, there has been a steady increase in scientific publications per year ever since research in this area began in 1983. The basic principle is rather simple. At each end of a hydrocarbon chain, which typically consists of 10 - 20 methylene units, a terminal functional group is attached. One of these groups features a strong tendency for preferential adsorption onto the substrate used, while the other terminal group defines the chemical characteristics of the generated film. Thiol (S-H) terminal groups, for instance, have been shown to work very effectively with gold substrates. The thiol molecules chemisorb readily from solution onto the gold, forming a densely packed, ordered monolayer film thanks to interchain van der Waals interactions. The tail group is thereby pointing outwards from the surface. The resulting chemical characteristics of the surface can be widely varied by using alkanethiols with differently functionalised tail groups. Alternatively, it is also possible to vary the functionalisation of the terminal groups by performing chemical reactions after the self-assembly of the SAM film.

One technologically interesting application of such ultrathin and well-defined self-assembled monolayers is the modification of biomaterial surfaces. The current boost in nanotechnology is therefore closely related to the ongoing boom in biomaterials research. Biomaterials, in general, comprise chemical, mechanical physical and biological properties that render them suitable for safe, effective and reliable use within a physiological environment. Today, they play an important role in orthopaedic, dental and neurological applications as well as drug delivery, and show great promise for potential future applications such as biosensors or microrobotic devices for disease detection. Rendering such materials biocompatible involves rendering the substance very well tolerated (i.e. non-toxic, bioinert, etc.) so as not to interfere with normal bodily functions. Put in general terms, the essence of biocompatibility is "the ability of a material to perform with an appropriate host response in a specific application" [3].

The interactions between a biological environment and, for example, body implants take place at the surface. Therefore, ultrathin surface coatings that prevent the growth of cells and resist the adsorption of proteins are of utmost importance in biomedicine and related areas. Of particular interest in the field of biosensors are films that have the capability to bind certain biomolecules *specifically*, while showing resistance to *non-specific* adsorption at the

same time. Non-specific adsorption often screens the specific signal to be detected and hampers reasonable signal intensity. The engineering and preparation of such functional coatings with high reliability and reproducibility is becoming a prerequisite for the tailoring of biosensor surfaces. It requires, however, a fundamental understanding and knowledge of the type of relevant forces and of the processes underlying the inertness.

The polymer poly(ethylene glycol) (PEG) has been recognised for some time for its outstanding protein-repelling properties [4-6]. These are believed to be due to the high conformational freedom of the chains and associated tightly bound water, summarised as so-called 'steric repulsion' [7,8]. Over the last decade self-assembled monolayers containing oligo(ethylene glycol) (OEG) have also demonstrated a remarkable ability to resist the adsorption of biomolecules [9,10].

It has been found, however, that the mechanism responsible for the repulsion of proteins by OEG-containing monolayers is different from that of the polymer. While the PEG chains exhibit a high degree of conformational freedom, this conformational freedom of the OEG tails is strongly restricted due to the densely packed SAM film, so that other mechanisms than those relevant in the case of the PEG must be responsible for the behaviour.

1.2 Objectives

The main objective of the study presented in this thesis is to explore the driving forces that render synthetic organic surfaces resistant to the non-specific adsorption of proteins.

In **Chapter 2** fundamental principles of the surface analytical techniques that have been applied in this work in order to study the properties of synthetic organic surfaces in various environments, are discussed. In addition, basic sample as well as probe preparation methods are described.

Chapter 3 illustrates two approaches to understanding the protein-resistant properties of end-grafted poly(ethylene glycol) films and oligo(ethylene glycol) monolayers. Both types of films are resistant to protein adsorption, but the underlying mechanisms differ

fundamentally. One strategy is to vary the oligomer length in order to find a transition between oligomer and polymer behaviour. In another approach the surface packing density of the film has been varied.

In **Chapter 4** ions from the so-called Hofmeister or lyotropic series have been employed in order to test the hypothesis of a long-range structured water interface at the monolayer surface and to explore the affinity of different ions to the ethylene glycol units in more detail [11,12]. Cations and anions are known to have influence on both water structure and the solution behaviour of (bio)molecules [13,14].

In order to further understand the origin of the electrostatic component in the observed interaction, in **Chapter 5** force measurements have been performed as a function of the pH-value of the electrolyte solution and the sign of the charge of the probe surface. pH-values have been shown to play a crucial role in the interaction of organic, self-assembled monolayers with their aqueous environments and therefore have to be taken into account [15,16].

The influence of another important parameter is studied in **Chapter 6** in order to clarify the origin and the character of the apparently electrostatically promoted interaction between oligo(ethylene glycol) monolayers and hydrophobic probes. Terminal alkyl groups are introduced additionally into tri(ethylene glycol)-containing monolayers in order to increase the hydrophobic character of the films and hinder the hydration of the ethylene glycol units in the film [17].

The study on the influence of additional terminal alkyl groups is continued in **Chapter 7**. Here, hexa(ethylene glycol)-containing monolayers are subject to force-distance analysis because of their better protein resistance capabilities compared to tri(ethylene glycol)-containing films [18]. Therefore, the effect of the number of ethylene glycol units and the length of the terminating alkyl tail on the surfaces' resistance to protein adsorption can be discussed in more detail.

Conclusions of the presented work are drawn, and a general outlook for future prospects is given in **Chapter 8**.

Finally, the **Appendix** is devoted to another interesting property of self-assembled monolayers that has attracted attention over recent years. The possibility of designing controlled, mixed organic/inorganic supramolecular architectures on surfaces promises a broad range of future applications. A two-step process is described, where first a chemically well-defined organic surface is prepared by molecular self-assembly followed by a chemical reaction with an inorganic compound forming a hybrid organic-inorganic bilayer.

1.3 Literature

[1] Ulman, A. *An Introduction to Ultrathin Organic Films*, Academic Press, San Diego, **1991**

[2] Ulman, A. *Thin Films, Self-Assembled Monolayers of Thiols*, Academic Press, San Diego, **1998**

[3] Williams, D. F. *The Williams Dictionary of Biomaterials,* Liverpool University Press, Liverpool, UK, **1999**

[4] Taunton, H. J.; Toprakcioglu, C.; Fetters, L. J.; Klein, J. *Nature* **1988**, 712

[5] Jeon, S. I.; Andrade, J. D. *J. Colloid Interface Sci.* **1991**, 159

[6] Harris, J. M. *Poly(Ethylene Glycol) Chemistry*; Plenum Press, New York, **1992**

[7] Sleifzer, I. *Curr. Opin. Solid State Mater. Sci.* **1996**, *2*, 337

[8] Halperin, A. *Langmuir* **1999**, *15*, 2525

[9] Prime, K. L.; Whitesides, G. M. *J. Am. Chem. Soc.* **1993**, *115*, 10714

[10] Harder P.; Grunze, M.; Dahint, R.; Whitesides, G. M.; Laibinis P. E. *J. Phys. Chem. B* **1998**, *102*, 426

[11] Hofmeister, F. *Arch. Exp. Natur. Pharmakol.* **1888**, *24*, 247

[12] Hofmeister, F. *Arch. Exp. Natur. Pharmakol.* **1890**, *27*, 395

[13] Cacace, M. G.; Landau, E. M.; Ramsden, J. J. *Quart. Rev. Biophys.* **1997**, *30*, 241

[14] Vogler, E. A. *Adv. Colloid Interface Sci.* **1998**, *74*, 69

[15] Scatena, L. F.; Brown, M. G.; Richmond, G. L. *Science* **2001**, *292*, 908

[16] Schweiss, R.; Welzel, P. B.; Werner, C.; Knoll, W. *Langmuir* **2001**, *17*, 4304

[17] Caldararu, H.; Caragheorheopol, A.; Schlick, S. *Bull. Pol. Acad. Sc. Chem.* **2000**, *48*, 367

[18] Schwendel, D.; Dahint, R.; Herrwerth, S.; Schloerholz, M.; Eck, W.; Grunze, M. *Langmuir* **2001**, *17*, 5717

Chapter 2

Experimental

Over the last twenty years there has been a strong tendency towards miniaturisation in the development of new products. It is cost effective to merge small units with separated single functions into bigger, multifunctional operational units. In principal, there are two possible approaches to achieve this aim, either by miniaturising already existing products and combining their functions or by starting from the molecular level and designing new functional units with the help of specific properties of single molecules. Most commonly, a technologically interesting substrate is used for the latter, which is modified by adsorption of a thin film of specific molecules. Langmuir-Blodgett (LB) films as well as self-assembling monolayers (SAMs) represent two promising classes of such ultrathin films. In addition, the need for surface structures on the micro- and nanometer scale has enhanced the development of surface patterning techniques such as photolithography, electron beam lithography or soft lithographic methods such as microcontact printing (µCP).

In order to characterise and determine the surface properties of such thin films, several surface analysis techniques have been applied in this work. These techniques include atomic force microscopy (AFM), X-ray photoelectron spectroscopy (XPS), time-of-flight secondary ion mass spectroscopy (ToF-SIMS) and contact angle measurements. In this chapter, these techniques as well as the preparation of samples and probes are described.

2.1 Atomic Force Microscopy (AFM)

2.1.1 Basic Principles

Scanning probe microscopy (SPM) techniques have proven to be a particularly suitable tool for determining surface properties from the atomic to the micron level. The term SPM covers a whole family of instruments featuring a microscopic probe, which is scanned over a surface in a very accurately controlled way on the nanometer scale with the help of piezoelectric elements. In this way, it is possible to acquire a spatially resolved image of the surface properties by plotting the probed quantity versus the position the probe.

The scanning force microscope (SFM) was developed in 1986 by Binnig, Quate and Gerber and constituted an advancement of the Nobel prize-winning scanning tunnelling microscope (STM), which was the first instrument to allow real-space imaging of the surface of silicon [1,2]. A significant disadvantage of the STM is its limitation to conducting samples. Instead of the tunnelling current between probe and sample, a SFM uses the interaction force between tip and sample surface and thus allows the measurement of forces between all kinds of materials.

The elementary parts of a SFM are the scanning stage, a force-sensing probe and the detection unit (see Figure 2.1). The scanning stage consists of piezoelectric elements, which allow a very well-defined positioning of the sample below the SFM tip in three dimensions. The probing tip is mounted at the free end of a mechanical beam, the so-called 'cantilever'. Forces between probe and sample cause the cantilever to bend. Thus, the cantilever translates the interaction force, F, between probe and sample into a mechanical deflection, Δz, as a function of the relative position of the SFM tip with respect to the probed sample. According to Hooke's law, the interaction force can be determined, if the spring constant, k, of the cantilever is known:

$$F = -k\Delta z \tag{2.1}$$

Several different techniques including tunnelling microscopy [2], optical interferometry [3,4], optical beam deflection [5], capacity measurements [6] or laser diode techniques [7] have been developed in order to detect the cantilever deflection precisely.

Nowadays, the most common detection method, which is typically employed in commercial systems, is the optical beam deflection. A typical SFM setup applying the optical beam deflection technique, as was used for the experimental work presented in this thesis, is displayed in Figure 2.1.
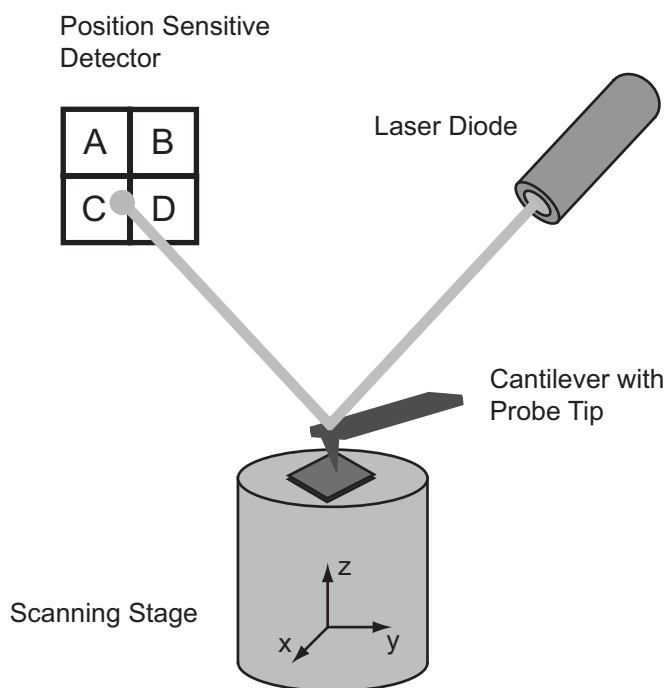
Figure 2.1: *Schematic of a scanning force microscope with scanning stage, laser diode, cantilever and detection unit.*

A collimated laser beam is focussed on the back of the cantilever. The reflected light is directed onto a position-sensitive detector (e.g. a four-segment photodiode as shown in Figure 2.1). As the cantilever bends, the position of the laser beam on the detector shifts. The differences in the voltages of opposing segments represent the detection signal that is used to control the distance between tip and sample surface. For the normal signal, a simple vertical deflection of the cantilever, the difference between the voltages of the two upper and lower segments, respectively, is detected $(V_A+V_B)-(V_C+V_D)$. The lateral signal, which represents the torsion of the cantilever, corresponds to the difference between the voltages of the left and right segments $(V_A+V_C)-(V_B+V_D)$.

Several forces typically contribute to the deflection of a SFM cantilever. The most prominent force associated with scanning force microscopy is the interatomic van der Waals

force. Figure 2.2 illustrates the dependence of the van der Waals force upon the distance between the SFM tip and a sample surface.
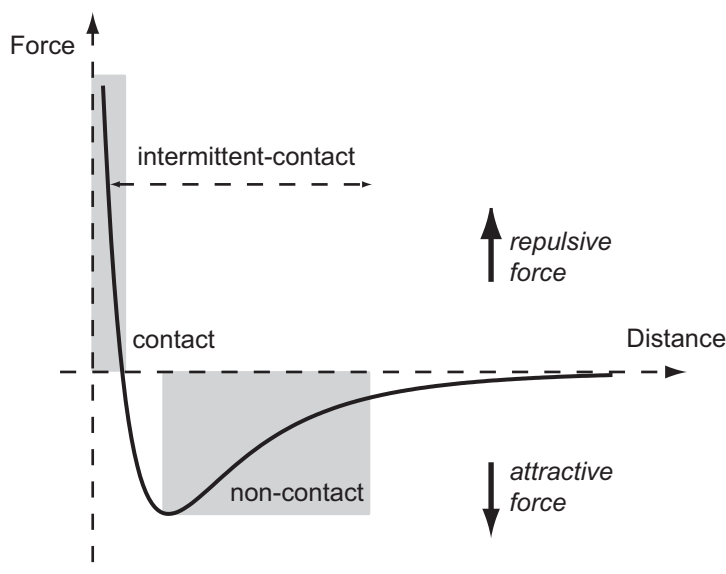
Figure 2.2: Interatomic force-versus-distance plot.

According to the position in the diagram displayed in Figure 2.2, two different regimes and therefore two principal modes of operation can be classified: 1) the contact mode and 2) the non-contact mode.

In contact mode, the SFM probe is brought into 'physical contact' with the sample, where the interatomic force between probe and sample surface is repulsive (DC mode). In non-contact mode, the probe is oscillated at a distance from the sample of the order of tens to hundreds of angstroms, where the interatomic forces are attractive (AC mode).

In DC mode, either the height of the sample is kept constant ('constant height' mode), while the deflection of the cantilever and therefore the change in the photodiode signal is recorded, or the deflection of the cantilever and therefore the exerted force is kept constant ('constant force' mode), while the voltage applied to the scanning stage is recorded. In AC mode, the cantilever is vibrated near its resonant frequency at a certain amplitude close to the surface of the sample, while shifts in frequency and phase as well as changes in amplitude are monitored.

SFM measurements can be performed in a variety of environments: in ultra-high vacuum, at low temperatures, under ambient conditions and in various liquids. Operation in

liquids is especially effective in reducing the total force exerted on the sample. This is an important prerequisite for studies of sensitive biological samples to avoid damage. Another advantage of liquid environments for the study of biological samples is the possibility of mimicking their natural environments and studying the environmental influences such as salt concentration or pH-value. Therefore, all force measurements performed in this study have been carried out under electrolyte solutions of various ionic strengths and pH-values.

2.1.2 Force Spectroscopy

Because forces on the atomic and molecular scale are probed with the SFM, it is also called atomic force microscope (AFM). Besides microscopic applications as, for example, the imaging of surface topographies, AFM is a very useful tool for studying local surface properties by performing so-called force-versus-distance measurements, where the normal deflection of the cantilever is recorded as a function of the normal displacement of the piezoelectric scanner.
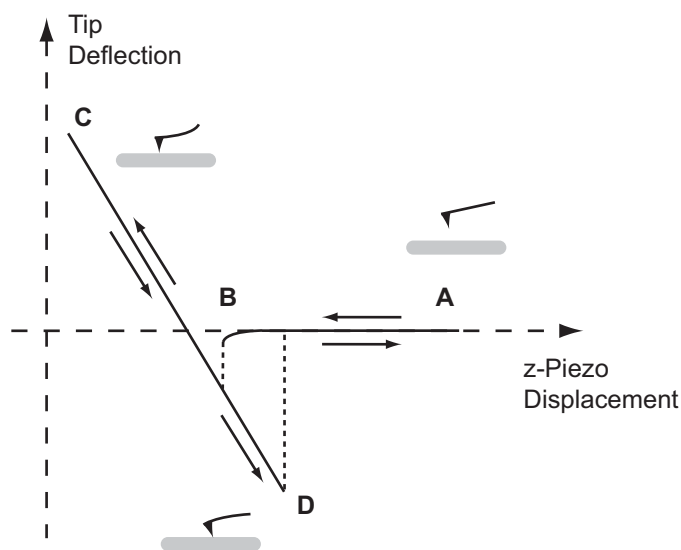
Figure 2.3: *Schematic diagram of a force-versus-distance measurement.*

Figure 2.3 shows a typical force-versus-distance measurement. At the right side of the diagram (A), the scanning stage is fully retracted and the cantilever is not deflected. With the z-extension of the scanner, the sample surface approaches the probe. The cantilever remains undeflected until it comes close to the sample surface. When the force gradient ($\Delta F/\Delta z$) overcomes the spring constant, k, of the cantilever eventually (B), the tip snaps into contact

with the sample surface. In fact, the probe already experiences an interaction force that causes the cantilever to bend shortly before the jump into contact occurs. Depending on the contributions to the interaction, the deflection of the cantilever can be negative (attractive), as shown in Figure 2.3, or positive (repulsive).

Further z-extension of the scanner causes the cantilever to deflect approximately linearly, because of the parallel movement of scanning stage and cantilever. At the left side of the diagram (C), the scanner is fully extended and starts to retract. When the spring constant overcomes the force gradient (D), the cantilever will jump away from the surface into its equilibrium position. The snap-off position (D) is often different from the snap-on position (B). This hysteresis emerges due to additional adhesive components. Finally, the cantilever is back in its rest position (A).

In order to convert the deflection of the cantilever into a force according to Hooke's law (see Eq. 2.1), it is essential to determine the normal force constant of the cantilever precisely. But the exact determination of the force constant is often difficult because in the submicron range, material properties of the cantilever, such as Young's modulus, are strongly influenced by increasing surface effects. Additional surface coatings (e.g. magnetic or conductive layers) as well as organic functionalisations complicate the determination further.

Several approaches have been suggested to calibrate the force constants of cantilevers of different shapes in the past. For a cantilever with rectangular cross-section, the force constant is given by

$$k = \frac{3EI}{l^3} \tag{2.2}$$

$$I = \frac{bd^3}{12} \tag{2.3}$$

where E is Young's modulus of the cantilever material, I is the geometrical moment of inertia, l the length, b the width and d the thickness of the cantilever.

Because the spring constant of the cantilever, k, is proportional to its resonant frequency, ω, a common calibration method is the determination of this frequency.

$$k = m_{eff}\omega^2 \tag{2.4}$$

To account for additional probe coatings, a combination of resonance frequency measurements and finite-element-analysis calculations has been proposed [8,9]. However, the estimation of the effective mass, m_{eff}, is often difficult and can incorporate errors to some extent.
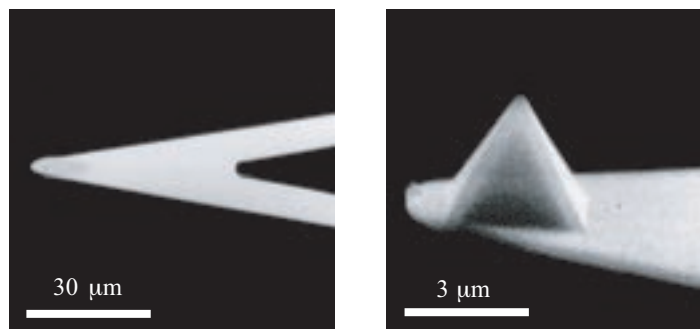
Figure 2.4: *Scanning electron microscopy images of a V-shaped cantilever with attached probe [10].*

For V-shaped cantilevers (see Figure 2.4), as were used in this work, a theoretical model has been suggested, which substitutes the cantilever by two parallel levers [11]. In addition, simple equations for all three dimensions depending only on cantilever geometry and material properties can be applied [12]. Other studies have drawn conclusions on the spring constant from the movement of the cantilever due to thermal noise [13,14].

This work concentrates primarily on the decay lengths of the measured forces, which are independent of the spring constant. Therefore, the values for the spring constants provided by the manufacturers have been used. All measurements were performed with a commercially available scanning probe microscope, Nanosope IIIa (Digital Instruments, Inc., Santa Barbara, CA), equipped with a liquid cell. All electrolyte solutions were introduced into the liquid cell using PTFE filters (Semadeni AG, Ostermundigen, Switzerland) with 0.2 and 0.45 µm pore size. Force-versus-distance measurements were collected with a cycle frequency of 0.3 - 1 Hz. At least 64 force curves per sample over an area of 2 µm × 2 µm were recorded using DI's 'force-volume' software. During a typical force-distance cycle, the measured experimental parameters were the deflection of the cantilever, obtained from the voltage of the four-quadrant photodiode, and the displacement of the piezo scanner, indicated by the applied voltages. Cantilever-deflection vs. piezo-displacement curves were converted into force-versus-distance curves according to a procedure described in the literature with 'zero distance'

corresponding to a hard-wall potential [15]. The individual force-distance curves were then averaged and further processed and evaluated using analytical as well as imaging software. Since the force measurements were performed in order to mimic the approaching of proteins towards synthetic organic surfaces, particular focus was spent on the approaching parts of the force-distance cycles. In the discussion of protein resistance of model organic surfaces in the following chapters, the displayed force-versus-distance plots thus illustrate the essential information determined from a large number of representative individual force curves. A detailed discussion of the experimental errors can be found in Chapter 3.

2.2 X-Ray Photoelectron Spectroscopy (XPS)

2.2.1 Basic Principles

X-ray Photoelectron Spectroscopy (XPS) - also called Electron Spectroscopy for Chemical Analysis (ESCA) - was developed in the mid 1960s by Siegbahn et al. and is based on the photoelectric effect outlined by Einstein in 1905 [16,17]. XPS is a powerful analytical tool for obtaining information about the chemistry, organisation and morphology of a surface [18]. It provides qualitative as well as quantitative information on all chemical elements, (except H and He).

The kinetic energy of photoelectrons, generated by irradiation of a sample by X-rays of known energy, can be measured with a spectrometer and is given by

$$E_{kin} = h\nu - E_b - \phi_{sp} \qquad (2.5)$$

where E_{kin} is the kinetic energy of the electrons, which is measured with the spectrometer, $h\nu$ is the known energy of the X-rays, E_b is the binding energy of the electrons and ϕ_{sp} is the spectrometer work function, which can be compensated electronically, leaving

$$E_{kin} = h\nu - E_b \qquad \Leftrightarrow \qquad E_b = h\nu - E_{kin} \qquad (2.6)$$

The binding energy of the different electronic states can thus be determined by measuring the kinetic energy of the corresponding photoelectrons [19,20]. Because binding

energies are characteristic for each element, an analysis of quantity and chemical state of the elements present at the probed surface can be performed. Due to the short mean free path of excited photoelectrons in solids (0.5 - 10 nm), XPS exhibits high surface specificity.

A typical XP spectrum, where the measured photoelectron intensity is plotted as a function of the binding energy, is shown in Figure 2.5.
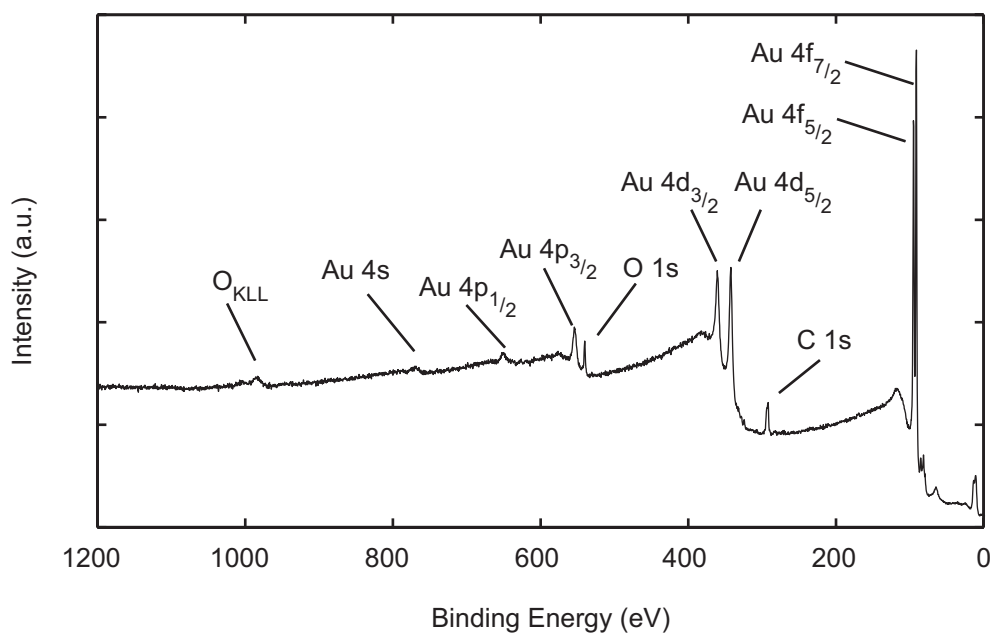
Figure 2.5: *Typical XP spectrum obtained from a self-assembled monolayer of a tri(ethylene glycol)-terminated alkanethiol adsorbed on a gold substrate.*

2.2.2 Instrumentation

For performing XPS measurements, some basic components are essential. These are the X-ray source, a sample-support system, an energy analyser and an electron detector. Since all measurements are performed under ultrahigh vacuum (UHV), an appropriate vacuum chamber is also necessary. Figure 2.6 displays a schematic of the important components for a XPS experiment.

Usually, commercial XPS systems are equipped with X-ray sources featuring dual Mg/Al anodes as standard. Both anodes generate stable and sufficiently narrow emission lines at 1253.6 eV for the Mg Kα and 1486.6 eV for the Al Kα line, respectively. The electron-energy analyser separates the photoelectrons emitted by the surface according to their energy. Electrostatic deflection analysers, such as Cylindrical Mirror Analysers (CMA) and

Concentric Hemispherical Analysers (CHA), where electrons pass through a dispersing field, in which the deflection is a function of their energy, are most commonly used [21-23]. Finally, due to the weak signal of single electrons, electron multipliers are usually used as detectors. Amplifiers are used additionally to increase the multiplier output signal, before the data are processed further.
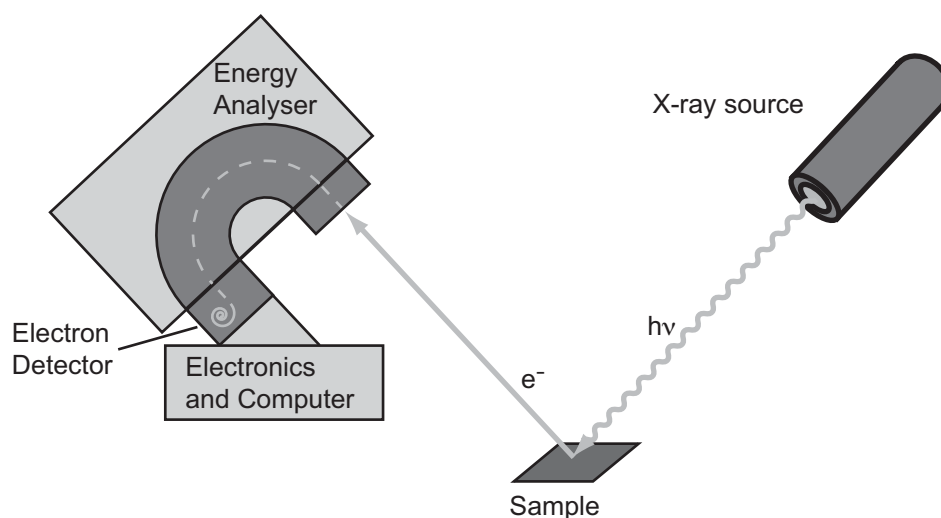
Figure 2.6: *Schematic of the main components of a XPS experiment.*

In this work, XP spectra (~400 μm spot size) were collected on a Physical Electronics PHI 5700 XPS instrument using monochromatic Al Kα radiation. The source was operated at 200 or 250 W, at a total X-ray exposure time per sample of less than 20 minutes. Control experiments confirmed that under the conditions applied, X-ray induced damage to the samples was negligible. The base pressure in the chamber was less then 10^{-9} mbar. The takeoff angle during acquisition was set to 30°, the pass energy of the analyser was chosen as 46.95 eV for single region scans (0.1 eV step size) and 187.85 eV in survey mode (0.4 eV step size).

The spectra were typically referenced to the Au 4f peak at 84.0 eV. Data were analysed using a least-squares fit routine following Shirley iterative background subtraction (PHI MultiPak V.5.0a software) and PHI sensitivity factors for quantification. Peaks were fitted using 80/20 mixed Gaussian-Lorentzian functions. Intensities were also corrected for the energy dependence of the transmission function.

2.3 Time-of-Flight Secondary Ion Mass Spectroscopy (ToF-SIMS)

Emission of secondary ions from surfaces after bombardment with primary particles was first observed in 1910 [24]. Invented in the early 1950's and 1960's, the mass spectrometry of these secondary ions developed rapidly due to interesting applications in the growing semiconductor industry [25-27]. Due to the intrinsically destructive character of this technique, the elemental analysis of materials depth profiles became of great interest. Later it was shown, that this technique could also be of importance in surface science, if a very low primary particle flux density (<1 nA per cm^2) was used [28-30].
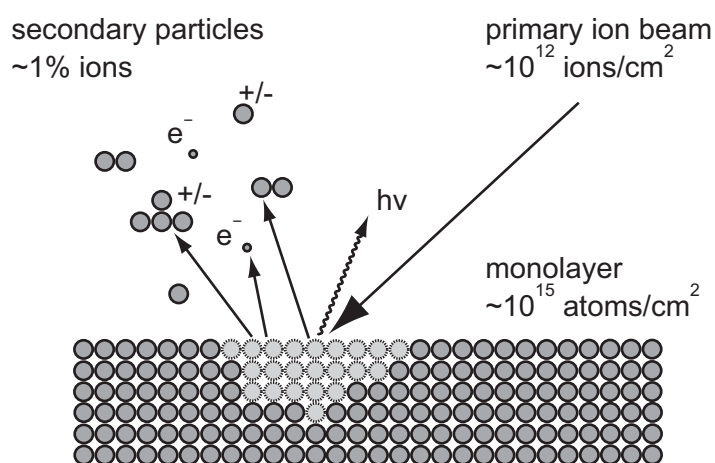
Figure 2.7: Schematic diagram of the basic principle of static SIMS.

In a Time-of-Flight Secondary Ion Mass Spectroscopy (ToF-SIMS) experiment, the top surface layer of a sample is typically bombarded with a microfocused, pulsed (<1 ns) primary ion beam of 1 - 30 keV kinetic energy [31,32]. Upon bombardment, kinetic energy and momentum of the impinging primary ions are transferred to the sample via a collision cascade process. Within the cascade, a small fraction of the momentum may be redirected to the surface and besides other particles, secondary ions are emitted by the surface in a very small proportion (<1%), if the transferred energy is higher than the surface binding energy. In principle, a ToF-SIMS experiment can be performed in two modes: in static and dynamic mode. In static SIMS mode, the total primary ion density hitting the surface is kept below 10^{12} ions/cm^2. Below this 'static limit', less then roughly one per thousand surface atoms or molecules are directly struck by primary ion bombardment. The dynamic SIMS mode is often used for depth profiling, because the sample surface is rapidly sputtered and eroded away due

to the high incident ion-beam density. The basic principle of static SIMS is illustrated schematically in Figure 2.7.

The secondary ions are extracted from the sample and injected into a specially designed Time-of-Flight mass spectrometer by applying a potential between sample surface and spectrometer. There, the ions are accelerated into a field-free space and dispersed in time proportional to their velocity during their drift. Because the acceleration voltage is of the order of 10 - 20 keV, the initial energy of the secondary ions can be neglected and the ions will all have the same kinetic energy, E_{kin}, that can be expressed by the following equation

$$E_{kin} = qV = \frac{1}{2}mv^2 \qquad (2.7)$$

where q the charge, m the mass and v the velocity of the secondary ions, and V is the applied acceleration voltage.

Therefore, the time-of-flight, t, the ions travel during their drift in the spectrometer of length, L, is only a function of the mass of the ions. According to Equation 2.8, heavier masses travel more slowly through the spectrometer than lighter masses.

$$t = \frac{L}{v} = \sqrt{\frac{m}{2qV}} \qquad (2.8)$$

The time difference between the primary ion pulse (start pulse) and the detection of the different secondary ions (end pulse) is measured and used to generate a mass spectrum. A typical ToF-SIMS spectrum is shown in Figure 2.8.

There are several major advantages of ToF-SIMS. It is an extremely sensitive technique, with a detection limit below 1 ppb. In addition, the system is highly surface sensitive in static SIMS mode, and probes only the topmost atomic layers (<1 nm). It is also possible to distinguish easily between different isotopes of the same element. And due to the detection of specific fragments of single molecules ("fingerprints"), information on chemical bonding at the outermost surface can be obtained. The major disadvantage of SIMS is the difficulty to obtain quantitative data.
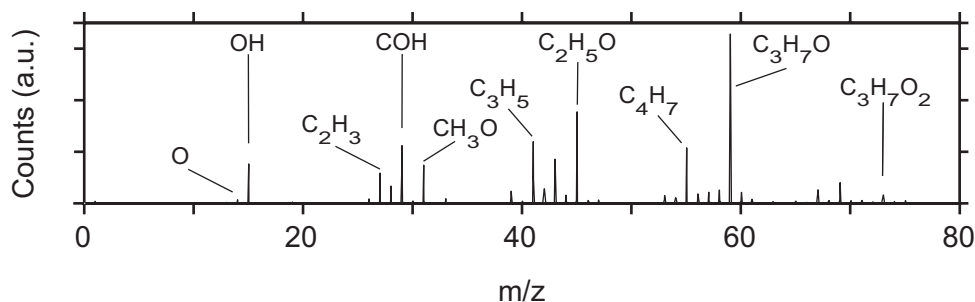
Figure 2.8: *Typical ToF-SIMS spectrum of a self-assembled monolayer of tri(ethylene glycol)-terminated alkanethiols adsorbed on a gold substrate.*

In this work, ToF-SIMS measurements were carried out on a Physical Electronics PHI 7200 imaging ToF-SIMS system (Physical Electronics, Eden Prairie, MN, USA). High-resolution mass spectra in the mass range of 2 - 700 amu were collected from areas covering $200 \times 200 \ \mu m^2$ using an 8 keV Cs^+ primary ion beam. The time per data point was 0.625 ns. The Cs^+ ion dose was around 2×10^{12} ions/cm^2 for the positive spectra and 5×10^{12} ions/cm^2 for the negative spectra, corresponding to values within the static regime. Mass resolution m/Δm was typically 6300 in the positive range and 3200 in the negative range. The mass scale was first calibrated using one set of signals each for the positive (CH_3^+, $C_2H_3^+$, $C_3H_5^+$ and Cs^+) and negative (CH^-, OH^-, C_2H^- and Au^-) mass spectra, followed by the assignment of species using the PHI TOFPAK V.2.0a software. Imaging ToF-SIMS measurements were performed using an In^+ liquid metal ion gun of 25 keV beam energy. To achieve a probe beam size in the micrometer range, it is necessary to use pulses of approximately 50 ns duration and therefore only moderate mass resolution is achieved in this mode. The ion dose during measurement was kept in the static regime (5×10^{12} ions/cm^2), well below the dynamic range.

2.4 Contact Angle Measurements

A droplet of water or another liquid put on a surface always assumes the shape that gives the lowest total energy (see Figure 2.9). This equilibrium situation between the solid, liquid and vapour phase allows the measurement of the corresponding interfacial energies, γ_i, using Young's equation

$$\gamma_{SL} + \gamma_{LV} \cos\theta = \gamma_{SV} \tag{2.9}$$

Measurements of the static contact angle, θ, are useful for wettability studies as well as for surface free energy estimation on a wide range of solid surfaces [33].

At hydrophilic surfaces (for example, if there are -OH or -COOH groups present in the topmost layer) it is favourable for the water droplet to spread out over the surface. Thus, low contact angles are measured. If the outermost surface layer mainly contains hydrophobic groups (such as $-CH_3$ or $-CF_3$ groups) the drop assumes a shape exposing a minimal area to the surface and high contact angles are measured. Therefore, contact angle measurements allow sensitive discrimination of the chemical state of different homogeneous sample surfaces. Due to the size of the droplet (typically 5 µl), only macroscopic surface properties can be determined. Defects in film composure, therefore, cannot directly be probed. Contact angles at such hydrophilic and hydrophobic surfaces, respectively, are illustrated in Figure 2.9 schematically.
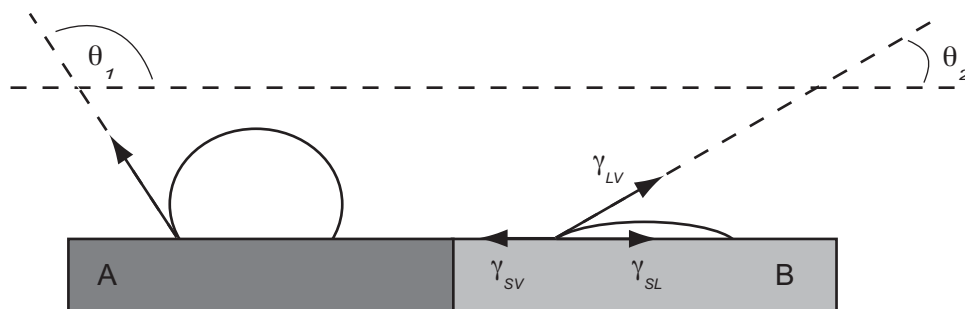

Figure 2.9: *Schematic of liquid droplets on either a hydrophilic or a hydrophobic surface.*

In this work, contact angle measurements have been performed using ultrapure water and n-hexadecane as polar and apolar test liquids, respectively. Measurements were taken at room temperature and ambient humidity conditions.

2.5 Sample and Probe Preparation

2.5.1 Self-Assembled Monolayers (SAMs)

Ultrathin organic films have become of great interest for biomaterials research in recent years. A promising class of such ultrathin films are self-assembled monolayers (SAMs). SAMs are molecular assemblies that form spontaneously upon immersion of a suitable substrate into a solution containing an active surfactant [34,35]. Due to their well-defined structural and chemical properties, their ease of preparation and long-term stability, SAMs represent suitable synthetic model systems to study properties such as protein adsorption [36,37]. In particular, SAMs of alkanethiols adsorbed on gold surfaces are widely used to produce model surfaces for a variety of applications including biomaterial and biosensor surfaces [38-40].

In principle, surfactant molecules forming SAMs consist of three parts: the surface-active head group (A), the (derivatised) alkyl chain (B), and the terminal functional group (C). Figure 2.10 displays a schematic diagram of an alkanethiol SAM on a gold substrate [34].
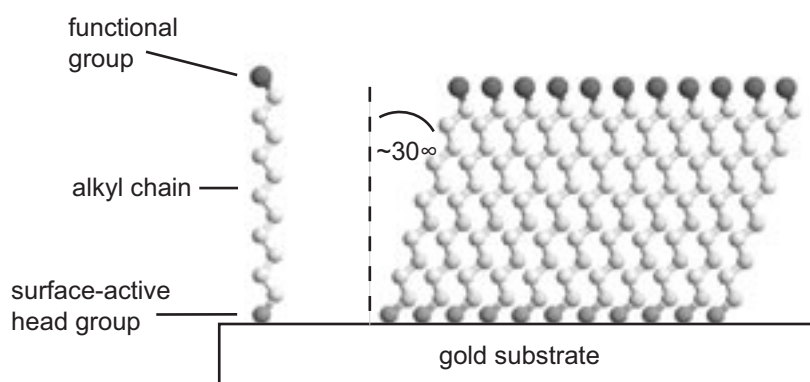
Figure 2.10: Schematic of a SAM of alkanethiols on a gold substrate.

The surface-active head group promotes the chemisorption of the surfactant molecule to the substrate surface. In the case of alkanethiols on gold, a covalent, but slightly polar Au-S bond is formed via a highly exothermic reaction. Following adsorption onto the surface, the formation of a well-ordered and closely packed assembly occurs. Here, the interchain van der Waals forces associated with the alkyl chain constitute the relevant interaction. Finally, the terminating functional group determines the surface-chemical properties of the SAM.

In this work, dilute ethanolic solutions (approximately 2×10^{-3} M) of several derivatised alkanethiols were used to functionalise freshly prepared polycrystalline gold samples. It was found, that in such dilute solutions, the adsorption kinetics feature two significant steps [37]. Within a quick first step of only a few minutes, 80 - 90% of the final monolayer thickness is reached, and the contact angles show almost their limiting values. The slower second step was found to take a few hours. At this, the order of the SAM is established due to the interchain van der Waals forces. Therefore, the gold samples were immersed for an extended period of time (typically 12 h) to ensure the formation of a well-ordered and closely packed film. In a final step, the samples were thoroughly rinsed with the pure solvent (ethanol), put into an ultrasonic ethanolic bath for one minute and dried in a nitrogen stream.

Prior to functionalisation, gold samples were prepared by slow thermal evaporation of an 80-nm-thick polycrystalline gold film (99.99%, Balzers Materials, Liechtenstein) preceded by an adhesion promoting layer of 5 nm of chromium (99.99%, Balzers Materials) onto silicon wafers. These single-side-polished silicon (100) wafer pieces (MEMC Electronic Materials Inc., St. Peters, MO) were cut to size, oxygen-plasma cleaned and placed in a metal evaporation chamber at a base pressure of less than 1×10^{-7} mbar.

2.5.2 Microcontact Printing (µCP)

Recently, considerable effort has been applied to submicrometer science and technology. In particular, the ability to control properties and structures on a submicrometer scale is currently a challenging goal in the applied materials sciences. One promising strategy of achieving this goal is to use microcontact printing (µCP) for the patterning of SAMs with feature sizes smaller than 0.5 µm [41-43].

In order to prepare adequately chemically structured samples for this work, polydimethoxysilane (PDMS) stamps were first obtained from structured silicon masters. For this, a silicon-elastomer (Sylgard 184, Dow Corning) of medium viscosity was mixed with the corresponding curing agent in a ratio of 10:1, poured over the master structure and kept at a temperature of 60° C for 4 hours in order to polymerise. After ultrasonic solvent cleaning and drying in a nitrogen stream, the stamps were then inked with the ethanolic solution of the first alkanethiol using a cotton swab (A), blown dry with nitrogen and carefully brought into

contact with the gold surface (B). When the stamp was removed after about 30 seconds, a laterally patterned SAM had formed (C). Subsequently, the gold sample was cleaned using hexane and ethanol, and the thiol-free regions backfilled with a second, differently terminated alkanethiol by immersion into solution for 1 minute (D+E). Finally, the sample was thoroughly rinsed with hexane and ethanol and dried in a nitrogen stream. The general procedure is illustrated in Figure 2.11.
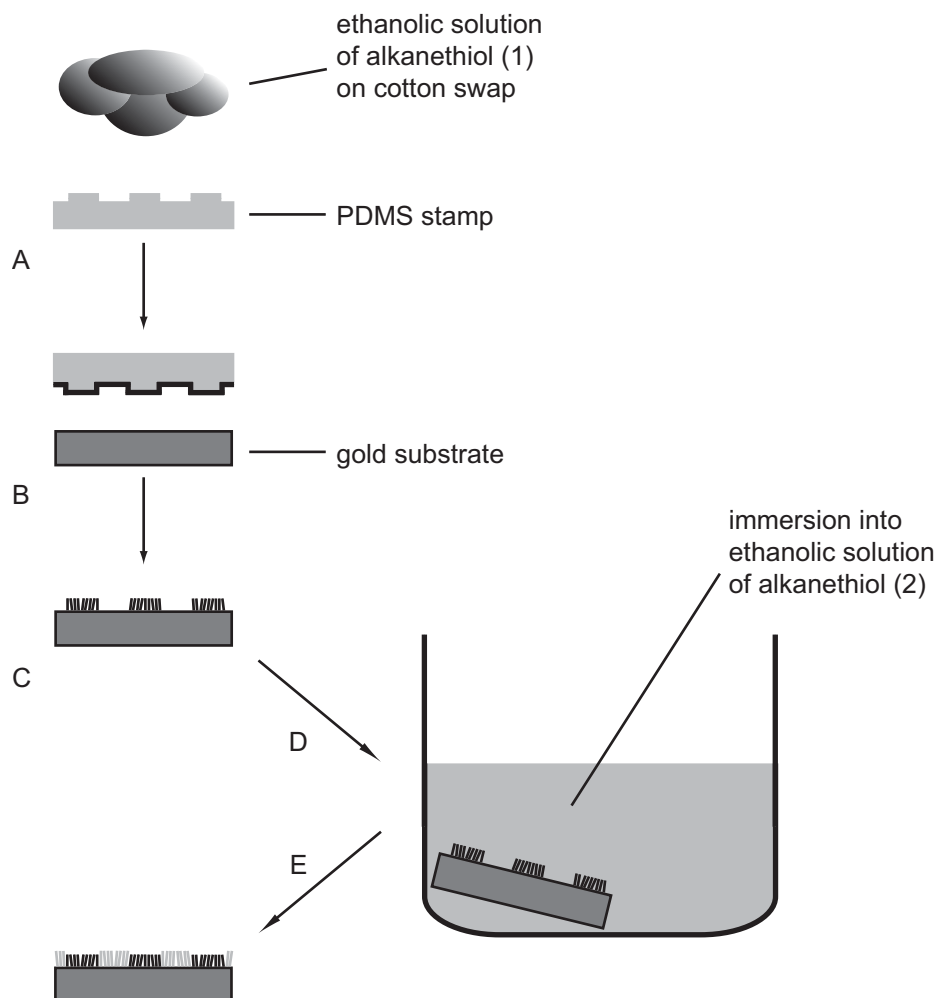
Figure 2.11: *Schematic of the preparation of a micropatterned surface by μCP.*

2.5.3 Cleaning Procedures

Cleaning procedures are an elementary prerequisite to ensure that samples and probes be free of contaminants. Besides cleaning purposes they also provide sterilising, oxidising or etching options [44-47].

Plasma Cleaning

Cleaning, however, is a very broad term, and it may be helpful to think of it as the first stage of the experiment, rather than cleaning as such. In many cases, etching for example is a more descriptive term for plasma cleaning. Plasma cleaning/etching is an effective technique for removing organic contaminants from a variety of materials and substrates [46-49]. In combination with a water-enriched atmosphere, surface hydroxylation is another result of plasma treatment.

A plasma can be defined as a partially or wholly ionised gas with a roughly even number of positively and negatively charged particles, which is generated at sufficiently low pressures using a high voltage.

In principle, there are four etching mechanisms in a low-pressure plasma: sputtering (energetic ion bombardment), chemical etching (chemical reaction of etchant gas phase atoms with the surface forming volatile products), ion-energy-driven etching (combination of the first two processes) and ion-inhibitor etching (etching occurs only, where the surface protecting inhibitor film is damaged due to focussed ion bombardment). Figure 2.12 illustrates the four processes schematically [48].

Figure 2.12: Schematic of the four basic plasma-etching processes: sputtering (A), chemical etching (B), ion-energy-driven etching (C), and ion-inhibitor etching (D).

For this work, silicon wafer pieces and silicon nitride SFM probes were treated in a water-enriched oxygen plasma before they were gold-coated and functionalised. A tubular-shaped, commercial RF-plasma cleaner (PDC-32G, Harrick Scientific Corporation, Ossining,

NY) was operated at 60 Watts for approximately 30 seconds, where chemical etching was the main process.

Chemical Etching in 'Piranha Solution'

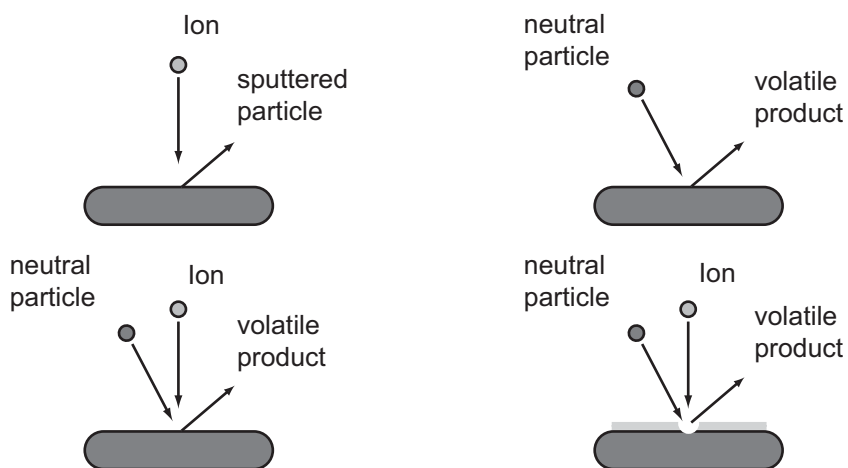Silicon nitride probes as well as alumina-coated probes, which were used without further organic functionalisation, were cleaned in a different way prior to the measurements. A mixture of sulphuric acid (H_2SO_4) and hydrogen peroxide (H_2O_2) was applied in the proportions: 7 parts H_2SO_4 [95% w/o] to 3 parts H_2O_2 [30% w/o] at approximately 90° C. This solution is a strong oxidising agent and is widely used as cleaning agent for oxide surfaces [34,50]. Due to its very strong interaction with many organic materials it is called 'piranha solution' and should be handled with extreme care.

The advantage of this treatment is that it results in a very hydrophilic surface. For silica surfaces, a Si-OH group concentration of $\sim5\times10^{14}$ per cm^2 was found [51,52]. This concentration of surface OH groups is approximately equivalent to the concentration of alkyl chains in a SAM.

In the present work, piranha solution was used to clean and hydroxylise the surfaces of standard silicon nitride and alumina-coated SFM probes. The tips were immersed in freshly prepared piranha solution for approximately 5 seconds and directly transferred to the SFM liquid cell.

2.6 Literature

[1] Binnig, G.; Rohrer, H.; Gerber, C.; Weibel, E. *Phys. Rev. Lett.* **1982**, *49*, 57

[2] Binnig, G.; Quate, C. F.; Gerber, C. *Phys. Rev. Lett.* **1986**, *56*, 930

[3] Mate, C.; McClelland, G. M.; Erlandsson, R.; Chiang, S. *Phys. Rev. Lett.* **1987**, *59*, 1942

[4] Erlandsson, R.; McClelland, G. M.; Mate, C.; Chiang, S. *J. Vac. Sci. Technol. A* **1988**, *6*, 266

[5] Amer, N.; Meyer, G. *Appl. Phys. Lett.* **1988**, *53*, 1045

[6] Neubauer, G.; Cohen, S.R.; McClelland, G.M.; Horn, D.: Mate, C. M. *Rev. Sci. Instrum.* **1990**, *61*, 2296

[7] Dandridge, A.; Miles, R. O.; Giallorenzi, T. G. *Electron Lett.* **1980**, *16*, 948

[8] Hazel, J. L.; Tsukruk,V. V. *Journal of Tribology* **1998**, *120*, 814

[9] Hazel, J. L.; Tsukruk,V. V. *Thin Solid Films* **1999**, *339*, 249

[10] Marti, A. PhD Thesis, ETH Zurich, Diss. No. 12320, **1997**

[11] Albrecht, T. R.; Akamine, S.; Carver, T. E.; Quate, C. F. *J. Vac. Sci. Tech. A* **1990**, *8*, 3386

[12] Neumeister, J. M.; Ducker, W. A. *Rev. Sci. Instrum.* **1994**, *65*, 2527

[13] Butt, H. J.; Jaschke, M. *Nanotechnology* **1995,** *6*, 1

[14] Florin, E. L.; Rief, M.; Lehmann, H.; Ludwig, M.; Dornmair, C.; Moy, V. T.; Gaub, H. E. *Biosens. Bioelectron.* **1995**, *10*, 895

[15] Ducker, W. A.; Senden, T. J.; Pashley, R. M. *Nature* **1991**, *353*, 239

[16] Siegbahn, K.; Nordling, C.; Fahlman, A.; Nordberg, R.; Hamrin, K.; Hedman, J.; Johansson, G.; Bergmark, T.; Karlsson, S.-E.; Lindgren, I.; Lindgren, B. *ESCA: Atomic, Molecular and Solid State Structure Studied by Means of Electron Spectroscopy*, Almqvist & Wiksells, Stockholm, **1967**

[17] Siegbahn, K.; Nordling, G.; Johansson, G.; Hedman, J.; Heden, P. F.; Hamrin, K.; Gelius, U.; Bergmark, T.; Werme, L. O.; Manne, R.; Baer, Y. *ESCA Applied to Free Molecules*, North-Holland, Amsterdam, **1969**

[18] Vickerman, J. C. *Surface Analysis: The Principle Techniques*, Wiley, New York, **2000**

[19] Berkowitz, J. *Photoadsorption, Photoioniazation, and Photoelectron Spectroscopy*, Academic Press, New York, **1979**

[20] Feldman, L. C.; Mayer, J. W. *Fundamentals of Surface and Thin Film Analysis*, North-Holland, New York, **1986**

[21] Roy, D.; Carette, J. D. *Canad. J. Phys.* **1971**, *49*, 2138

[22] Sevier, K. D. *Low Energy Electron Spectrometry*, Wiley, New York, **1972**

[23] Roy, D.; Carette, J. D. *Topics in Current Physics*, Springer-Verlag, Berlin, **1977**

[24] Thomson, J. J. *Phil. Mag.* **1910**, *20*, 252

[25] Herzog, R. F. K.; Viebock, F. P. *Phys. Rev.* **1949**, *76*, 855

[26] Castaing, R.; Slodzian, G. *J. Microscopic* **1962**, *1*, 395

[27] Liebl, H. J.; Herzog, R. F. K. *J. Appl. Phys.* **1963**, *34*, 2893

[28] Benninghoven, A. *Z. Physik* **1970**, *230*, 403

[29] Müller, A. and Benninghoven, A. *Surf. Sci.* **1973**, *39*, 427

[30] Müller, A. and Benninghoven, A. *Surf. Sci.* **1973**, *41*, 493

[31] Benninghoven, A.; Ruedenhauer, F. G.; Werner, H. W. *Secondary Ion Mass Spectrometry*, Wiley, New York, **1987**

[32] Vickerman, J. V.; Brown, A.; Reed, N. *Secondary Ion Mass Spectrometry*, Oxford University Press, Oxford, **1989**

[33] Mittal, K. L. *Contact Angle, Wettability and Adhesion*, VSP, Netherlands, **1993**

[34] Ulman, A. *An Introduction to Ultrathin Organic Films*, Academic Press, San Diego, **1991**

[35] Ulman, A. *Thin Films, Self-Assembled Monolayers of Thiols*, Academic Press, San Diego, **1998**

[36] Nuzzo, R. G.; Allara, D. L. *J. Am. Chem. Soc.* **1983**, *105*, 4481

[37] Bain, C. D. Troughton, E. B.; Tao Y. T.; Evall J.; Whitesides G. M.; Nuzzo, R. G. *J. Am. Chem. Soc.* **1989**, *111*, 321

[38] Prime, K. L.; Whitesides, G. M. *J. Am. Chem. Soc.* **1993**, *115*, 10714

[39] Harder, P.; Grunze, M.; Dahint, R.; Whitesides, G. M.; Laibinis, P. E. *J. Phys. Chem. B* **1998**, *102*, 426

[40] Feldman, K.; Hähner, G.; Spencer, N. D.; Harder, P.; Grunze, M. *J. Am. Chem. Soc.* **1999**, *121*, 10134

[41] Kumar, A.; Whitesides, G. M. *Appl. Phys. Lett.* **1993**, *63*, 2002

[42] Kumar, A.; Biebuyck, H. A.; Whitesides, G. M. *Langmuir* **1994**, *10*, 1498

[43] Jackman, R. J.; Wilbur, J. L.; Whitesides, G. M. *Science* **1995**, *269*, 664

[44] Coburn, J. W. *Plasma Processing* **1982**, *2*, 1

[45] Sze, S. M. VLSI Technology: 2nd Edition, McGraw-Hill International **1988**

[46] Korner, N.; Beck, E.; Dommann, A.; Onda, N.; Ramm, J. *Surf. Coat. Technol.* **1995**, *76*, 731

[47] Petasch, W.; Kegel, B.; Schmid, H.; Lendenmann, K.; Keller, H. U. *Surf. Coat. Technol.* **1997**, *97*, 176

[48] Manos, R. G.; Flamm, D. L. *Plasma Etching*, Academic Press, San Diego, **1989**

[49] Kafader, U.; Sirringhaus, H.; von Känel, H. *Appl. Surf. Sci.* **1995**, *90*, 297

[50] Pintchovski, F.; Price, J. B.; Tobin, P. J.; Peavey, J.; Kobold, K. *J.Electrochem. Soc.* **1979**, *126*, 1428

[51] Madeley, J. M.; Richmond, C. R. *Anorg. Allg. Chem.* **1972**, *289*, 92

[52] Zhuravlev, L. T. *Langmuir* **1987**, *3*, 316

Chapter 3

Force-vs.-Distance Analysis on Poly(Ethylene Glycol) Films and Oligo(Ethylene Glycol)-terminated SAMs

Proteins are the micromachines that drive cells and, ultimately, living organisms. They are essential components of all human organs and play a vital role in all biochemical processes in the body.

Proteins are composed of single unit cells called amino acids. The general structure of an amino acid is shown in Figure 3.1. It contains an amino group ($-NH_2$), an acidic carboxyl group (-COOH) and a residual side chain (-X) that determines its specific properties [1,2]. These amino acids are linked together in particular sequences by peptide bonds between the carboxyl and the amino groups of each pair of amino acids to form a polypeptide, i.e. a protein. The only fundamental difference between proteins is their length and their sequence of residues. Due to their chemical structure the usually carbon-based residues have varying properties [3]. Some are hydrophobic, while others are hydrophilic. Some residues are basic, while others are acidic. Some are ring-like, while others are chain-like. Therefore, proteins comprise hydrophilic and hydrophobic as well as charged regions [1].

The understanding of protein adsorption on synthetic surfaces is of great interest in areas concerned with biomaterials, biosensors or artificial organs [4-6]. The first level of concern deals with non-specific adsorption: that is, adsorption reflecting hydrophobic or electrostatic interactions between protein and surface [7-11].
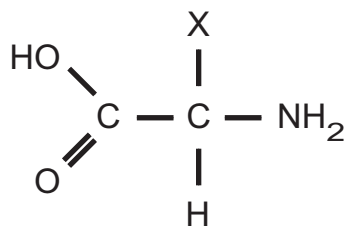
Figure 3.1: *A generic amino acid*

In particular, surfaces coated with poly(ethylene glycol) ($H\text{-}(OCH_2CH_2)_n\text{-}OH$) (PEG) films have been recognised for a long time for their remarkable protein-resistant properties [4,12,13]. In general, PEG is a simple, linear or branched, nonionic and water-soluble polyether. It is available in a huge variety of molecular weights and has various properties pertinent to biomedical applications [4]. The outstanding protein-resistance properties of PEG-coated surfaces are associated with a high conformational freedom of the chains and tightly bound water in the near-surface region [4]. A protein that approaches a PEG-coated surface and reaches the interface region, will compress the polymer chain and therefore restrict its conformational freedom. This is associated with the simultaneous dehydration of the PEG chain. Both the entropic component of the interaction due to the conformational freedom of the polymer chain and the osmotic component arising from the solvation of the PEG chain, constitute the 'steric repulsion' effect [14,15].

More recently, it has been found that self-assembled monolayers containing oligo(ethylene glycol) (OEG) can also resist the adsorption of biomolecules [16-18] and prevent the growth of cells on surfaces [4]. SAMs are easy to prepare while offering at the same time some flexibility towards functionalisation and have therefore attracted a lot of interest over the last two decades. The mechanism responsible for the repulsion of proteins by OEG-containing monolayer films, however, is different from that of the polymer. In a densely packed film, the conformational freedom of the OEG tails is strongly restricted and mechanisms other than those relevant in the case of the PEG must become effective. Therefore, the chain-length dependence of the protein resistance of OEG-terminated SAMs has been subject to intensive study [17,19-22].

Figure 3.2 illustrates the chemical structure of methoxy-tri(ethylene glycol) undecanethiolate (EG_3-OMe) exemplarily. Basically, these molecules are composed of an alkane chain featuring eleven methylene units, a surface-active thiol group (SH) that accounts

for the chemisorption to the gold substrate and a functional head group consisting of three ethylene glycol units terminated by a methoxy group. SAMs consisting of these molecules have been investigated extensively in this work.
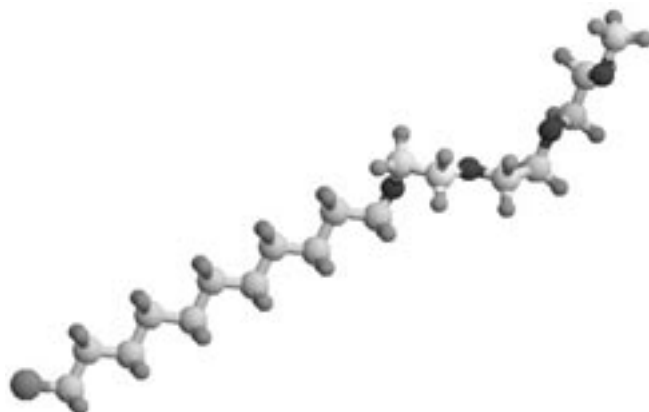
Figure 3.2: *Methoxy-tri(ethylene glycol) undecanethiolate (EG$_3$-OMe)*

Chemically modified SFM probes have been found to be a suitable tool to study both hydrophobic and electrostatic interactions with synthetic model surfaces separately and hence to mimic independently the different contributing forces to protein-surface interactions. In particular, measurements with hydrophobic tips have provided interesting insights into protein-surface interactions [23]. Therefore, most of the chemical force spectroscopy measurements in this work have been performed with hydrophobic C$_{16}$-tips in order to investigate different (ethylene glycol)-containing films and their interaction behaviour towards proteins.

3.1 Results

3.1.1 SFM Measurements on PEG and EG$_3$ SAMs

The advancing parts of concentration-dependent force-versus-distance curves with hydrophobic probes (referred to below as C$_{16}$-probes) on end-grafted PEG2000 (approximately 45 EG units on average) modified gold surfaces are shown in Figure 3.3. The electrolyte solutions were prepared by dissolving KNO$_3$ salt in ultrapure water covering ionic strengths from 0.1 mM to 0.1 M. The exponential fit of the approaching part of the force-

distance curves displayed repulsive interactions with decay lengths of approximately 1 nm that did not vary significantly for different ionic strengths. The independence of the salt concentration as well as the range of the repulsive forces are characteristic features of the 'steric repulsion' effect typically observed in combination with PEG films [13].
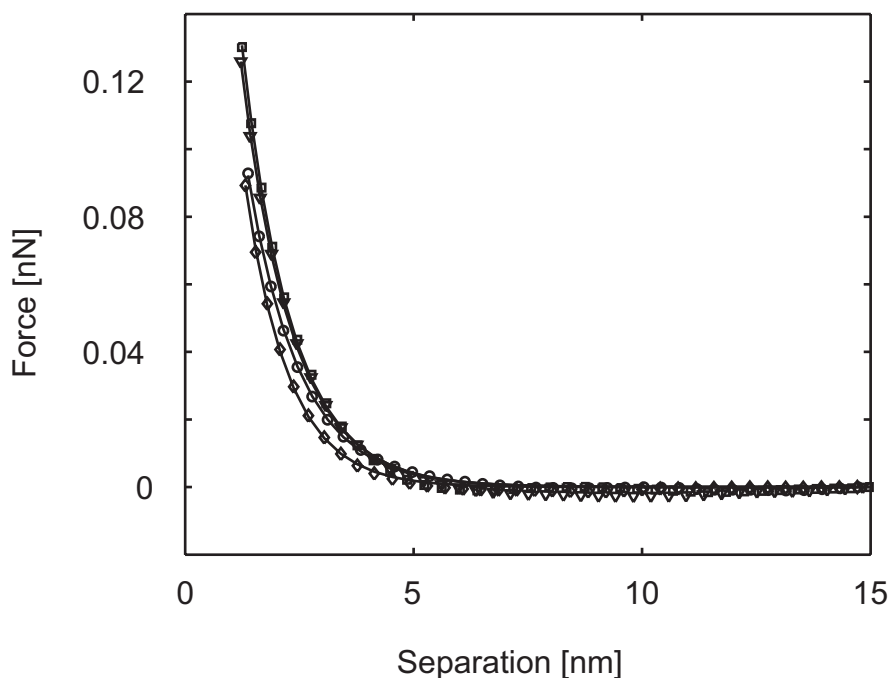
Figure 3.3: *Advancing force-versus-distance curves (averaged) measured with a C_{16}-probe on PEG2000 thiolates adsorbed on gold in aqueous KNO_3 solution of different salt concentrations ($\diamondsuit$ - 0.1M; $\bigcirc$ - 0.01M; $\triangledown$ - 1mM; $\square$ - 0.1mM).*

Oligo(ethylene glycol)-terminated films such as EG_3-OMe self-assembled monolayers on gold are also protein resistant, while the same films on silver are not, although in both cases the conformational freedom of the ethylene glycol tails is restricted in a densely packed film [18,23]. Despite the fact that EG_3-OMe monolayers adsorbed on gold and silver display macroscopically identical contact angles [18], they exhibit surprisingly different properties on the nanometer scale.

Figure 3.4 displays force-distance curves recorded for an EG_3-OMe (3 EG units) terminated gold surface employing a hydrophobic AFM tip under aqueous KNO_3 solution. The interaction comprises a long-range repulsive force detectable for low salt concentrations. At a concentration of 0.1 mM the exponential decay length is 17.3 nm. Increasing the concentration to 1 mM results in a smaller decay length of 9.1 nm. After further increasing the

salt concentration to 0.01 M, the decay length of this repulsive force decreases even more with an absolute value of 2.4 nm. For the highest concentration (0.1 M) investigated in this measurement, a very short decay length of 1.5 nm can be observed.
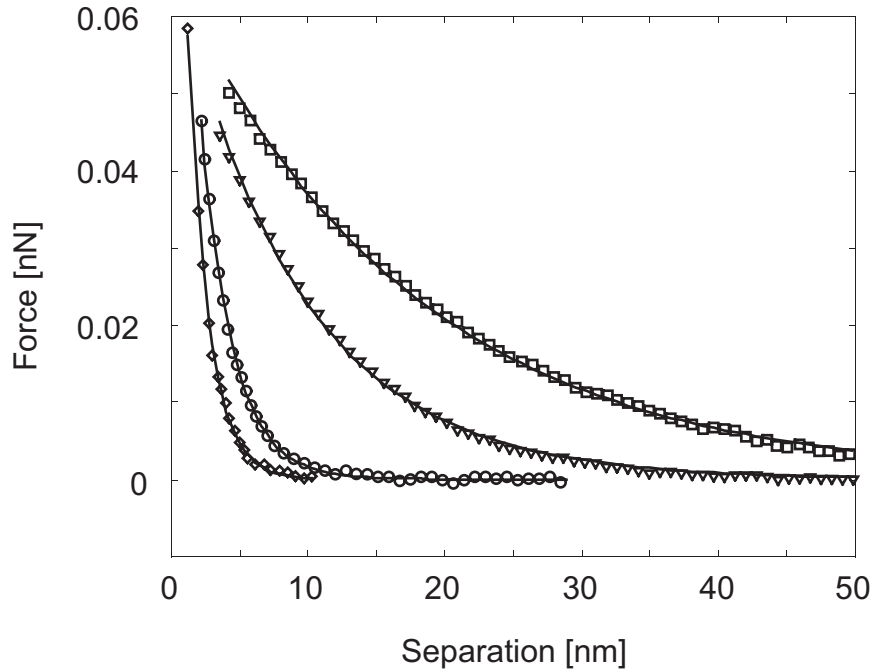
Figure 3.4: *Advancing force-versus-distance curves (averaged) measured with a hydrophobic C₁₆-probe on an EG₃-OMe SAM on gold in aqueous KNO₃ solution of different ionic strengths (◇ - 0.1M; ◯ - 0.01M; ▽ - 1mM; ☐ - 0.1mM).*

The strong dependence of the exponential decay length on the concentration of the solution suggests an electrostatic contribution to the interaction and hence a DLVO-type force. In general, DLVO theory describes the interaction between charged bodies under electrolyte solution taking into account both electrostatic and van der Waals contributions to the force [24]. For a sphere of radius R and a flat surface with charge densities σ_1 and σ_2 and 'low' potentials (<25 meV), the interaction force was found to be best described by the following equation [25,26]

$$F = \frac{4\pi R \sigma_1 \sigma_2}{\varepsilon_o \varepsilon_r \kappa} \exp(-\kappa s) \tag{3.1}$$

where ε_o is the permittivity of free space, ε_r is the dielectric constant of the electrolyte solution, $1/\kappa$ is the Debye length and s is the separation between the two bodies.

According to DLVO theory, the exponential decay length, the so-called Debye length, scales with the inverse of the square root of the ion concentration [24].

$$\kappa^{-1} = 0.304 \big/ \sqrt{C} \text{ nm} \qquad \text{for 1:1 electrolytes, e.g. KCl} \qquad (3.2)$$

$$\kappa^{-1} = 0.176 \big/ \sqrt{C} \text{ nm} \qquad \text{for 2:1 electrolytes, e.g. } K_2SO_4 \qquad (3.3)$$

One possible source for errors in our measurements is the concentration of the salt solution. The preparation process itself as well as contamination during the measurement cycles might lead to deviations from the nominal ionic strength. We estimate this error to be on the order of 5%, resulting in an error of the same magnitude for the decay length. Other (systematic) errors such as unknown tip radius or spring constant of the probe do not affect the decay length, since they do not change during the measurement. Errors of the theoretical fit have been determined based on least-squares fits of the exponential function (see Eq. 3.1) to the experimentally determined curves. Generally, noise in single force curves did not exceed 0.01 nN. The decay lengths showed an error in the range of 5 - 10% for a fixed ionic strength. The overall error in the decay length can then be estimated to be well below 20%.

A more rigorous quantitative analysis of the absolute values of the forces acting between probe and sample surface is not possible, because force constants and radii of curvature of the probes were not determined after functionalisation. Note, however, that the decay length is independent of both of these parameters.

Although there are no free charges associated with the organic films involved *per se*, the EG$_3$-OMe SAM seems to generate sufficiently strong dipolar fields to cause a screenable electrostatic interaction with the hydrophobic probe. Thus, the repulsive force between the C$_{16}$-probe and the monolayer film on gold under electrolyte solution exhibits an interaction behaviour that is intrinsically different from that detected for the PEG polymer, which shows short-range steric repulsion. In order to investigate the nature of this interaction in more detail, principally two strategies can be employed.

One is to study various monolayers of the short chain oligomer with different lengths of the terminating functional group, in order to trace the assumable transition from the interaction detected for the oligomer to the steric repulsion correlated with the polymer. Another possible approach might be to concentrate on the polymer films and vary their density and therefore the thickness of the films.

3.1.2 Varying the Oligomer Length

In order to study the influence of the number of EG units on the interaction behaviour of a SAM towards hydrophobic probes, monolayer films containing 1, 6 and 9 ethylene glycol units have been employed additionally to the EG_3-OMe SAM described above.

SAM	Contact Angle [°]
EG_1-OMe	72 ± 3
EG_3-OMe	65 ± 3
EG_6-OMe	66 ± 3
EG350	63 ± 3
PEG2000	38 ± 3

Table 3.1: *Advancing contact angle measurements at the different OEG SAM surfaces.*

Prior to force-distance analysis, advancing contact angle measurements have been performed. Within the experimental error, all OEG SAMs display similar values around 65° (see Table 3.1). For the EG_1 monolayer a slightly higher value can be observed resembling the highly ordered, strongly hydrophobic backbone of the film, whereas the PEG2000 film shows noticeably lower water contact angles around 40°.

Figure 3.5: *Advancing force-versus-distance curves (averaged) measured with a hydrophobic C_{16}-probe on an EG_1-OMe SAM on gold in aqueous KNO_3 solution of different salt concentrations ($\diamond$ - 0.1M; $\bigcirc$ - 0.01M; $\triangledown$ - 1mM; $\square$ - 0.1mM).*

In principle, it must be noted that the structures of the different OEG films may vary due to their differing surface coverage. Near-Edge X-ray Adsorption Fine-Structure Spectroscopy (NEXAFS) measurements have revealed a distinct decay in order of the monolayers with increasing number of terminating EG units [27]. While the EG_1 film still shows a preferential organisation comparable to a reference C_{16} film, this order subsequently decreases for EG_3 and EG_6 monolayers. For the EG350 SAM as well as for the PEG2000 film order was no longer detectable.

Force-distance measurements performed on the EG_1-OMe monolayers (1 EG unit) adsorbed on gold have been performed under aqueous KNO_3 solution. Again, various salt concentrations ranging from 0.1 mM to 0.1 M have been employed. For all ion concentrations the observed interaction is attractive, as can be seen in Figure 3.5. This attractive interaction between SAM and C16-probe suggests low resistance to non-specific protein adsorption and, in fact, EG_1-OMe monolayers on gold have been shown to adsorb proteins [17].

Figure 3.6: *Advancing force-versus-distance curves (averaged) measured with a hydrophobic C_{16}-probe on an EG_6-OMe SAM on gold in aqueous KNO_3 solution of different salt concentrations ($\diamond$ - 0.1M; $\bigcirc$ - 0.01M; $\triangledown$ - 1mM; $\square$ - 0.1mM).*

EG_6-OMe monolayers (6 EG units) adsorbed on gold were found to exhibit a similar behaviour as EG_3-OMe concerning protein adsorption properties, but a higher variety in the

conformational state of the ethylene glycol tails was observed with IR spectroscopy [18]. The EG tails showed a higher amount of gauche conformations and hence a more amorphous character compared to EG_3-OMe monolayer films. When probed with hydrophobic tips (see Figure 3.6), however, the forces observed are very similar to those found for EG_3-terminated SAMs. The determined decay lengths, $1/\kappa$, are on the same order of magnitude as those for EG_3-OMe and as expected on the basis of Debye theory.

The interaction force between a hydrophobic C_{16}-probe and a polycrystalline gold surface functionalised with a self-assembled monolayer of EG350 alkanethiols, which comprise 8 to 9 EG units on average, also shows a repulsive interaction for salt concentrations between 0.1 mM and 0.01 M and becomes attractive for 0.1 M (see Figure 3.7). The range of interaction is again strongly dependent on the ionic strength of the electrolyte solution. The force-distance dependence is best fitted with an exponential curve again. Consequently, the experimentally determined decay lengths are also close to the theoretical values predicted for the Debye lengths as expected for electrostatic interactions, with some deviation for the lowest concentration.
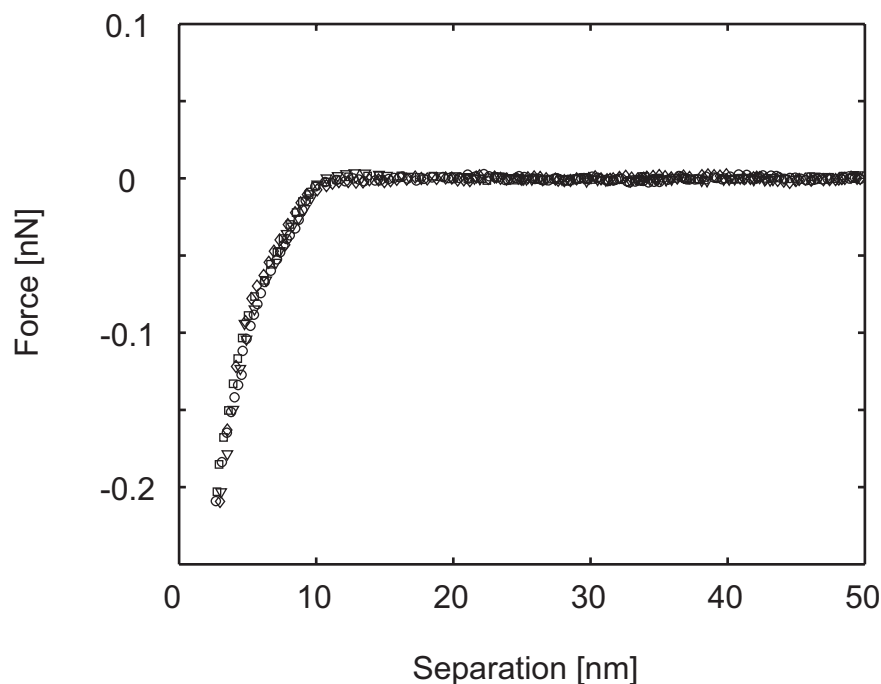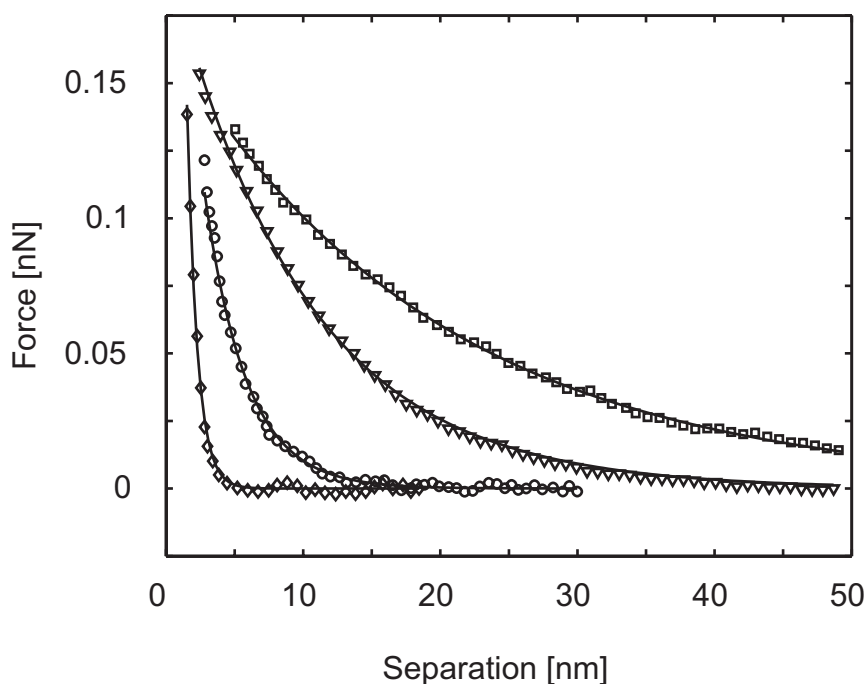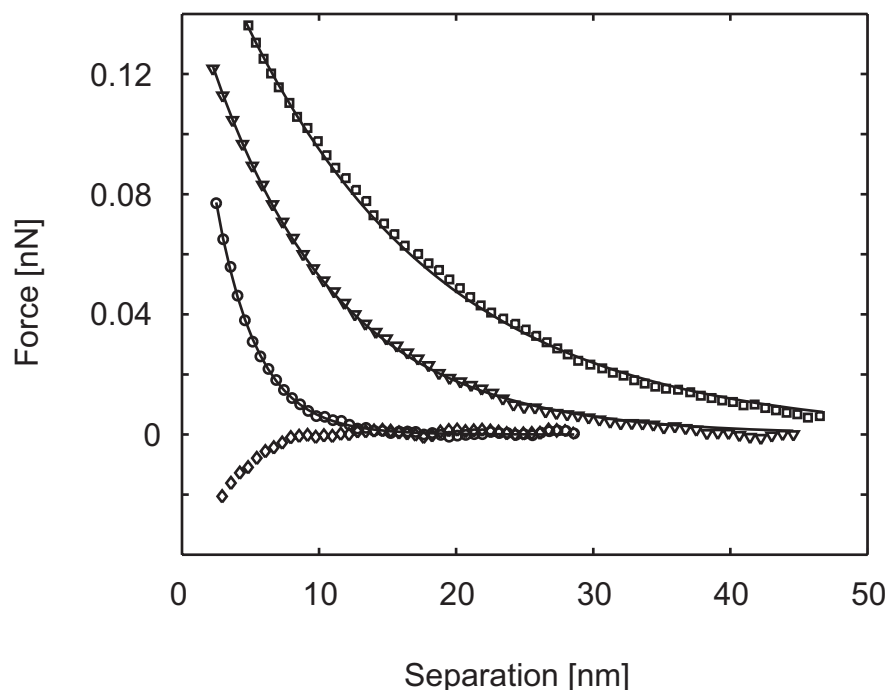

Figure 3.7: *Advancing force-versus-distance curves (averaged) measured with a C_{16}-probe on an EG350 SAM on gold in aqueous KNO_3 solution of different concentrations ($\diamond$ - 0.1M; $\bigcirc$ - 0.01M; $\triangledown$ - 1mM; $\square$ - 0.1mM).*

3.1.3 Varying the Density of the Polymer Film

In another approach to elucidate the difference in the interaction behaviour between polymer and oligomer films towards hydrophobic C_{16}-probes, the density of the polymer film was varied. It has been shown, both in experimental and theoretical studies, that the polymer density is a crucial parameter for protein resistance [13,28]. Molecular dynamics simulations emphasise the importance of mobility and density of the end-grafted polymeric surface to the extent of the protein-polymer interaction [4]. In addition, polymer density was found to strongly influence the distribution of water molecules in its very proximity. At an optimum packing density the PEG chain will adopt trans-gauche-trans conformation, which makes it fit best into the hydrogen-bonded network of water molecules [29,30].

According to the adsorption kinetics as discussed by Grunze and coworkers (displayed in Figure 3.8) [31], polymer films with relative densities of approximately 25% and 50% of a fully covered film have been prepared by immersion into a 50 μM DMF solution of PEG2000 for approximately 15 and 30 minutes, respectively. Compared to these films, the PEG layer in Figure 3.1 was established by immersion into the same solution for approximately 500 minutes to ensure full coverage.
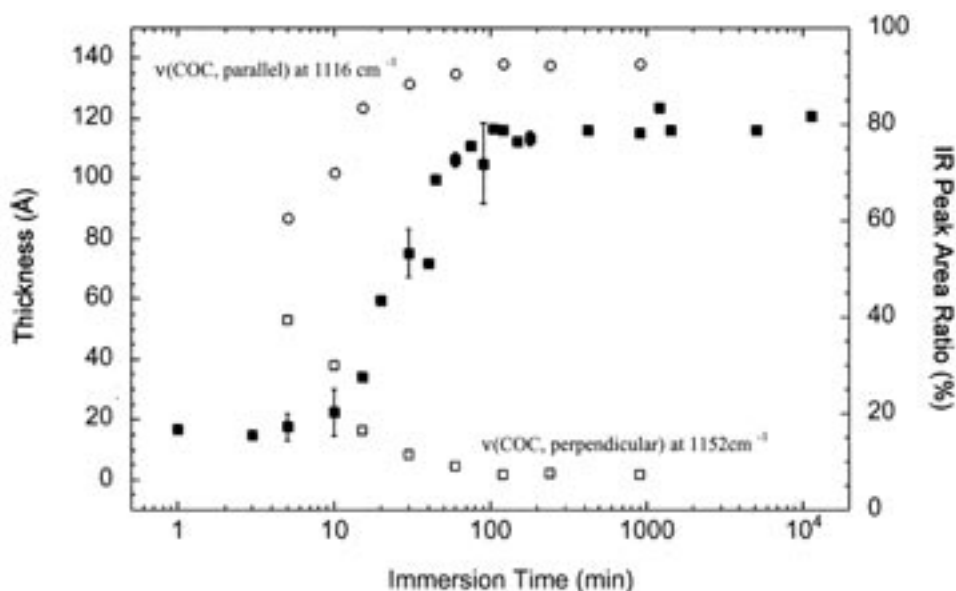
Figure 3.8: *Evolution of film thickness of end-grafted PEG2000 thiolate films on gold after different times of immersion into 50 μM DMF solution as measured by ex-situ ellipsometry (filled squares) (published by Tokumitsu et al.) [31].*

Grunze and coworkers found the morphologies of these films to be strongly dependent on the PEG grafting density [31]. At low surface coverage (25% films), they observe a coil-like structure similar to that found in solution. At medium surface coverage (50% films), the molecules experience a lateral confinement forcing the single chains into a brush-like structure. For a densely packed polymer film (100% coverage), they propose a preferential helical conformation of the PEG molecules with an orientation normal to the surface.

Figure 3.9: *Advancing force-versus-distance curves (averaged) measured with a C_{16}-probe on PEG2000 thiolates (50% coverage) adsorbed on gold in aqueous KNO_3 solution of different concentrations ($\Diamond$ - 0.1M; $\bigcirc$ - 0.01M; $\triangledown$ - 1mM; $\square$ - 0.1mM).*

Force-distance measurements on a PEG film with 50% coverage reveal a long-range repulsive force at a salt concentration of 0.1 mM, as shown in Figure 3.9. The exponential decay length of the repulsion is similar to the value observed for the oligomer films. Note the remarkable jump-into-contact distance of approximately 10 nm, which is a strong indication for an additional long-range attractive force. After increasing the ion concentration to 1mM, a decrease in the decay length similar to the measurements on the OEG films can be observed. In addition to this long-range repulsion, again an attractive contribution established in the long jump-into-contact distance can be observed. For the 0.01 M solution a very interesting effect occurs. After introduction of the solution into the liquid cell, the system was given approximately five minutes to equilibrate. After this time, force-distance measurements were

performed in several cycles. Continuing the effect observed for the lower salt concentrations, the first curves revealed a rather long-range repulsive force with a decay length similar to the value expected on the basis of DLVO theory (full circles). With ongoing measurements, the decay length of the repulsion and the jump-into-contact distance decreased (open circles). At higher concentrations (0.1 M), the typical short-range steric repulsion known from the fully saturated polymer film can be observed. This clearly concentration-dependent force-distance behaviour is not reversible. After sample storage in the pure solvent overnight, only steric repulsion could be observed for the whole range of concentrations employed. The long-range repulsive forces measured at low ionic strengths therefore seem to diminish permanently, after the sample was exposed to solutions with higher ionic strengths.
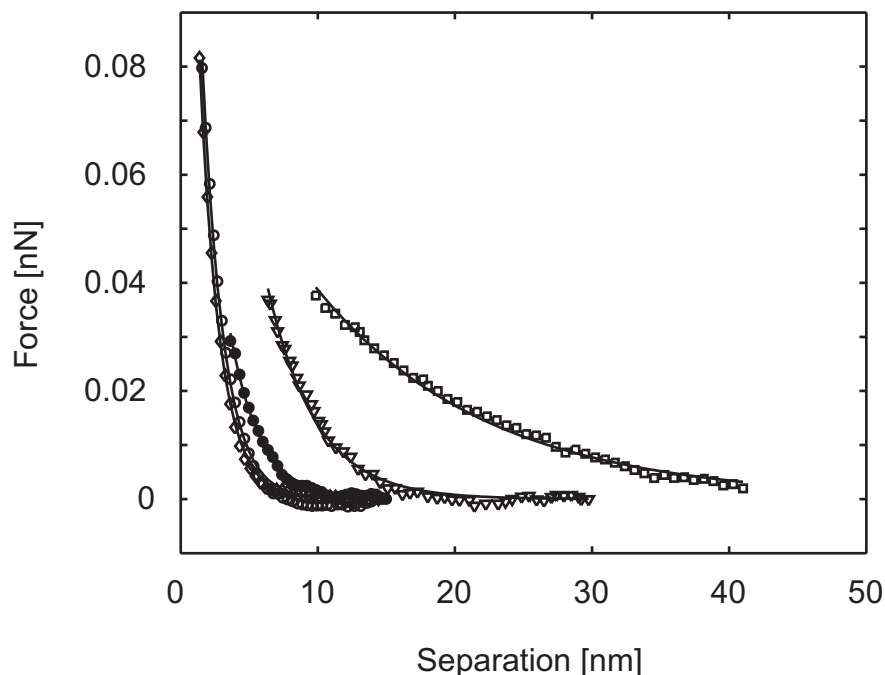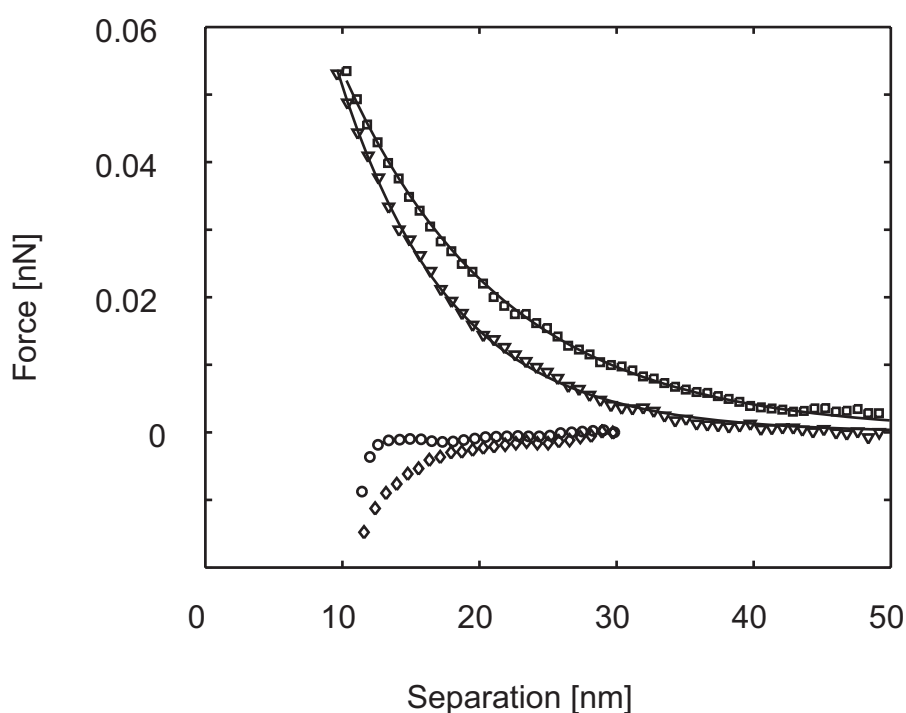

Figure 3.10: *Advancing force-versus-distance curves (averaged) measured with a C_{16}-probe on PEG2000 thiolates (25% coverage) adsorbed on gold in aqueous KNO_3 solution of different concentrations ($\diamond$ - 0.1M; $\bigcirc$ - 0.01M; $\triangledown$ - 1mM; $\square$ - 0.1mM).*

Figure 3.10 displays force-distance curves for a gold sample coated with a PEG2000 layer of 25% coverage. At low salt concentrations again long range repulsive forces as well as long jump-into-contact distances of around 10 nm can be observed. The order of magnitude of the decay lengths at 0.1 mM and 1 mM is once again in very good agreement with the values observed for the OEG SAM covered samples at these concentrations. At more elevated ion

concentrations of 0.01 M and 0.1 M the long-range repulsive interaction completely vanishes and clearly attractive forces with a jump-into-contact at 10 nm are measured. This interaction is very similar to force-distance measurements performed with hydrophobic C_{16}-probes on bare gold surfaces and implies a strong hydrophobic character. Again, these measurements are not reversible. Sample storage overnight in the pure solvent did not help to re-establish the long-range repulsive interaction at low ionic strengths. The interaction remained attractive for all investigated salt concentrations. Obviously, these surfaces are not resistant to protein adsorption [31].

3.2 Discussion

3.2.1 SFM Measurements on OEG SAMs

For all oligomers adsorbed on gold, a long-range repulsive interaction upon approach with a hydrophobic C_{16}-probe was observed at low salt concentration (0.1 mM), which dramatically reduces with increasing ionic strength. The force-distance dependence suggests an electrostatic character of the interaction. Therefore, the EG oligomers with 3 - 9 ethylene glycol units seem to carry an effective surface charge. The fully covered PEG polymer film, however, shows pure steric repulsion, i.e., its overall effective charge can be assumed to be zero. The EG monomer film shows attractive forces towards hydrophobic probes over the whole range of investigated ion concentrations indicating the loss of protein resistance. In fact, these films have been shown to adsorb proteins to some extent, whereas films with terminally attached ethylene glycol oligomers (n ≥ 2) prevent protein adsorption, provided the density of EG functional groups in the SAM exceeds a threshold value [17].

For high ion concentrations (0.1 M), an attractive interaction was also measured for the EG350 film. This might be due to van der Waals forces or the hydrophobic character of the film, which can dominate when the electrostatic forces are completely screened by high ion concentration. The purely repulsive and short-range forces observed for high ion concentration for the EG_3-OMe and EG_6-OMe monolayers might be due to hydration forces associated with the ions from the electrolyte. A similar behaviour was reported for high ion concentrations and charged surfaces [25]. The highest deviation from the expected Debye values is found for the lowest ion concentration, indicating that a slightly higher amount of

ions might be present in the liquid. This is likely due to small amounts of contaminants (e.g. dissolved gas) from the environment.

Although the EG tails of EG_6-OMe and EG350 on gold are in a more amorphous state compared to those of EG_3-OMe, they still exhibit a similar concentration-dependence of the forces. Note, however, that the *range of interaction* depends solely on parameters of the electrolyte and not on any surface properties. Different effective surface charges, for example, result in different strength of the forces but not in different decay lengths.

While EG_3-OMe molecules adsorbed on gold carry some effective surface charge in a densely packed film, this vanishes when the molecules are adsorbed on silver [23]. Hence, the probably induced dipole moment crucially depends on the configuration in the adsorbed state. While the OEG monolayers adopt a helical to amorphous state on gold surfaces, it was shown that an all-trans configuration is the dominant phase on silver [18]. The helical configuration was found to fit best into the hydrogen-bonded water network, while PEG chains in all-trans configuration do not [32,33]. In combination with the high order at the top of the densely packed SAM film and the observed DLVO-type forces, a dipole field is likely to be established at the SAM/water interface. In fact, a dipole moment per molecule on the order of 2 D could be attributed to the EG3-OMe SAM on gold [23].

3.2.2 SFM Measurements on End-grafted PEG Films

Force-versus-distance measurements on partially established PEG2000 films display different characteristics. While both investigated films (at 25% and 50% coverage) establish long-range repulsive interaction forces towards the hydrophobic C_{16}-probe at low salt concentrations, they show different interactions at higher ionic strengths. For the films with lower PEG coverage (25% films) attractive forces similar to hydrophobic forces between C_{16}-tips and bare gold surfaces become dominant at higher salt concentrations, whereas for the PEG films with medium coverage (50% films) features typical for steric repulsion known from fully covered films become apparent. In particular, the traceable stepwise transition from long-range to steric repulsion at 0.01 M provides information about film architecture and dynamics. From these results it might be concluded, that PEG2000 films with 50% coverage still remain resistant to protein adsorption, whereas films comprising 25% cover rate lose this capability.

In fact, it was found that PEG cover density is a crucial parameter in protein resistance [4]. Jeon et al. defined concrete conditions for an optimal PEG packing density for resistance to protein adsorption by simulations [13,34]. In these studies, the polymer chains were examined in the "brush" structure, meaning that the average distance between the chains was less than the Flory radius, r_F, of the polymer (see Figure 3.11) [35]. They proposed a quantitative model for protein adsorption taking into account steric repulsion as well as van der Waals and hydrophobic attraction. From these simulations it was concluded that the concentration of PEG chains at the interface that is required to resist the adsorption of proteins decreases as the size of the proteins increases.

a) $d \gg 2r_F$ **b)** $d \sim 2r_F$ **c)** $d < 2r_F$
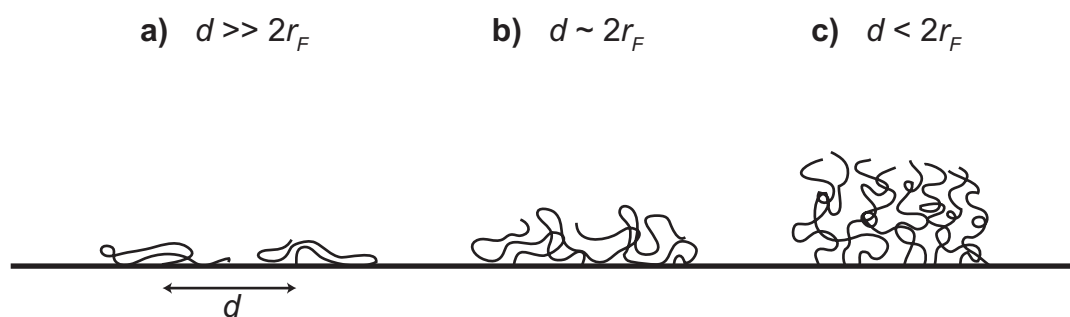
Figure 3.11: Schematic of PEG2000 chains adsorbed on a gold surface at various surface concentrations: a) non-overlapping 'mushrooms', b) weakly-overlapping 'mushrooms', and c) dense 'brushes'.

The influence of different structural states of PEG films on their protein resistant properties has been reported elsewhere [36]. In particular, the importance of interchain coupling at the very surface has been emphasised. Due to the strong interaction of the EG units with water molecules, isolated, hydrated PEG chains normally resist overlapping, i.e., interchain coupling. Upon increasing the grafting density above a critical surface concentration, the PEG chains experience a lateral confinement that finally forces the single chains to overlap. According to Figure 3.11, this critical surface concentration is reached, when the average distance, d, between two PEG chains is of twice as much the Flory radius, r_F [22,34].

Depending on the surface concentration, three different regimes have been defined elsewhere (compare Figure 3.11): a) non-overlapping 'mushrooms', b) weakly-overlapping 'mushrooms' and c) dense 'brushes' [22]. The picture of 'mushroom'-like structures may mislead in case of PEG2000 molecules due to their limited length and the relatively small number of 45 EG units. A more suitable image might be a planar orientated random coil or

flat 'pancake'. From this point of view, the 25% film consists of non-overlapping coil-like amorphous moieties, which are chemisorbed to the gold substrate by the thiol group and most likely feature additional surface linkages due to van der Waals interactions but no interchain coupling due to the low surface coverage. Furthermore, the denser 50% film shows some additional interchain coupling, while the fully covered film comprises dense 'brushes', which are responsible for the observed steric repulsion effect as described in literature [13].

In this picture, the long-range repulsive interactions observed at lower salt concentrations can be explained by a comparison with the OEG-terminated monolayer films. In fact, the PEG films at lower grafting densities correspond to OEG SAMs with an average number of 3 - 6 EG units [31]. These SAMs have been found to comprise EG units in helical to amorphous states under aqueous solution [37]. This amorphous structure can also be presumed in the case of the partially covered surfaces, where the polymer chains are spread more laterally on the surface so that a similar electrostatic character of the long-range repulsive interaction can be assumed. At more elevated salt concentrations, the solubility of the polymer chains increases [23,24]. Therefore, it is more favourable for the PEG molecules to expose more EG units to the solvent and so to extend into the solution rather then occupying the van der Waals adsorption sites on the surface. Thus, the partly exposed bare gold surface in case of the 25% film gives rise to the attractive interaction towards the hydrophobic C_{16}-probe.

The transition observed for the 50% film, however, cannot be solely explained with this picture. Due to the weak overlap of the polymer chains a thin but closed surface layer might be assumed. The transition from long-range electrostatic to short-range steric repulsion, which is observed for higher electrolyte concentrations, can be explained in terms of an extension of the PEG chain into the liquid. This is associated with a stronger solvation of the polymer chains and an increase in their conformational freedom, which gives rise to the steric repulsion effect [13].

3.3 Conclusions

Oligo(ethylene glycol)-terminated alkanethiols adsorbed on polycrystalline gold substrates show repulsive interactions towards hydrophobically functionalised C_{16}-probes under electrolyte solution. The observed repulsive force depends strongly on the salt concentration indicating an electrostatic origin. SAMs containing short-chain oligomers with 3 - 9 EG units seem to carry an effective surface charge, while this vanishes for a polymer chain consisting of 45 units. The electrostatic character is likely caused by induced dipoles but is completely absent for the densely packed EG_3-OMe films on silver.

PEG2000 coated gold surfaces display a characteristic force-distance dependence that is strongly dependent on their film density. While films with 25% and 50% coverage both show long-range repulsive forces for low ionic strenghts, fully covered PEG films display the well-known steric repulsion effect. In electrolyte solutions with higher ion concentrations, partially established PEG films feature a diverse behaviour. While PEG films with 50% coverage undergo a transition in their interaction behaviour to steric repulsion as observed for fully covered films, PEG films with lower density (25% coverage) show an attractive interaction very similar to the hydrophobic interaction between C_{16}-tips and bare gold surfaces. The three different surface concentration regimes including interchain coupling described above and the solubility dependence of PEG molecules on the electrolyte concentration play a crucial role in the observed interactions. The long-range repulsive forces are likely caused by a conformation, in which the PEG chains are closely linked to the gold surface by additional van der Waals interactions generating a two-dimensional layer similar to the EG tail at OEG SAMs.

3.4 Literature

[1] Branden, C.; Tooze, J. *Introduction to protein structure*, Garland Publishing, NY, **1999**

[2] Voet, D.; Voet, J. G.; Pratt, C. W. *Fundamentals of Biochemistry*, Wiley, New York, **1999**

[3] Creighton, T. E. *Proteins: Structures and Molecular Properties*, Freeman, NY, **1997**

[4] Harris, J. M. *Poly(Ethylene Glycol) Chemistry*, Plenum Press, New York, **1992**

[5] Bergström, K.; Holmberg, K.; Safranj, A.; Hoffman, A. S.; Edgell, M. J.; Hovanes, B. A.; Harris, J. M. *J. Biomed. Mater. Res.* **1992**, *26*, 779

[6] Topchieva, I. N. *Russ. Chem.Rev.* **1980**, *49*, 494

[7] Prime, K. L.; Whitesides, G. M. *Science* **1991**, *252*, 1164

[8] Spinke, J.; Liley, M.; Schmitt, F. J. *J. Chem. Phys.* **1993**, *99*, 7012

[9] Dahint, R.; Seigel, R. R.; Harder, P.; Grunze, M.; Josse, F. *Sensor Actuat B* **1996**, *36*, 497

[10] Silin, V.; Weetall, H.; Vanderah, D. J. *J. Coloid. Interf. Sci.* **1997**, *185*, 94

[11] Ide, M.; Mitamura, A.; Miyashita, T. *Bull. Chem. Soc. Jap.* **2001**, *74*, 1355

[12] Taunton, H. J.; Toprakcioglu, C.; Fetters, L. J.; Klein, J. *Nature* **1988**, *332*, 712

[13] Jeon, S. I.; Andrade, J. D. *J. Colloid Interface Sci.* **1991**, *142*, 159

[14] Sleifzer, I. *Curr. Opin. Solid State Mater. Sci.* **1996**, *2*, 337

[15] Halperin, A. *Langmuir* **1999**, *15*, 2525

[16] Pale-Grosdemange, C.; Simon, E. S.; Prime, K. L.; Whitesides, G. M. *J. Am. Chem. Soc.* **1991**, *113*, 12

[17] Prime, K. L.; Whitesides, G. M. *J. Am. Chem. Soc.* **1993**, *115*, 10714

[18] Harder, P.; Grunze, M.; Dahint, R.; Whitesides, G. M.; Laibinis, P. E. *J. Phys. Chem. B* **1998**, *102*, 426

[19] Dicke, C.; Feldman, K.; Eck, W.; Herrwerth, S.; Hähner, G. *Pol. Prep.* **2000**, *41*, 1444

[20] Zhu, B.; Eurell, T.; Gunawan, R.; Leckband, D. *J. Biomed. Mater. Res.* **2001**, *56*, 406

[21] Schwendel, D.; Dahint, R.; Herrwerth, S.; Schloerholz, M.; Eck, W.; Grunze, M. *Langmuir* **2001**, *17*, 5717

[22] Efremova, N. V.; Sheth, S. R.; Leckband, D. E. *Langmuir* **2001**, *17*, 7628

[23] Feldman, K.; Hähner, G.; Spencer, N. D.; Harder, P.; Grunze, M. *J. Am. Chem. Soc.* **1999**, *121*, 10134

[24] Israelachvili, J. *Intermolecular and Surface Forces*, Academic Press: San Diego, CA, **1992**

[25] a) Butt, H.-J. *Biophys. J.* **1991**, *60*, 777; b) Butt, H.-J. *Biophys. J.* **1991**, *60*, 1438

[26] Butt, H.-J.; Jaschke, M.; Ducker, W. *Bioelectrochem. Bioenerg.* **1995,** *38*, 191

[27] Zwahlen, M.; Hähner, G.; Herrwerth, S.; Eck, W.; Grunze. M. *in preparation*

[28] Atha, D. H.; Ingham, K. C. *J. Biol. Chem.* **1981**, *256*, 12108

[29] Tanford, C.; *The Hydrophobic Effect*, Wiley-Interscience, New York, **1980**

[30] Kjellander, R.; Florin, E. *J. Chem. Soc., Faracday Trans. 1* **1981**, *77*, 2053

[31] a) Herrwerth, S. *private communication*; b) Tokumitsu, S., Liebich, A.; Herrwerth, S.; Eck, W.; Himmelhaus, M.; Grunze, M. *Langmuir,* **2002**, *18*, 8862

[32] Narten, A. H. *J. Chem. Phys.* **1972**, *56*, 5681

[33] Jeon, S. I.; Lee, J. H.; Andrade, J. D.; De Gennes, P. G. *J. Colloid Interface Sci.* **1991**, *142*, 149

[34] Takahashi, Y.; Tadokoro, H. *Macromolecules* **1973**, *6*, 672

[35] Flory, P. J. *Principles of Polymer Chemistry*, Cornell University Press, New York, **1953**

[36] Sofia, S. J.; Premnath, V.; Merrill, E. W. *Macromolecules* **1998**, *31*, 5059

[37] Zolk, M.; Eisert, F.; Pipper, J.; Herrwerth, S.; Eck, W.; Buck, M. Grunze, M. *Langmuir* **2000**, *14*, 5849

Chapter 4

Force-Distance Analysis on Tri(Ethylene Glycol)-terminated Self-Assembled Monolayers, Part 1[*]

The force measurements discussed in the last chapter suggest that a strong electrostatic component is involved in the interaction of hydrophobic SFM probes with OEG-terminated SAM surfaces. In order to study the origin of the observed effective negative surface charge density generated at these surfaces in aqueous solutions the force-distance measurements presented in this chapter focus on SAMs of methoxy-tri(ethylene glycol) undecanethiolates (EG$_3$-OMe) prepared on polycrystalline gold substrates. These molecules basically consist of an alkane chain containing eleven methylene units, a surface active thiol group, which is responsible for the covalent attachment to the gold substrate and a functional head group containing three ethylene glycol units and a terminal methoxy group (see Figure 3.2).

Different suggestions have been made in order to explain the ability of these ultrathin films to resist the non-specific adsorption of proteins. Ethylene glycol units are known to interact strongly with the surrounding aqueous environment: For an EG$_3$-OMe SAM on gold, for example, a helical to amorphous conformation was found in vacuum [1], while under water, the order present in the OEG tail diminishes [2]. In another study, it was observed that water molecules penetrate into micrometer-thick PEG films in ambient and finally form dimers and trimers with other water molecules [3]. IR-visible sum-frequency generation spectroscopy at the water/PEG interface revealed the presence of water molecules that are

strongly bonded to the oxygen atoms of the ethylene glycol entities and of further water species located in the vicinity of the PEG surface organised in an 'ice-like' film [4]. The maximum hydration number per EG monomer for PEG molecules has been determined experimentally to vary between 1.6 and 3.3, depending on the molecular weight of the polymer [5,6]. Some attention has also been directed at the interface of EG functional groups and a hydrophobic backbone under water, for PEG modified with alkane chains [7]. A very low hydration of the PEG units near the PEG/hydrocarbon interface was found, which increased towards the outer region of the PEG tail.

Due to the strong interaction of EG units with water it has been hypothesised that water might establish a transition layer at the film/liquid interface of the OEG-functionalised SAMs, which is different from the bulk solution [8]. A 'thick water interface (several nm) with unusual properties' might be responsible for the inertness towards the adsorption of proteins. This could be a water layer that is structured or exhibits a reduced density compared to the bulk. Similarly it has been suggested that hydrophobic interactions are due to the influence of the surface on water structure [9]. The surface is assumed to induce order into the water molecules in close proximity. This order decays into the liquid and gives rise to a long-range interaction with the same decay length as the order profile.

Apart from the strong affinity between OEG and water molecules, it has also been reported that a specific interaction of certain (cat)ions with EG units is possible. Ab-initio calculations performed for 1:1 complexes of triglyme (i.e., triethylene glycol dimethyl ether) with different cations revealed several stable complexes for different metal ions, with Li^+ forming the most stable and energetically most favourable one [10]. All four ether oxygens are involved in complexing the cation, which can lead to different configurations. However, in all of them the ethylene glycol units 'encage' the cation.

Complexation reactions have also been subject to intensive studies in connection with electrochemical devices such as rechargeable batteries. Small alkali ions are of particular interest in this field of research. Several studies were concerned with PEG/alkali salt complexes, where Li^+, Na^+ or K^+ ions form stable crystalline complexes with PEG via coordination of the cations to the ether oxygens [11-14]. In general, 5:1 complexes, where five ether oxygens are coordinated to one cation, are found to be most stable, while several PEG chains can cooperatively contribute oxygens to the constituted complex. Due to these complexing properties, poly(ethylene glycol) has been considered to form so-called 'flexible

crown ethers' [15]. Alkanethiols, in turn, functionalised with different crown ethers have been shown to react specifically with cations depending on their size and can be utilised for recognition [16-20].

EG$_3$-OMe SAMs have also been investigated with regards to their resistance to polyelectrolyte adsorption at ionic concentrations between 1mM and 0.1M. It was concluded that resistance is caused by a swelling of the EG interface, and the hydrated brush structure of the EG repeat units is stabilised by small ions [21]. In addition, it was found that Li$^+$ ions in particular 'fit' into the hydrated structure of the EG-brushes giving it additional stability. Na$^+$ ions showed a similar but weaker tendency to support the hydrated brush, as did K$^+$ ions. An incorporation of certain cations into the OEG tail of the alkanethiol molecules in the monolayer can therefore not be excluded *a priori*.

In order to test the hypothesis of a long-range structured water interface and to explore the affinity of different ions to the EG units in more detail we have performed the present investigation. In the previous chapter, force-versus-distance measurements on PEG and OEG monolayers are described, where repulsive forces with decay lengths depending on the ionic strength of the aqueous solution were found. These experiments suggested that there is an electrostatic component involved in case of the oligomers [22].

In this chapter, ions from the so-called Hofmeister or lyotropic series have been employed [23,24]. This series emerges from a combination of a general effect of cosolutes on solvent structure and of specific interactions between the cosolutes and the solute [23-28]. Cations and anions are known to have influence on both water structure and the solution behaviour of (bio)molecules [28,29]. The ability of the ions in the lyotropic series to disturb the hydrogen bond network between the water molecules varies. While some of them effectively 'break' water structures (so called chaotropes such as Cs$^+$ or Li$^+$), others are water structure 'supporting' (so called polar kosmotropes, e.g. NH$_4$$^+$ or N(CH$_3$)$_4$$^+$).

The different ions employed shall give an idea about the order profile of an extended structured water interface, if present, as well as indication for a specific interaction with the OEG tails.

4.1 Results

4.1.1 Contact Angle Measurements

Advancing contact angle measurements were performed prior to force-distance analysis. Various electrolyte solutions with a concentration of 1 mM were used to study the influence of different ions on the wettability of the EG_3-OMe-terminated SAM film. The ions dissolved in the aqueous solution were chosen according to the Hofmeister series (compare Table 4.2) and cover chaotropic as well as kosmotropic anions and cations, respectively. Table 4.1 displays all measured advancing contact angles, which show values at approximately 65° for all investigated electrolyte solutions and therefore prove good comparability within the experimental error.

Salt	Contact angle [°]
$LiNO_3$	62 ± 3
KNO_3	65 ± 3
$N(CH_3)_4NO_3$	65 ± 3
KI	67 ± 3
K_2SO_4	64 ± 3

Table 4.1: *Contact angle measurements on EG_3-terminated SAMs on gold using different electrolyte solutions with a salt concentration of 1 mM.*

4.1.2 Force Measurements with Hydrophobic Probes

In order to check the chemical quality and stability of the hydrophobised SFM probes that were employed for the force measurements on OEG-terminated films during and after exposure to electrolyte solution, we first measured a system consisting of two hydrophobic alkanethiol films adsorbed on both probe and countersurface. Figure 4.1 shows advancing force-versus-distance curves recorded under KNO_3 solution for hexadecanethiol films adsorbed on gold.
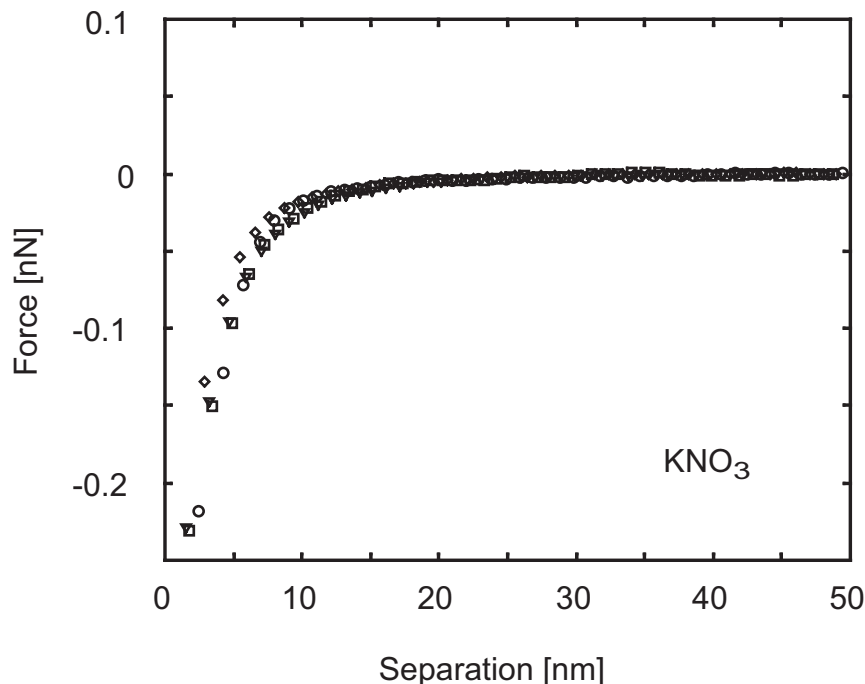
Figure 4.1: *Advancing force-versus-distance curves (averaged) for a hydrophobic hexadecanethiol-covered probe and a hexadecanethiol SAM on gold in aqueous KNO$_3$ solution for different concentrations ($\diamond$ - 0.1M; $\bigcirc$ - 0.01M; $\triangledown$ - 1mM; $\square$ - 0.1mM).*

The concentration was varied between 0.1 mM and 0.1 M, the same range as used for the measurements on the EG$_3$-OMe system. The measurement cycle was started with the lowest concentration, which was then increased stepwise by factors of ten. Over the whole range of concentrations an attractive interaction was found as displayed in Figure 4.1. This attractive interaction showed a constant range and appeared to be independent of the ionic strength. Finally, the measurement with the lowest concentration of 0.1 mM was repeated to check for a possible alteration of the tip or the sample surface. No difference to the first measurements with the same concentration was detectable. The retracting parts of the force curve cycles, which are not displayed in the figure, showed high adhesion forces (~50 nN), which remained rather constant for all electrolyte concentrations, as has been reported earlier in the literature [30,31].

The forces between a hydrophobic C$_{16}$-probe and an EG$_3$-OMe-terminated alkanethiol film adsorbed on a gold substrate were also recorded in KNO$_3$ solution and for different ionic strengths (see Figure 4.2). As already discussed in Chapter 3, the interaction features a strong dependence on the ionic strength of the electrolyte solution with repulsive forces of long range.

Figure 4.2: *Advancing force-versus-distance curves (averaged) for a hydrophobic probe and an EG$_3$-OMe SAM on gold in aqueous KNO$_3$ solution for different concentrations ($\diamond$ - 0.1M; $\bigcirc$ - 0.01M; $\triangledown$ - 1mM; $\square$ - 0.1mM). The solid lines represent exponential fits to the experimental data. For details see text.*

4.1.3 Hofmeister Series

Kosmotropic						**Chaotropic**				
Anions: F^- PO_4^{3-} SO_4^{2-} CH_3COO^- NO_3^- Cl^-						Br^- I^- CNS^- $CF_3SO_4^-$				
Cations: $(CH_3)_4N^+$ $(CH_3)_2NH_2^+$ NH_4^+ K^+ Na^+ Cs^+						Li^+ Mg^{2+} Ca^{2+} Ba^{2+}				

Table 4.2*: Hofmeister series - Kosmotropic ions are water structure supporting while chaotropic ions are assumed to be structure breaking.*

Aqueous KNO$_3$ solution was chosen as 'standard electrolyte' for the following force-distance analysis. According to the empirical Hofmeister series, the K^+ and the NO_3^- ion are both supposed to be 'neutral', i.e., they are neither water structure breaking (chaotropic) nor structure supporting (kosmotropic) (see Table 4.2). The interaction between a C_{16}-probe and an EG$_3$-OMe-terminated gold sample displayed in Figure 4.2 shows an exponentially decaying long-range repulsive force at low ionic strength. At the lowest investigated salt

concentration of 0.1 mM, a decay length of 17.3 nm was detected. Increasing the salt concentration resulted in lower values for the decay length: 9.1 nm were found for 1 mM and 2.4 nm for 10 mM solutions. For the highest ion concentration (0.1 M) adjusted in the liquid cell a value of 1.5 nm was observed.

The strong dependence of the decay length on the salt concentration of the solution suggests an electrostatic contribution and a DLVO-type force, although there are no free charges associated with the organic films involved *per se*. According to DLVO theory, the Debye length scales with the inverse of the square root of the ionic strength [25]. Table 4.3 summarises the values determined for the theoretical Debye lengths and the experimental decay lengths of the repulsive forces depending on the ionic strength. They are in reasonable agreement except for the lowest concentration of 0.1 mM.

Errors in the force-distance measurements have been determined using least-squares fits based on Equation 3.1 as already described in Chapter 3. Again, the overall error in the decay length could be estimated to be well below 20%.

Ionic Strength [mM]	Debye Length [nm] (theo.)	$1/\kappa$ [nm] (exp.)
0.1	30.7	17.3
1	9.6	9.1
10	3.1	2.4
100	1.0	1.5

Table 4.3: *Comparison between experimentally and theoretically determined exponential decay lengths for the normal force between a hydrophobic probe and an EG$_3$-containing SAM recorded under KNO$_3$.*

In order to test the hypothesis of a long-range (several nm) *structured* water layer adjacent to the EG$_3$-interface, force-distance measurements were performed under different electrolyte solutions. These experiments targeted to a determination of the influence of various dissolved ions on the resulting force between SFM tip and sample surface.

Both chaotropic as well as kosmotropic ions from the lyotropic series (see Table 4.2) have been employed. While maintaing the same anion, NO$_3^-$, measurements with various

cations were performed in order to investigate their influence on water structure and interaction with the ethylene glycol units of the SAM.
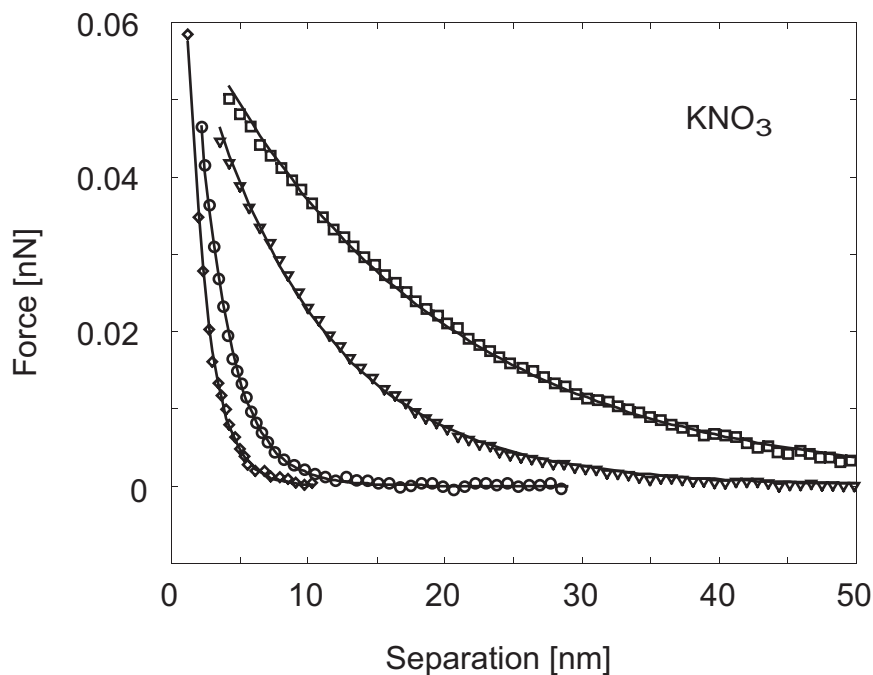

Figure 4.3: *Advancing force-versus-distance curves (averaged) for a hydrophobic probe and an EG₃-OMe-terminated SAM on gold in aqueous LiNO₃ solutions for different concentrations (◇ - 0.1M; ○ - 0.01M; ▽ - 1mM; □ - 0.1mM). The solid lines represent exponential fits to the experimental data.*

Figure 4.3 shows exemplary force-distance curves performed under LiNO₃ solution. The same concentration-dependent interaction behaviour as already recorded for force measurements under KNO₃ solution can be observed. The exponential decay length of the repulsive force decreases with increasing ionic strength and the experimentally determined values for the different decay lengths are again in good agreement with the theoretical values predicted for the Debye length.

Figure 4.4 summarises the experimentally determined decay lengths for the different cations employed, depending on the solution concentration. The results of the force-distance measurements are displayed in slightly different fashion in order to illustrate the experimental decay lengths of the repulsive forces in dependence of the salt concentration and the type of dissolved ion simultaneously. As a guide to the eye, dashed lines are inserted into the diagram to visualise the theoretical values of the Debye length predicted by DLVO theory.

Figure 4.4: *Measured decay lengths for different cations from the Hofmeister series depending on the ionic strength (● - 0.1M; ▲ - 0.01M; ■ - 1mM; ♦ - 0.1mM). Dashed lines correspond to values expected on the basis of the DLVO theory.*

In another series the cation, K$^+$, was maintained constant while the influence of different anions was investigated (see Figure 4.6). Figure 4.5 illustrates exemplarily force-distance measurements in K$_2$SO$_4$ solution. Again, all force-distance curves showed a similar interaction behaviour depending on the ionic strength of the electrolyte solution. Figure 4.6 summarises these force-measurements, displaying the observed decay lengths of the repulsive force curves depending on the ionic strength and the anion dissolved.

For a fixed salt concentration, all different electrolytes show a similar force-distance behaviour as was also observed for the 'standard' KNO$_3$ solution (compare Figure 4.2). As can be seen from Figures 4.4 and 4.6, the experimentally determined values of the decay lengths and the theoretical Debye lengths as predicted by DLVO theory are in reasonable agreement within the error bars for all Hofmeister ions, with the exception of the lowest concentration.
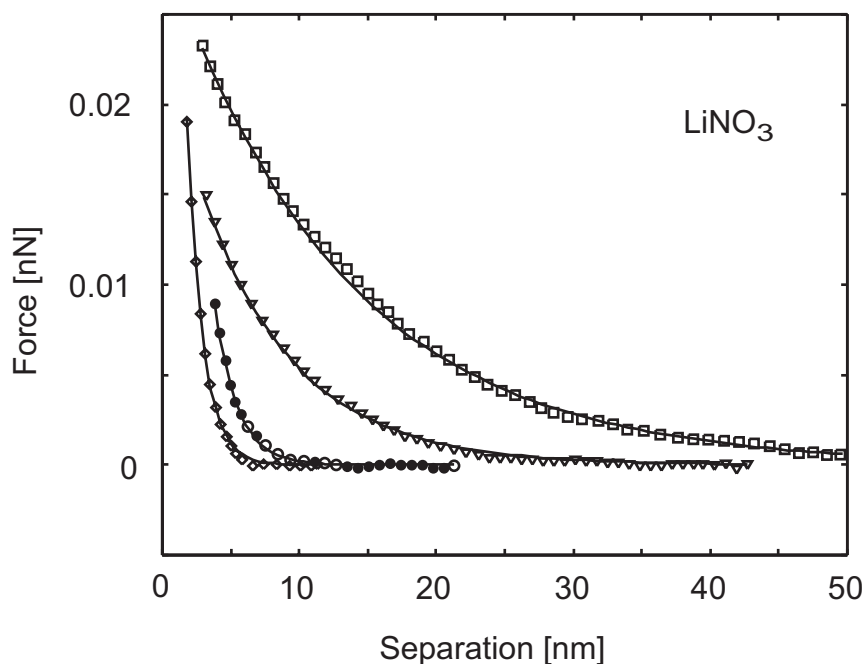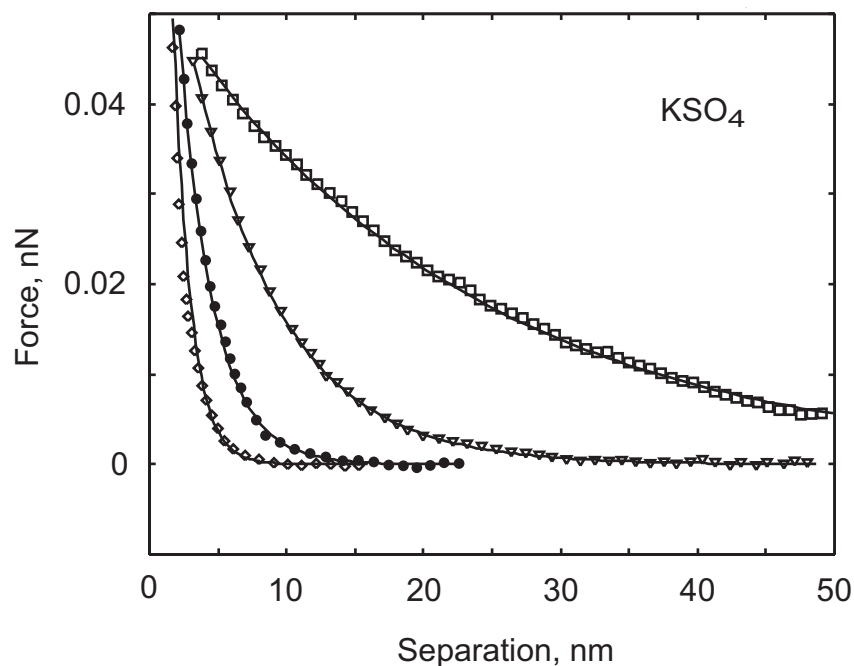
Figure 4.5: *Advancing force-versus-distance curves (averaged) for a hydrophobic probe and an EG$_3$-OMe-terminated SAM on gold in aqueous K$_2$SO$_4$ solutions for different concentrations ($\diamondsuit$ - 0.1M; $\bigcirc$ - 0.01M; ∇ - 1mM; $\square$ - 0.1mM). The solid lines represent exponential fits to the experimental data.*

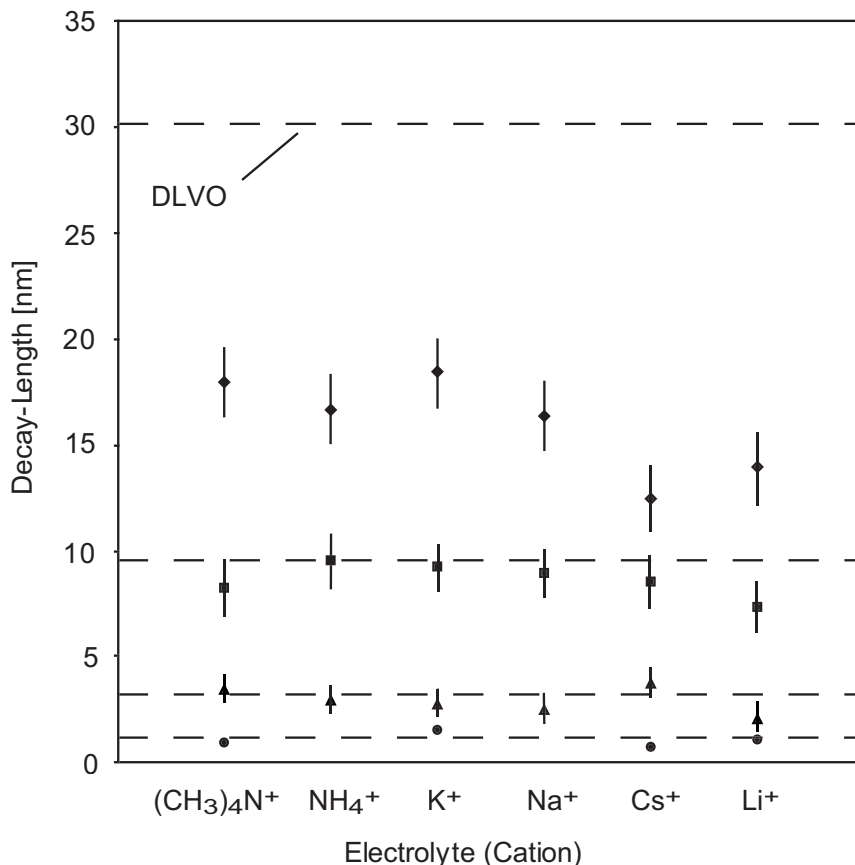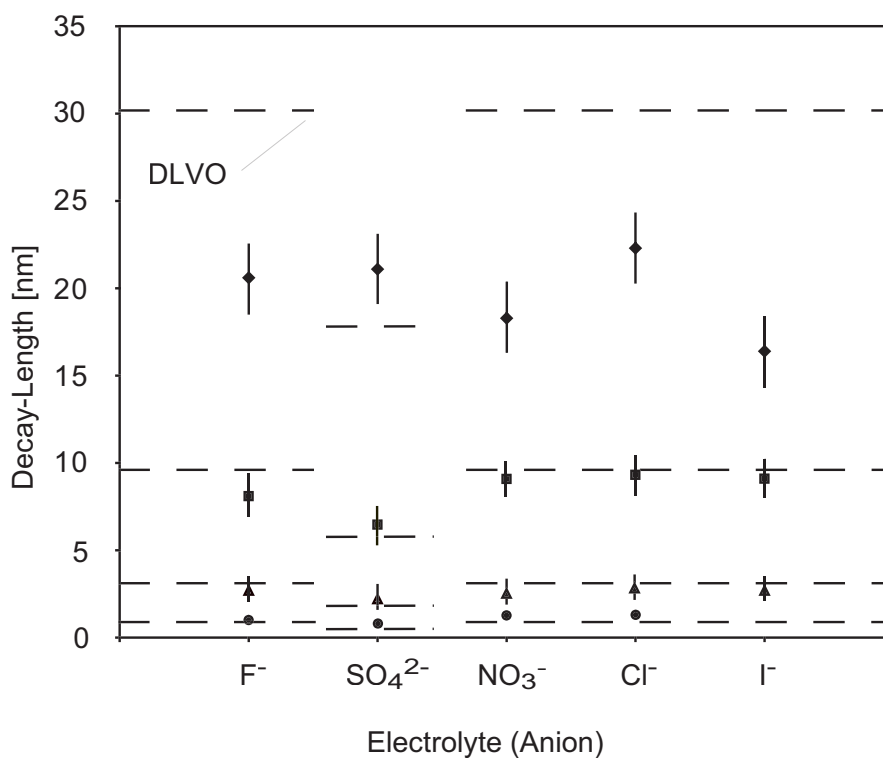***Figure 4.6:*** *Measured decay lengths for different anions from the Hofmeister series depending on the ionic strength ($\bullet$ - 0.1M; $\blacktriangle$ - 0.01M; $\blacksquare$ - 1mM; $\blacklozenge$ - 0.1mM). Dashed lines correspond to values expected on the basis of DLVO theory.*

4.1.4 XPS and ToF-SIMS Analysis

Different cations can have different affinities to the OEG part of the SAM film. The incorporation of cations into the OEG interface might result in a charge separation, and a dipolar field could be established. In order to test the possibility of ion incorporation of some of the cations from electrolyte solution into the OEG tail of the SAM films, additional XPS and ToF-SIMS measurements were performed. After preparation of the EG₃ SAM surface, samples were immersed into 0.01 M solutions of the different electrolytes for 12 hours. Subsequently, the samples were removed and thoroughly rinsed with ultrapure water, dried with nitrogen and immediately introduced into the vacuum chamber. All XPS survey spectra recorded showed the same characteristics as were found for the untreated, freshly prepared sample with the same elemental ratios and species. Besides the prominent peaks of the gold substrate and the carbon as well as the oxygen peaks characteristic for the EG₃-OMe SAM, no additional peaks (compared to the fresh, untreated EG₃ SAM as shown in Figure 2.5) indicative of the various ions dissolved in the electrolytes investigated were observable as can be seen in Figure 4.7.
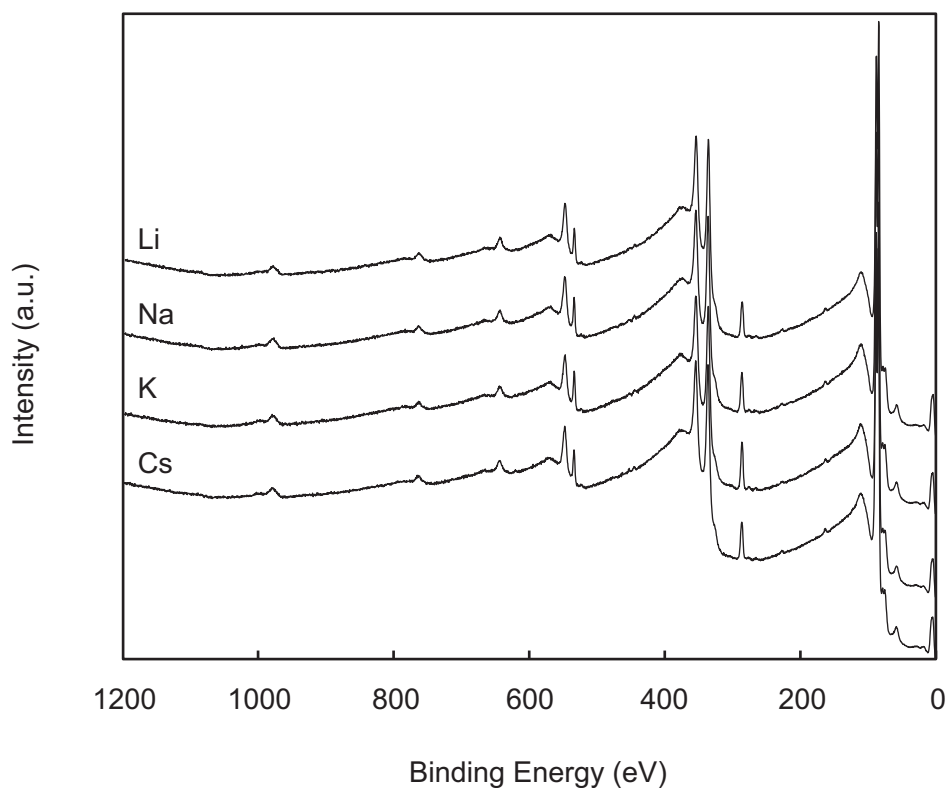
Figure 4.7*: XPS survey spectra of EG₃-OMe-terminated SAMs after immersion into different electrolyte solutions for 12 hours. For peak assignment compare Figure 2.5.*
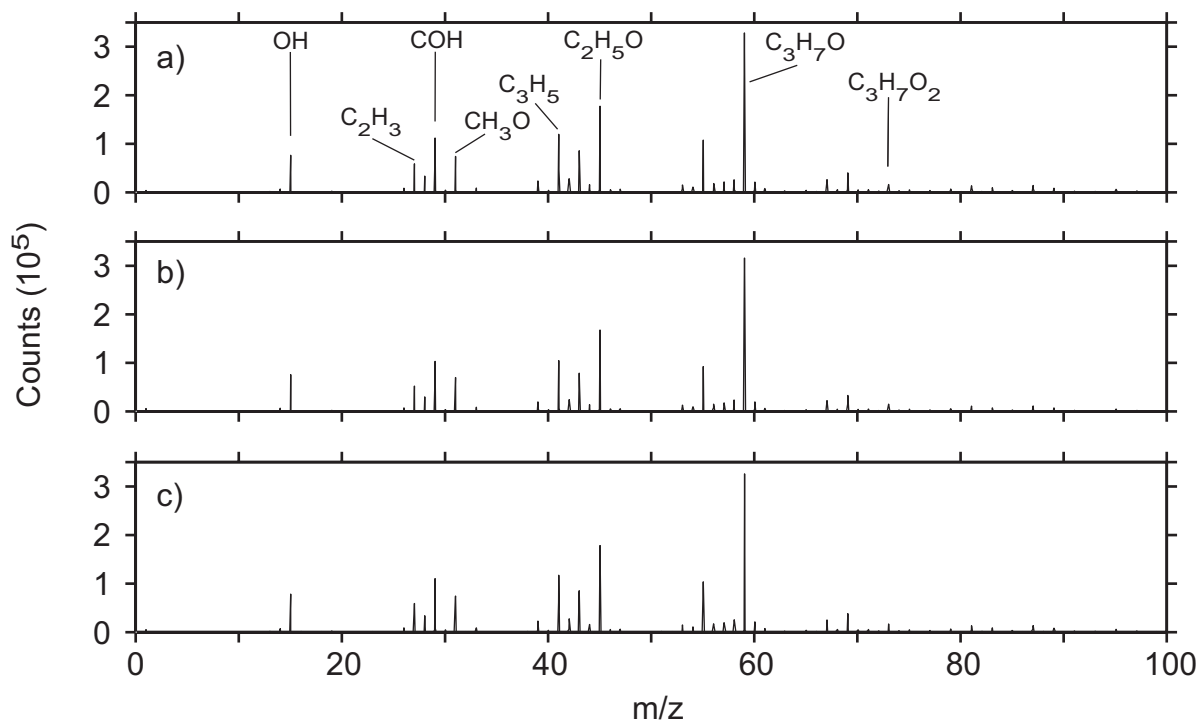
Figure 4.8: *Positive static ToF-SIMS spectra of a) a freshly prepared EG$_3$-OMe SAM, b) an EG$_3$-OMe SAM after 12h exposure to 10mM aqueous KNO$_3$ solution and c) an EG$_3$-OMe SAM after 12h exposure to 10mM aqueous K$_2$SO$_4$ solution. Some of the species related to the SAM are labelled exemplarily.*
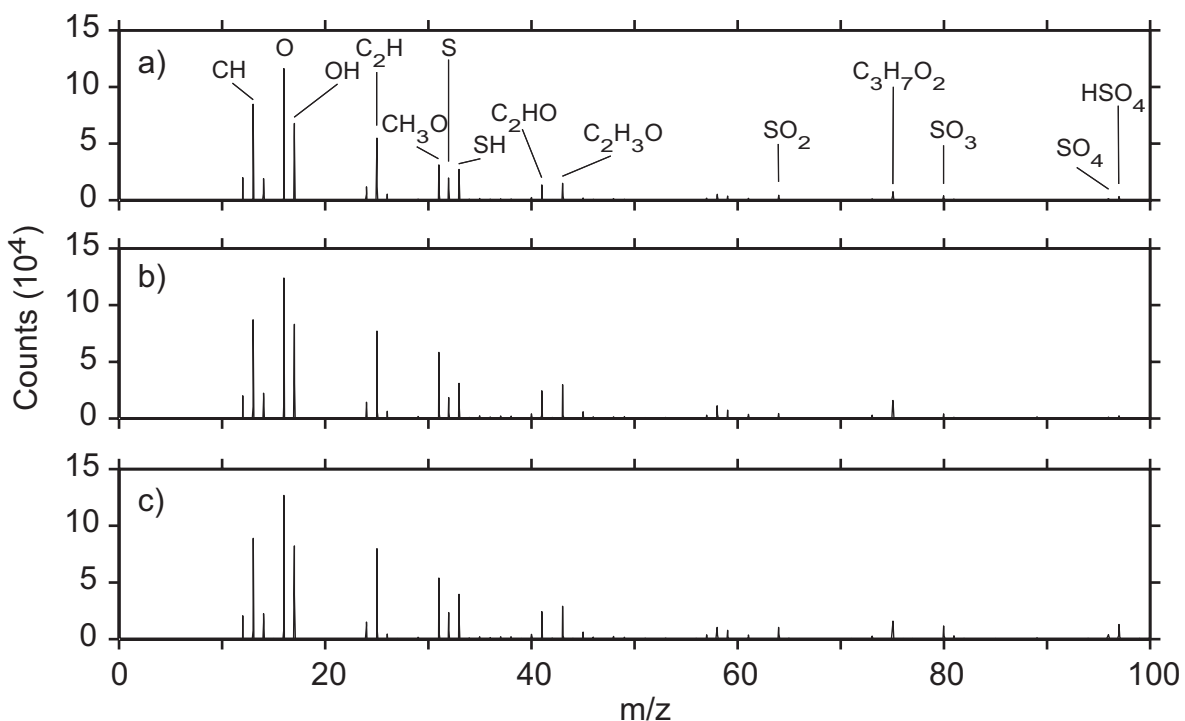
Figure 4.9: *Negative static ToF-SIMS spectra of a) a freshly prepared EG$_3$-OMe SAM, b) an EG$_3$-OMe SAM after 12h exposure to 0.01 M aqueous KNO$_3$ solution and c) an EG$_3$-OMe SAM after 12h exposure to 0.01 M aqueous K$_2$SO$_4$ solution. Note the increase in intensity of the oxysulfur species for the latter. Some species related to the SAM are labelled exemplarily.*

The ToF-SIMS measurements displayed in Figures 4.8 and 4.9 also failed to reveal any indication of a strong affinity between the cations and/or anions and the monolayer film for most of the salts. There was, however, a slight increase in the oxysulfur peaks and the potassium intensity observable after immersion of the films into the corresponding aqueous solution (K$_2$SO$_4$). Figure 4.8 shows the positive mass peaks in the range of 0.2 to 100 amu. Some of the peaks that can be assigned to the alkanethiol SAM are labelled with the corresponding fragments. Negative SIMS spectra acquired in the mass range of 3 to 100 amu are displayed in Figure 4.9. No evidence for specific complexation of cations with the EG entities was found.

4.2 Discussion

The measurements described above were performed in order to explore the influence of different ions from the Hofmeister series on the repulsive interaction between hydrophobic probes and OEG-terminated monolayer films. The interactions in electrolyte solutions are mediated by water. Cosolutes can influence both the structure of the liquid and the surfaces of the solids by specific adsorption or dissociation processes [26-29,32-34].

The reference measurement displayed in Figure 4.1shows an attractive interaction between two methyl-terminated alkanethiol monolayers at pH ~6, independent of the ion concentration of the solution. The observed force-distance curves resemble those published in the literature for the same system and reflect a 'typical hydrophobic' interaction [25]. Replacement of the hydrophobic film on the gold substrate by an EG$_3$-OMe-terminated film, however, results in a completely different interaction. A repulsive force, strongly dependent on ion concentration, was found under KNO$_3$ solution, as was reported earlier [22].

Replacing the - according to the Hofmeister series - 'neutral' K$^+$ ion in the electrolyte by more kosmotropic ions such as NH$_4$$^+$ and N(CH$_3$)$_4$$^+$, which are supposed to be water structure breaking, or by more chaotropic ions such as Cs$^+$ and Li$^+$, which are considered to be structure-supporting, resulted in very similar force-distance curves to those observed under KNO$_3$, showing a strong dependence on ionic strength. Fitting exponential curves to the experimental data revealed decay lengths very close to those expected on the basis of DLVO theory, except for the lowest concentration. Accordingly, there is no clear trend observable for

the measured decay lengths within the Hofmeister series for constant ionic strength from Figure 4.4. A similar observation was made for the different anions investigated. The determined decay lengths displayed in Figure 4.6 do not show a clear trend with increasing chaotropic or kosmotropic character.

In case of a pronounced network of organised water molecules at the interface between organic surface and bulk electrolyte, different ions from the Hofmeister series are expected to have a different effect on the *order profile* of the network, which should reflect itself in the observed force profile and especially the range of the repulsive interaction. Addition of polar kosmotropes to the electrolyte should break an extended water structure more efficiently than chaotropic ions and reduce the range of the repulsion experienced by the AFM tip for a fixed ionic strength, if it is due to an order profile. However, as evidenced by Figures 4.4 and 4.6, no clear trend can be identified in our experiments within the experimental error bars. Instead, a typical DLVO-like behaviour was observed, independent of the type of ion, with the exception of the lowest concentration. For higher concentrations the repulsive force between the C_{16}-probe and the EG_3-OMe-coated sample surface strongly depends on the ion concentration and scales approximately with the Debye length. We interpret this as a strong hint for a significant electrostatic contribution to the interaction force between the hydrophobic probe and the EG_3-OMe-terminated gold surface, suggesting that there is no long-range (>2 nm), highly ordered water interface.

A final answer for the deviation of the force from standard DLVO behaviour in case of the solutions with lowest ionic strength cannot be given. It has been reported in the literature, however, that for such low concentrations and low surface charging an additional attractive component is expected in colloidal systems [35]. The latter is due to an increase in ion concentration between the two surfaces when approaching each other [36]. This effect might also be responsible for the consistently observed shorter decay lengths in our system.

The origin of the charges in case of an electrostatic interaction, however, remains to be resolved. It has recently been reported that hydrophobic alkanethiol films on gold display a negative zeta potential in electrolyte solution at neutral pH-values and below [37]. Our probe will similarly acquire a negative charge. Consequently, the OEG-terminated films must be also negatively charged, because a repulsive interaction was observed. The charge density can be estimated to be on the order of -0.05 C/m^2, based on our experiments described in [22].

Since the observed interaction appears to be of electrostatic nature, the question arises if there is some contribution from a specific interaction between certain cations and the OEG tails. An incorporation of ions into the OEG tails, for instance, might lead to an effective charge separation and result in a dipolar field. In such a case a 'high' surface charge density should be established for ions with higher affinity to the EG strands, in contrast to those, that do not show any preferred reaction with EG units. A possible complexation should then reflect itself in higher absolute force values between probe and surface.

All probes were prepared following an identical procedure described in Chapter 2. Therefore it appears reasonable to assume that all force constants are affected similarly by the functionalisation process. However, for a fixed ion concentration, the force curves showed values within the same order of magnitude for all different ions (see Figures 4.2 to 4.6). Strongly hydrated cations such as Li$^+$ and Na$^+$ which can complex with EG units [10,38,39], showed no hint of any specific interaction with the EG tails by displaying significantly higher repulsive force values within our limited resolution. As a consequence, it seems unlikely that ion binding and the specific interaction with ions play a major role for the observed interaction. This is supported by the X-ray photoelectron spectroscopy and ToF-SIMS analysis. These measurements did not show a clear indication of an irreversible ion incorporation into the films, supporting that specific adsorption or coordination of various ions to the ethylene glycol tail do not play a major role. However, difficulties in detecting salt ions in these systems with XPS have been reported earlier [21,40]. The ions are removed during the rinsing process with high probability. It should also been borne in mind that both XPS and ToF-SIMS measurements were performed under vacuum conditions, while the interaction was probed under aqueous solution. However, a strong and irreversible interaction between the ions and the organic film seems unlikely at least.

A possible complexation between the EG units and a cation requires a certain amount of space, which might not be available in the densely packed SAMs. There will be, however, defects in the films, which create less densely packed regions where ions might preferentially interact with the film and the substrate. This view is supported by the ToF-SIMS measurements, where no ions except traces of oxysulfur related species and the counterion were found in the films, which we attribute to the high affinity of the sulfur to the gold and a penetration of the ions into the film. This is most likely to occur at defect sites and has been reported in previous SIMS studies [41-43].

The origin of the effective negative charge, however, cannot be assigned to the ions from the salt dissolved in the solution, since no difference was observed for different electrolytes. In addition, methyl-terminated alkanethiol films are also not free of defects. If adsorbing ions from the electrolyte were responsible for the charging, this effect should have also been observable for the pure hexadecanethiol films. In that case, the ion concentration should have had a similar effect on the force-distance curves of the 'reference system' to that observed for the EG films.

So far, a final explanation for the effective negative charge that appears to be established at the EG_3 interface cannot be derived from the results presented above. It is possible, however, that the conformation of the OEG strands in connection with water is responsible for it. The charges obviously associated with the EG_3-terminated monolayer might, for instance, be due to the interaction of hydroxyl and/or hydronium ions with the EG_3 interface as the autoprotolysis equilibrium of water is altered by the ethylene glycol entities at the top of the SAM. Another possible explanation for the observed charge might be found in a preferential orientation of the water molecules in the OEG tail of the synthetic organic surface. It has recently been reported that weakly interacting interfacial water molecules can be oriented by interactions with an organic phase [44]. A similar effect might play a central role in the observed interaction here.

The studies described in this chapter underline the strong interaction between ethylene glycol units and water and its importance for the resulting chemical and physical properties of the monolayer films. The observed repulsive force appears to be mainly of electrostatic nature and is in urgent need of further investigation. The described interaction is also likely to play also some role in the protein-repelling properties of EG-terminated films. Additionally, a water interface of lower density as has been suggested earlier could also contribute to the overall repulsive behaviour. Also a short-range structured water interface (<2 nm) cannot be excluded. A long-range *structured* water interface or a specific interaction of ions with the OEG tails, however, appear to be less important.

4.3 Conclusions

Force-versus-distance measurements between OEG-containing self-assembled monolayer films and hydrophobic probes were performed under different electrolyte solutions and for varying ionic strength. The force curves showed no indication of a long-range (>2 nm) order profile due to a *structured* water interface or a preferred 'reaction' with or higher affinity of some of the cations to the ethylene glycol interface. The latter is supported by additional XPS and ToF-SIMS analysis. Instead, it appears that a significant electrostatic component is involved in the repulsive interaction observed. From the force measurements performed so far, the effective negative surface charge established on the OEG SAM might be due to oriented water molecules and/or the interaction with hydroxyl and hydronium ions from solution.

4.4 Literature

[1] Harder P.; Grunze, M.; Dahint, R.; Whitesides, G. M.; Laibinis P. E. *J. Phys. Chem. B* **1998**, *102*, 426

[2] Zolk, M.; Eisert, F.; Pipper, J.; Herrwerth, S.; Eck, W.; Buck, M. Grunze, M. *Langmuir* **2000**, *14*, 5849

[3] Ide, M. I.; Yoshikawa, D.; Maeda, Y.; Kitano, H. *Langmuir* **1999**, *15*, 926

[4] Dreesen, L.; Humpert, C.; Hollander, P.; Mani, A. A.; Ataka, K.; Thiru, P. A.; Peremans, A *Chem. Phys. Lett.* **2001**, *333*, 327

[5] Huang, L.; Nishinari, K. *J. Polymer Sci. Part B* **2001**, *39*, 496

[6] Kjellander, R.; Florin, E. *J. Chem. Soc. Faraday Trans* **1981**, *77*, 2053

[7] Caldararu, H.; Caragheorheopol, A.; Schlick, S. *Bull. Pol. Acad. Sc. Chem.* **2000**, *48*, 367

[8] Wang, R. L. C.; Kreuzer, H. J.; Grunze, M. *J. Phys. Chem. B* **1997**, *101*, 9767

[9] Kokkoli, E.; Zukoski, C. F. *Langmuir* **1998**, *14*, 1189

[10] Johansson, P.; Shridhar, P. G.; Tegenfeldt, J.; Lindgren, J. *Solid State Ionics* **1996**, *86-88*, 297

[11] Spevacek, J.; Dybal, J. *Macromol. Rapid Commun.* **1999**, *20*, 435

[12] Banka, P. A.; Selser, J. C.; Wang, B.; Shenoy, D. K.; Martin, R. *Macromolecules* **1996**, *29*, 3956

[13] MacGlashan, G. S.; Andreev, Y. G.; Bruce, P. G. *Nature* **1999**, *398*, 792

[14] Annis, B. K.; Kim, M.-H.; Wignall, G. D.; Borodin, O; Smith, G. D. *Macromolecules* **2000**, *33*, 7544

[15] Harris, J. M.; Hundley, N. H.; Shannon, T. G.; Struck,E. C. in *Crown Ethers and Phase-Transfer Catalysis in Polymer Science*; Mathias, L.; Carreher, C. E. Eds., Plenum: New York, **1984**, 371

[16] Bandyopadhyay, K.; Liu, H.; Liu, S.-G.; Echegoyen, L. *Chem. Commun.* **2000**, 141

[17] Liu, H.; Liu, S.; Echegoyen, L. *Chem. Commun.* **1999**, 1493

[18] Flink, S.; van Veggel, F. C. J. M.; Reinhoudt, D. N. *J. Phys. Chem B* **1999**, *103*, 6515

[19] Manege, L. C.; Takayanagi, T. Oshima, M.; Iwachido, T.; Motomizu, S. *Bull. Chem. Soc. Jpn.* **1999**, *72*, 1301

[20] Talanova, G. G.; Elkarim, N. S. A.; Talanov, V. S.; Hanes, R. E.; Hwang, H.-S.; Bartsch, R. A.; Rogers, R. D. *J. Am. Chem. Soc.* **1999**, *121*, 11281

[21] Clark, S. L.; Montague, M. F.; Hammond, P. T. in *Organic Thin Films, ACS Symp. Ser. 695* **1997**, Chapter 15

[22] Feldman, K.; Hähner, G.; Spencer, N. D.; Harder, P.; Grunze, M. *J. Am. Chem. Soc.* **1999**, *121*, 10134

[23] Hofmeister, F. *Arch. Exp. Natur. Pharmakol.* **1888**, *24*, 247

[24] Hofmeister, F. *Arch. Exp. Natur. Pharmakol.* **1890**, *27*, 395

[25] Israelachvili, J. *Intermolecular and Surface Forces*, 2nd ed., Academic Press: San Diego, CA, **1992**

[26] Napper, D. H. *J. Colloid Interface Sci.* **1970**, *33*, 384

[27] Collins, K. D.; Washabaugh, M. W. *Quart. Rev. Biophys.* **1985**, *18*, 323

[28] Cacace, M. G.; Landau, E. M.; Ramsden, J. J. *Quart. Rev. Biophys.* **1997**, *30*, 241

[29] Vogler, E. A. *Adv. Colloid Interface Sci.* **1998**, *74*, 69

[30] v. d. Vegte, E. W.; Hadziioannou, G. *J. Phys.Chem. B* **1997**, *101*, 9563

[31] Vezenov, D. V.; Noy, A.; Rozsnyai, L. F.; Lieber, C. M. *J. Am. Chem. Soc.* **1997**, *119*, 2006

[32] Franks, F. *Water: a matrix of life,* 2nd ed., Cambridge: Royal Society of Chemistry, **2000**

[33] Klose, M. *Wasser: Struktur und Dynamik*, Berlin: Akademie Verlag, **1986**

[34] Vogler, E. A. *J. Biomater. Sci. Polymer Ed.* **1999**, *10*, 1015

[35] Knott, M.; Ford, I. *J. Phys Rev. E* **2001**, *6303*, 1403

[36] Knott, M. *J. Phys Rev. E* **2002**, *65*, 061401

[37] Schweiss, R.; Welzel, P. B.; Werner, C.; Knoll, W. *Langmuir* **2001**, *17*, 4304

[38] Rogers, R. D.; Bauer, C. B. *J. Chromatogr. B* **1996**, *680*, 237

[39] MacGlashan, G. S.; Andreev, Y. G.; Bruce, P. G. *Nature* **1999**, *398*, 792

[40] Lvov, Y. M.; Decher, G. *Crystallography Reports* **1994**, *39*, 628

[41] Hutt, D. A.; Cooper, E.; Leggett, G. J. *J. Phys. Chem. B* **1998**, *1*,174

[42] Cooper, E.; Leggett, G. J. *Langmuir,* **1998**, *14*, 4795

[43] Rading, D.; Kersting, R.; Benninghoven, A. *J. Vac. Sci. Technol. A* **2000**, *18*, 312

[44] Scatena, L.F.; Brown, M.G.; Richmond, G.L. *Science* **2001**, *292*, 908

Chapter 5

Force-Distance Analysis on Tri(Ethylene Glycol)-terminated Self-Assembled Monolayers, Part 2[*]

In the previous chapters it has been shown that the EG_3-OMe-terminated SAMs establish a net negative surface charge under aqueous solution. This effective surface charge density is responsible for the observed DLVO-like interaction forces towards the hydrophobic SFM probes. The interaction of the EG entities with water has been found to be strongly dependent on the conformation of the EG strands. It has been suggested that water molecules in the interfacial surface region are associated to the alcohol and ethylene oxygens via hydrogen bonding [1]. Because of the dense and highly ordered SAM film an overall average orientation of the water molecules was proposed leading to an effective surface dipole moment [2,3]. Continuing the study on the influence of different salts on this interfacial water structure presented in the previous chapter, this chapter focuses on possible effects of pH-value of the electrolyte solution.

It is known that interfacial water can be highly ordered in comparison to bulk water [4]. The particular structure depends on the prevailing pH [4,5]. Ionic strength, charges and pH-value have all been shown to exert a crucial influence on interfacial water structures [6]. In their vibrational study of water at hydrophobic surfaces, Richmond and coworkers have shown that the pH-value of an aqueous solution is a crucial parameter in the orientation of water molecules at an organic surface [7]. Upon changing pH from very low to very high values they have observed a "flip" in orientation of about 180° for these interfacial water

---

molecules at a hydrophobic surface, which they have assigned to a change in interfacial potential caused by a change in interfacial OH⁻ concentration. They stress weakly hydrogen bonded water molecules in the interfacial region of the hydrocarbon/water system, while other studies point out the strong interaction of water with the oxygen atoms in the ethylene glycol entities, which act as hydrogen bond acceptors [7-10]. In another study utilising streaming potential as well as streaming current measurements, the preferential adsorption of H_3O^+ and OH⁻ ions, respectively, on methyl- and carboxyl-terminated self-assembled monolayers on gold under strange pH conditions is also stressed [11,12].

Applying these concepts of hydrogen bonded interfacial water molecules on the one hand and preferential adsorption of hydroxyl and/or hydronium ions on the other to the interpretation of the interaction of water with OEG-terminated SAMs turns out to be a useful approach for understanding the driving force for protein resistance of synthetic surfaces.

Apart from the pH-value of the electrolyte solution, the influence of another parameter has been investigated in order to study the mechanism of charge establishment in some more detail. So far, only hydrophobically functionalised SFM probes have been utilised to mimic proteins approaching a surface, because they have proven to be very effective in previous studies [1]. However, besides hydrophobic patches, proteins also exhibit locally charged structures. Thus, in this chapter, additional force-distance measurements have been performed utilising oxidised Si_3N_4 probes (referred to below as SiO_x-probes) and alumina-coated Si_3N_4 probes (referred to below as AlO_x-probes), which establish net surface charges in response to the pH-value of the surrounding solution. In this way, the effect of sign of charge on the interaction could be explored.

5.1 Results

5.1.1 Concentration-Dependence of Force at Constant pH

Commercially available oxide-sharpened silicon nitride probes were used for force spectroscopy measurements on an EG_3-OMe sample under aqueous KNO_3 solution at a constant (neutral) pH-value. Tips have been exposed to oxygen plasma in order to enhance the native oxide layer. Before use they have been cleaned and 'hydroxylised', respectively, in

piranha solution. The isoelectric point (IEP) of Si_3N_4-probes typically varies between 5.5 and 7 [13], depending on the history of the tips and the amount of oxide present. The IEP of SiO_2 has been reported as being around 2 [14]. Hence, for oxidised Si_3N_4-tips, the isoelectric point decreases to values between 3.5 and 5 [15]. The pH-value of the electrolyte solution was adjusted to a pH ~5.8 according a procedure described in Chapter 3. Similar values for such aqueous solutions are reported in the literature [16]. At this pH-value, SiO_x-probes are known to establish a net negative surface charge [13].

Force-versus-distance curves have again been recorded with DI's 'force-volume' software at a cycle frequency of ~0.5 Hz averaging at least 64 force curves per sample. According to Chapter 3, errors in the decay lengths of the repulsive forces observed in the curves have been calculated to be well below 20% [2]. In general, errors in the normal force within a single force curve due to noise did not exceed 0.01 nN [2].

Figure 5.1: *Advancing force-versus-distance curves (averaged) measured with a (negatively charged) SiO_x-probe on an EG₃-OMe SAM on gold in aqueous KNO_3 solution at different concentrations and constant pH ~5.8.*

Figure 5.1 shows averaged force-versus-distance curves at salt concentrations ranging from 0.1 mM to 0.1 M. At the lowest concentration of 0.1 mM, which was introduced into the liquid cell first, there is a long-range repulsive force with exponential behaviour detectable.

The decay length of this force is 11.2 nm, determined by fitting an exponential to the experimental data [2]. For an ionic strength of 1 mM, the repulsive force shows a decay length of 7.7 nm. Increasing the ionic strength further to 0.01 M reduces the decay length of the repulsive force even more to 2.8 nm. At the highest salt concentration (0.1 M) introduced into the liquid cell, a short-range repulsive interaction is detectable featuring a decay length of 1.1 nm.

In a next step, the sign of the probe's surface charge was changed in order to probe the electrostatic properties of the organic film independently. This was realised by coating the tip with an amorphous alumina layer. The isoelectric point of such AlO_x-tips is typically found to be around ~9 [14]. Literature values for the IEP of alumina surfaces vary between 8 and 10 [14,17], but values as low as 6.7 have also been reported [18]. In consequence, these tips carry a net positive surface charge at pH ~5.8 [14,17].
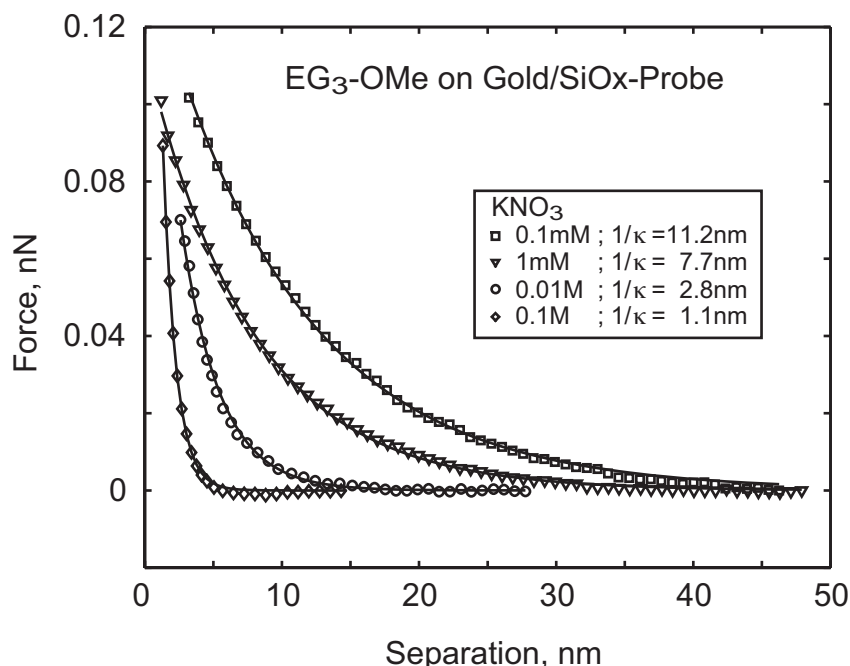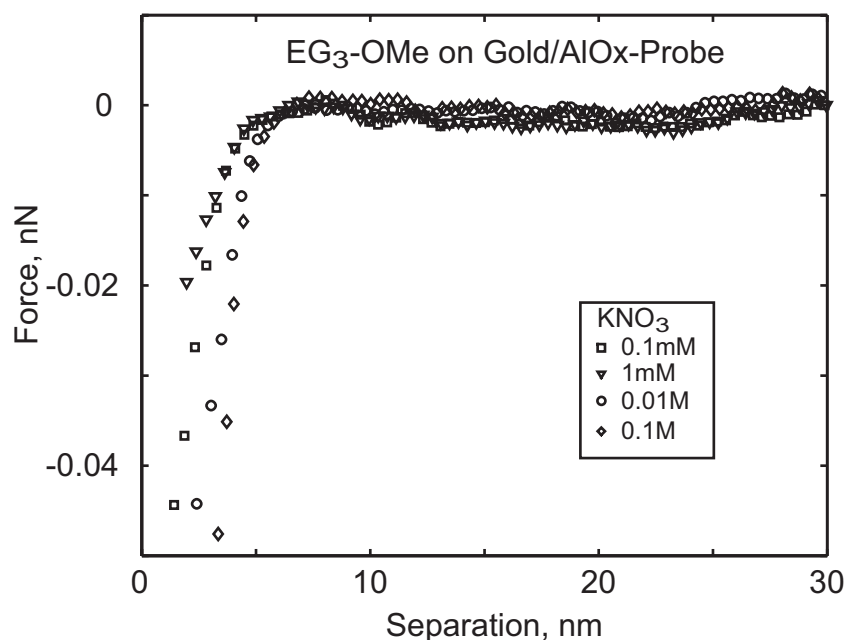

Figure 5.2: *Advancing force-versus-distance curves (averaged) measured with a (positively charged) AlO_x-probe on an EG_3-OMe SAM on gold in aqueous KNO_3 solution at different concentrations and constant pH ~5.8.*

Using these probes, force-versus-distance measurements were recorded utilising the same experimental set up as described before. The corresponding force curves are displayed in Figure 5.2. Over the whole range of ionic strengths explored in the electrolyte solution, no long-range repulsive interaction was detectable between the EG_3-OMe-terminated gold sample and the positively charged alumina SFM-probe. Instead, all force curves show an

attractive interaction of constant range lacking a significant dependence on the ionic strength of the aqueous salt solution.

In another measurement we changed the properties of the AFM probe again keeping all the other parameters (such as sample functionalisation, electrolyte solution, pH-value and range of salt concentrations, etc.) constant. After utilising charged tips with both negative and positive surface charge, a hydrophobically functionalised probe was chosen to perform force-distance measurements on this system.
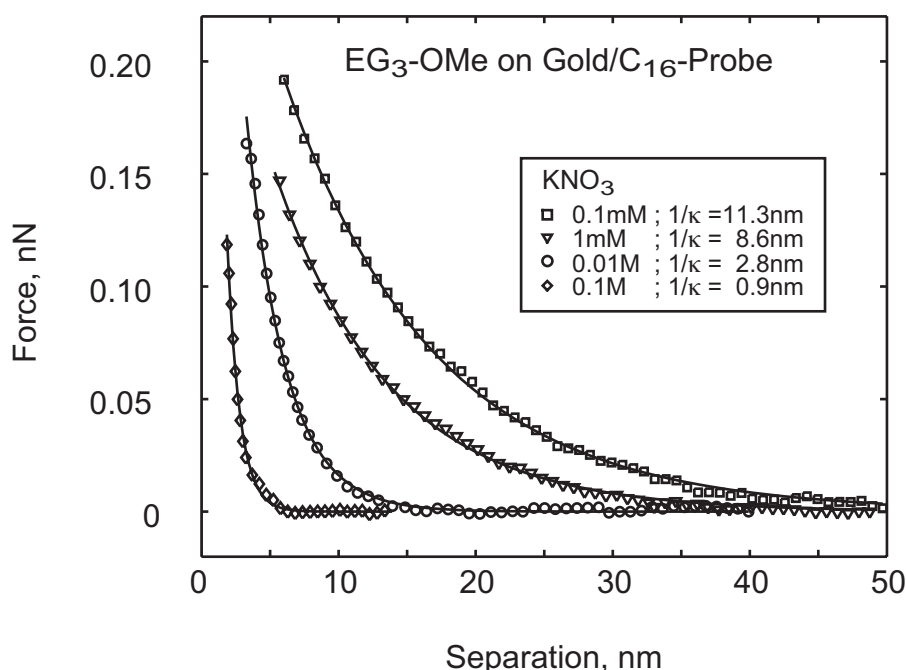
Figure 5.3: *Advancing force-versus-distance curves (averaged) measured with a (hydrophobic) C$_{16}$-probe on an EG$_3$-OMe SAM on gold in aqueous KNO$_3$ solution at different concentrations and constant pH ~5.8.*

Force measurements with hydrophobic probes on EG$_3$ films depending on the ionic strength and the type of electrolyte have been already discussed in Chapter 4 [2]. Figure 5.3 exemplarily displays the interaction forces between the EG$_3$-OMe sample and a hydrophobic C$_{16}$-probe at different salt concentrations. Again, the solution with the lowest ionic strength (0.1 mM) was introduced first. A repulsive force with an exponential decay length of 11.3 nm as is plotted in Figure 5.3 was observed. Subsequently, the ionic strength of the aqueous solution was increased stepwise by factors of ten. This resulted in a subsequent decrease in decay length of the repulsive force. At 1 mM, the decay length of the repulsive force was

found to be 8.6 nm. A decay length of 2.8 nm can be observed in case of the 0.01 M solution. Finally, for the highest introduced ionic strength a decay length of 0.9 nm was calculated. As discussed in the previous chapters, this concentration-dependent interaction resembles a typical DLVO-like behaviour with both surfaces involved in the interaction carrying similar charges [2,19].
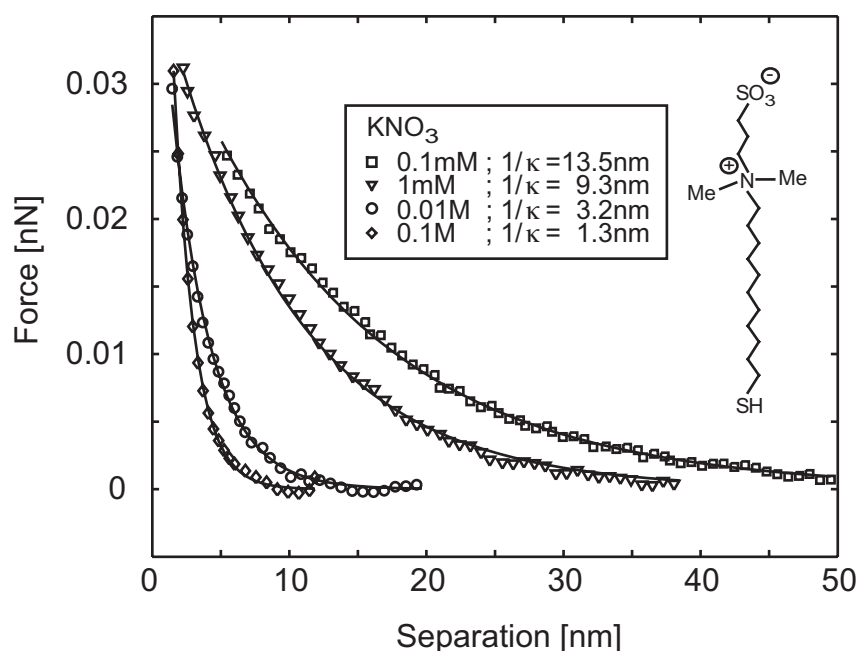
Figure 5.4: *Advancing force-versus-distance curves (averaged) measured with a (hydrophobic) C_{16}-probe on a SAM containing an inner salt on gold in aqueous KNO_3 solution at different concentrations and constant pH ~5.8. The inset illustrates the structure of the molecule.*

In addition, force-distance measurements for a different sample system have been performed, in order to compare the interaction behaviour observed for the OEG-containing SAMs with a SAM featuring a permanent static dipole moment. The orientation of the dipole moment is arranged normal to the surface in a way that the negative charge faces the SAM/water interface. In Figure 5.4, the chemical structure of 11-(Mercapto-N,N-dimethyl-N-3-sulfopropyl)-1-undecanaminium is illustrated. The recorded force-versus-distance curves displayed in Figure 5.4 show a concentration-dependent, exponentially decaying repulsive force. At the lowest concentration of 0.1 mM introduced into the liquid cell, a decay length of 13.5 nm has been observed. Increasing the ionic strength by a factor of ten to 1 mM has resulted in a lower value for the decay length of 9.3 nm. For a salt concentration of 0.01 M a further decrease in decay length to 3.2 nm can be observed. For the highest ion concentration

(0.1 M) investigated a value of 1.3 nm has been detected. This interaction behaviour is in very good agreement with the concentration-dependent force measurements performed on the OEG-containing SAMs described above.

Force measurements have also been performed on the symmetric C$_{16}$/C$_{16}$ system. Both the interaction at neutral pH of ~5.8 and at high and constant pH of ~9.5 have been studied depending on the ionic strength. While the force at pH ~6 showed no dependence on ion concentration (as already discussed in the Chapter 4) the force at pH ~9.5 exhibits a strong dependence on the solution's ionic strength similar to the EG$_3$ systems described above and therefore corroborates the electrostatic nature of the interaction force (see Figure 5.5).
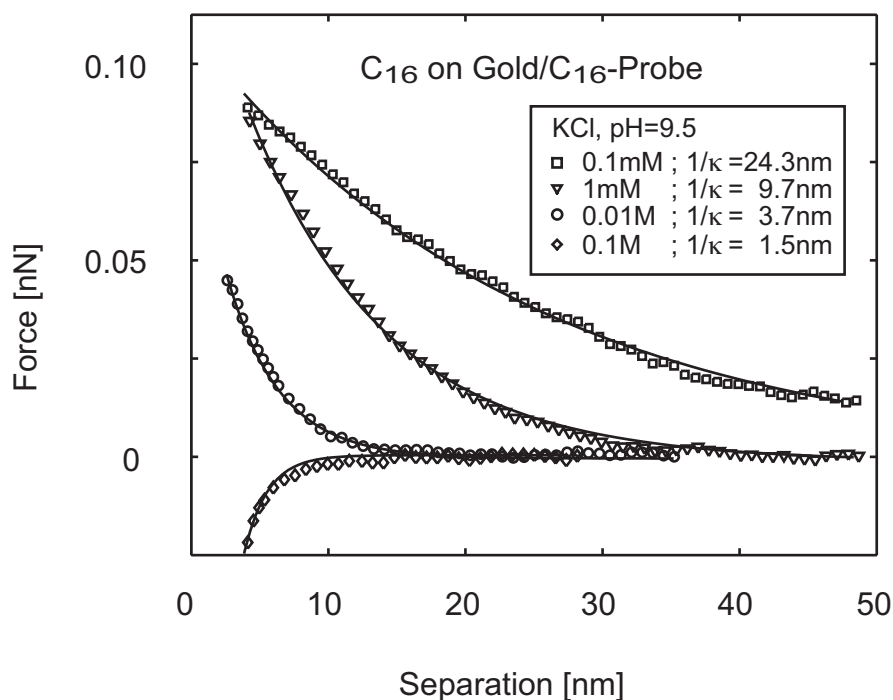
Figure 5.5: Advancing force-versus-distance curves (averaged) measured with a C$_{16}$-probe on a C$_{16}$ SAM on polycrystalline gold in aqueous KNO$_3$ solution at different concentrations and constant pH ~9.5.

5.1.2 pH-Dependence of Force at Constant Ionic Strength

In order to scrutinise the type and origin of the observed repulsive force, the pH-value of the electrolyte solution was varied systematically. Keeping the ionic strength of the aqueous KCl solution at a constant level of 1 mM during these measurements, the pH-value was varied by addition of 1 mM KOH for the alkaline range and 1 mM HCl for more acidic

conditions, respectively. pH-values between pH ~3.5 and pH ~10 could easily be adjusted this way. The measurement cycles were started with the 'standard' pH ~5.8 without any addition of KOH or HCl. The pH-value was then reduced to acidic values. Subsequently, the neutral starting value was set up again and a test measurement was made to check for any possible film instabilities. All films showed reproducible results at this value. The pH-value was then increased to the more alkaline regime. Finally, another control measurement with the standard pH-value was performed for a further check, which again confirmed good reproducibility of the data and stability of the monolayer films.

Figure 5.6: *Advancing force-versus-distance curves (averaged) measured with a SiO_x-probe on an EG_3-OMe SAM on gold in aqueous KCl solution at varying pH-values and constant concentration of 1mM.*

Figure 5.6 displays the pH-dependent force-distance measurements with a SiO_x-tip recorded on an EG_3-OMe sample. Aqueous KCl solution at a constant ionic strength of 1 mM was used as electrolyte. 1mM HCl and 1mM KOH were used to adjust acidic and alkaline conditions ranging from pH ~3.5 to pH ~10. All interaction forces found for pH-values above 4.9 are repulsive and of long range. The two lowest pH-values (3.9 and 4.4) only display attractive forces. Here, the sign of the interaction force changes, and the interaction turns to attractive. The repulsive curves all show comparable absolute values of the normal force and, of course, similar decay lengths due to the constant ionic strength of the electrolyte solution.

Performing pH-dependent force-distance measurements with the AlO$_x$-probe at constant ionic strength of 1 mM, a different interaction behaviour can be observed from Figure 5.7. For high pH-values (8.3 and 9.8), the probe experiences a long-range repulsion of about 10 nm. All other force curves recorded at lower and more acidic pH-values indicate attractive interactions close to the sample surface with a similar shape.

Figure 5.7: *Advancing force-versus-distance curves (averaged) measured with an AlO$_x$-probe on an EG₃-OMe SAM on gold in aqueous KCl solution at varying pH-values and constant concentration of 1mM.*

Using a hydrophobic C₁₆-probe with the same pH-dependent experimental setup, additional force-versus distance measurements have been acquired. Figure 5.8 displays the corresponding force curves. Long-range repulsive forces for pH-values above 4.2 are observed. An attractive interaction can be found solely for the lowest and most acidic value at pH ~3.6. It is also noteworthy that the absolute value of the repulsive force at a distance close to the sample surface is maximal at the highest pH-value and decreases successively with lower hydroxyl ion concentration until the interaction force finally becomes attractive, i.e., there is a gradual transition from repulsion to attraction.

The influence of the terminating methoxy group at the top of the EG₃ SAM has also been investigated by additional pH-dependent force measurements on a chemically very similar system.
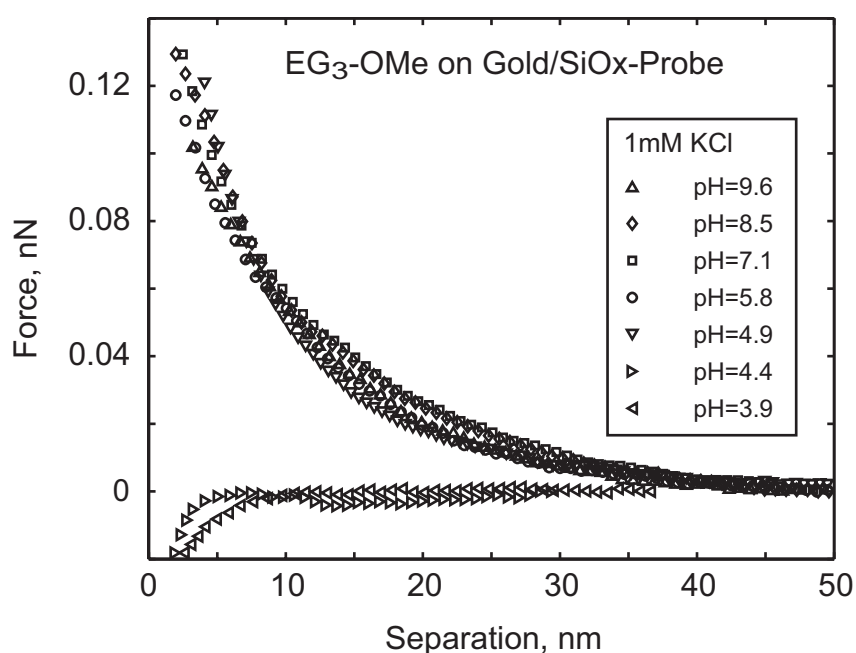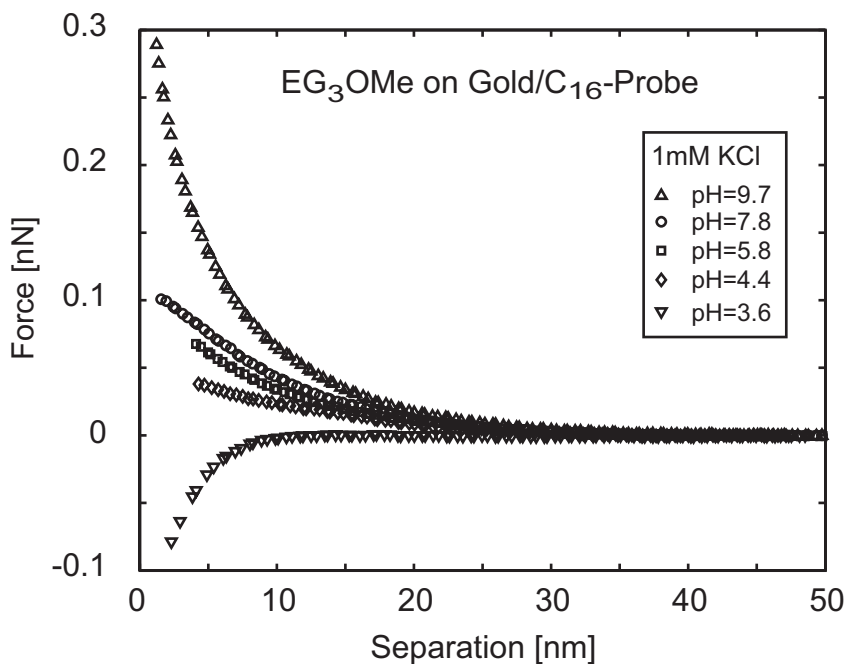
Figure 5.8: *Advancing force-versus-distance curves (averaged) measured with a hydrophobic C₁₆-probe on an EG₃-OMe SAM on gold in aqueous KCl solution at varying pH-values and constant concentration of 1mM.*
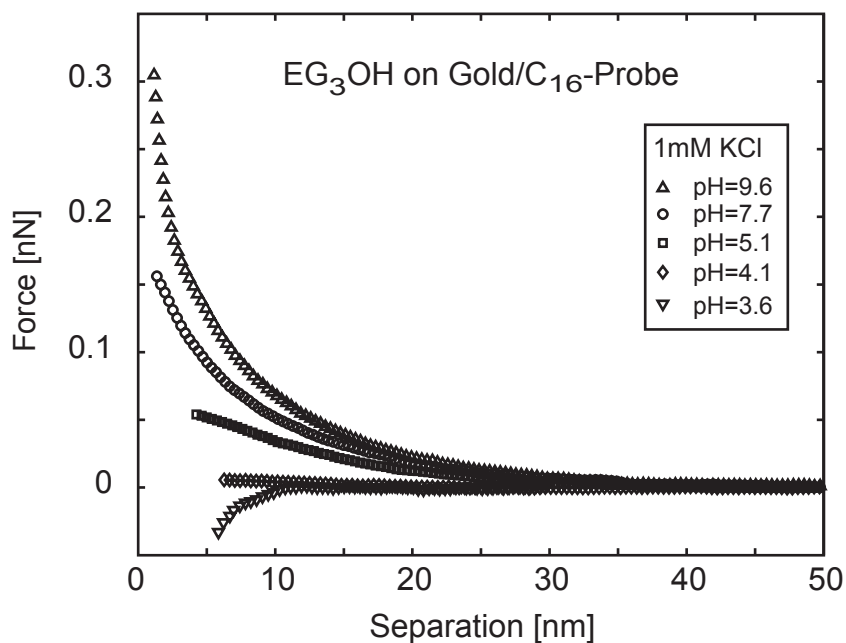
Figure 5.9: *Advancing force-versus-distance curves (averaged) measured with a hydrophobic C₁₆-probe on an EG₃-OH SAM on gold in aqueous KCl solution at varying pH-values and constant concentration of 1mM.*

Figure 5.9 displays the normal forces experienced by a hydrophobic C_{16}-probe when approaching an EG$_3$ SAM featuring a terminal hydroxy group. Again, various pH-values ranging from ~3.5 to ~10 have been adjusted in the electrolyte. For the lowest pH-value employed, an attractive interaction is detectable. At a slightly higher pH-value of ~4.1, the measured normal force exerted on the tip changes its sign and the interaction becomes repulsive. By further increasing the pH-value and thus adjusting more alkaline conditions the absolute value of the repulsive force increases, subsequently. Note the similarity in the interaction behaviour of EG$_3$-OH and EG$_3$-OMe SAMs towards the hydrophobic SFM probes (compare Figures 5.8 and 5.9).
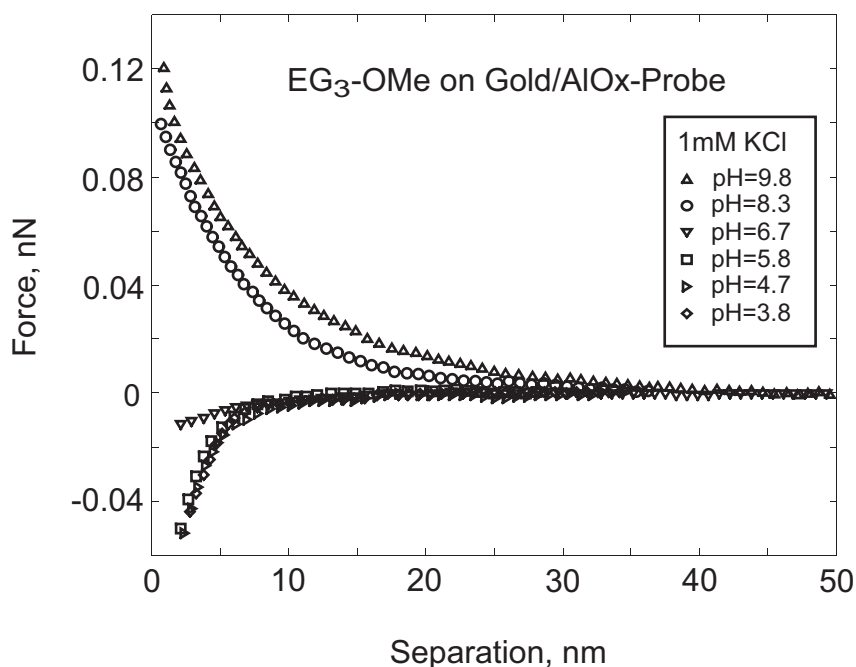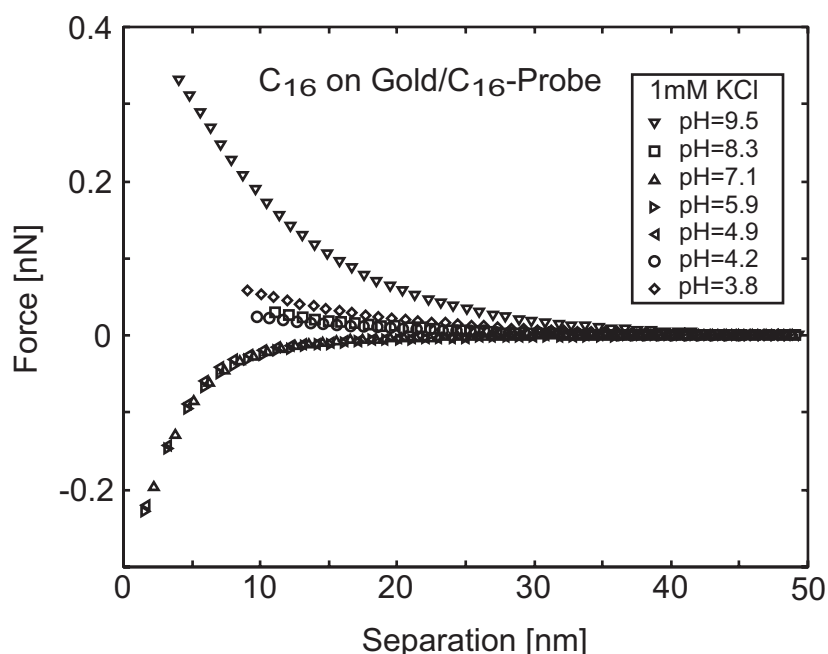

Figure 5.10: *Advancing force-versus-distance curves (averaged) measured with a C_{16}-probe on a C_{16} SAM on gold in aqueous KCl solution at varying pH-values and a constant salt concentration of 1mM.*

In order to learn more about the observed interaction and the behaviour of hydrophobic films under different pH conditions, additional measurements were performed for the symmetric system of two hexadecanethiol films adsorbed on gold.

A series of pH-dependent force-distance curves for hexadecanethiol-covered tip and surface recorded at constant ionic strength of 1 mM is shown in Figure 5.10. The force curves are attractive at 'neutral' pH-values ~6 and become repulsive for pH-values below ~4 and above ~8. While featuring slightly repulsive forces, the jump-into-contact distances for pH-

values 3.8, 4.2 and 8.3 were found to be surprisingly large compared to the OEG systems described above. Only at the highest investigated pH-value of 9.5, where the strongest normal force can be observed, is a repulsive interaction similar to the systems involving EG_3 detectable.

5.1.3 pH-Values of Vanishing Force

In order to gain more information about the pH-dependent interaction behaviour of the model organic surfaces towards the variably functionalised tips, Figure 5.11 summarises the results of Figures 5.6 to 5.8 and 5.10 and displays them in a slightly different fashion. The figure presents the nominal values of the interaction forces at a constant distance between AFM-probe and 'hard wall'-potential depending on the pH-value of the solution for the different probe/surface combinations investigated. According to literature the isoelectric point of an oxide surface can be determined at the point of vanishing force, i.e., the zero-crossing of the graphs [8]. For the synthetic organic surfaces involved the term 'point of zero charge' seems to be a more appropriate expression to label this significant change in the interaction behaviour with respect to the solution's pH-value.

All graphs in Figure 5.11 show a transition from attractive to repulsive interaction forces with increasing pH-values for those systems involving EG_3-OMe monolayer films. The exact pH-value of vanishing force varies with the probe used.

For pH-values above the zero-crossing at pH ~4.5 in Figure 5.11a, which can clearly be assigned to the isoelectric point of the oxidised silicon nitride probe according to values reported in literature [13], a plateau of repulsive forces with similar nominal values can be observed for the EG_3-OMe/SiO_x system. Figure 5.11b illustrates a plateau of low nominal negative force values up to a pH ~6.9 for the EG_3-OMe/AlO_x system. The transition from negative to positive force values occurs at pH ~7.3 and represents the isoelectric point of the amorphous alumina tip surface [14,17].

In Figure 5.11c, the change in sign of the normal force for the EG_3-OMe/C_{16} system emerges already at pH ~3.8. The subsequent increase of the repulsive force with higher pH-values known from Figure 5.8 can be observed clearly in this graph. According to Knoll and coworkers, this zero-crossing can be assigned to the isoelectric point of the hydrophobic probe [11,12].
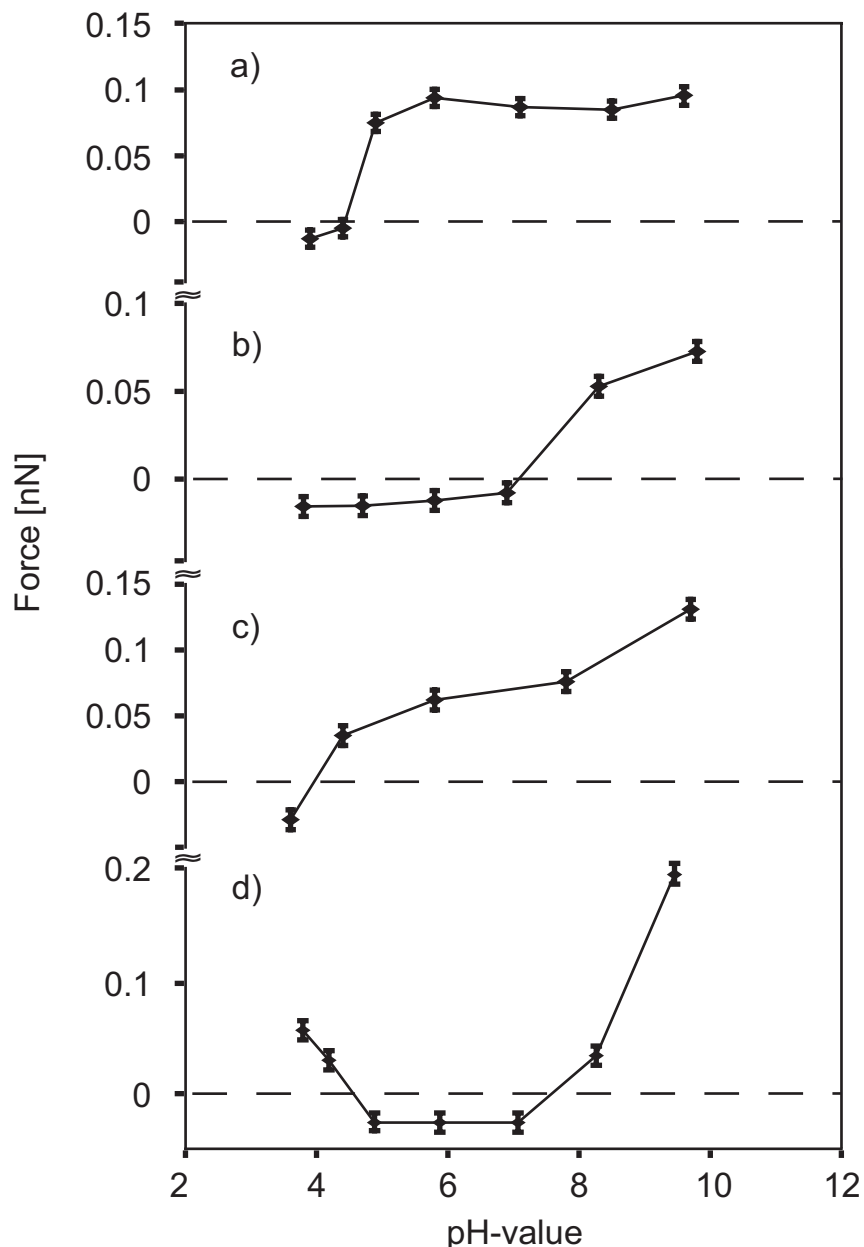
Figure 5.11: *Normal force between tip and sample surface in 1mM aqueous solution depending on pH for a) a SiO$_x$-probe and EG$_3$ film; b) an AlO$_x$-probe and EG$_3$ film; c) C$_{16}$-probe and EG$_3$ film; d) two C$_{16}$ films at constant distance of 5nm for a),b) and c and 10nm for d), respectively.*

Remarkably, solely the symmetric C$_{16}$/C$_{16}$ system displayed in Figure 5.11d features two of the prominent pH-values where the resulting overall interaction cancels. The measurement shows that in addition to pH 4, the overall interaction force is also zero at pH 8. The lower value around 4 is similar to that found for the EG$_3$/C$_{16}$ system in Figure 5.11c. In contrast to that combination, C$_{16}$/C$_{16}$ shows attractive forces for the pH range 4 - 8, which at least at pH ~6 does not depend on the ionic strength as is shown in the previous chapter.

5.2 Discussion

5.2.1 Concentration-Dependence of Force at Neutral pH

All force-versus-distance curves recorded at constant 'neutral' pH involving EG$_3$ films show a strong dependence on the ionic strength of the aqueous salt solution. The exponential decay lengths at various ion concentrations are in reasonable agreement with theoretical values predicted by DLVO-theory, indicating that the dominant component of the observed interaction is electrostatic. According to Butt [20], the total interaction force between a charged sphere with radius, R, and a plane in electrolyte solutions can be described by the following equation (5.1), which is derived from DLVO-theory assuming low surface potentials ($\Psi < 25$ mV) [20]

$$F_{el} = \frac{2\pi R}{\kappa \varepsilon_o \varepsilon_r} \left[\left(\sigma_1^2 + \sigma_2^2 \right) e^{-2\kappa s} + 2\sigma_1 \sigma_2 e^{-\kappa s} \right] \tag{5.1}$$

with σ_1 and σ_2 being the surface charge densities, $1/\kappa$ the so-called Debye length and s the separation between the two bodies. Note that an overall electrostatic interaction and consequential a finite force results even if only one of the two surfaces involved in the interaction does not carry a net charge and hence the second term cancels. The resulting force is then repulsive. In such a case, however, the decay length of the exponential force would be half the value of the Debye length. In contrast, the decay lengths found in the force curves correlate quite well with the Debye lengths (except for the lowest concentration [2]), and hence those expected if both surfaces are charged. In consequence, the EG$_3$-OMe monolayer must carry an effective surface charge. Its sign can be derived from the interaction with the negatively and positively charged probes. Since there is a repulsive interaction with negatively charged and an attractive interaction with positively charged tips, the effective surface charge of the OEG interface can be concluded to be negative.

Comparison with force measurements performed on a SAM featuring a static dipole moment (see Figure 5.4) with the negative charge facing bulk solution confirms this hypothesis.

In contrast to the systems where EG$_3$-OMe-terminated surfaces are involved, the symmetric C$_{16}$/C$_{16}$ combination discussed in Chapter 4 features typical hydrophobic attraction

at pH ~6 and shows no dependence on the salt concentration at this pH-value [2]. It can be concluded from the measurements on the C$_{16}$/EG$_3$ combination, however, that C$_{16}$ films also carry a negative surface charge at pH ~6. This is confirmed by recent streaming current measurements [11,12]. Since there is no sign of any ion concentration dependence at pH ~6, the electrostatic component for C$_{16}$/C$_{16}$ is negligible and the observed force is dominated by the attractive hydrophobic interaction (see Figure 4.1 or 5.10).

5.2.2 pH-Dependence of Force at Constant Ionic Strength

Oxide surfaces such as silica and alumina are well know to establish surface charges in aqueous environments with the sign of charge strongly dependent on the pH-value of the aqueous solution. They display characteristic isoelectric points, or points of zero charge, if there is no specific adsorption of ions other than H$_3$O$^+$ or OH$^-$. Regarding the association of water molecules to organic surfaces a similar pH-dependent behaviour has been reported recently [7], where water molecules adjacent to a hydrocarbon surface were found to "flip" their orientation ~180° when pH-value of the solution was changed from the alkaline to the acidic regime.

The pH-values of 4.4 and 7.1 for vanishing force found in Figures 5.11a and b when approaching the EG$_3$-OMe SAM with SiO$_x$- and AlO$_x$-probes, respectively, are in reasonable agreement with IEPs reported in the literature [14,17,18]. At pH ~4.4 the interaction between the silica tip and the EG$_3$-OMe SAM turns from attractive to repulsive due to the change in sign of the surface charge at the silica tip from positive to negative. The same pattern can be observed for the alumina tip at pH ~7.1. The probes' surface charge becomes negative for higher values and the interaction turns to repulsive. Conclusively, these pH-values have to be assigned to the IEPs of the amphoteric silica and alumina probes.

Remarkably, such a distinctive pH-value can also be found in the EG$_3$/C$_{16}$ system, although two intrinsically uncharged surfaces are involved in the interaction. The DLVO-like behaviour of the force in the concentration-dependent measurements at constant pH has already been discussed above (see Figure 5.3). At a pH of ~4 the overall force vanishes and changes sign (Figure 5.11c), i.e., the C$_{16}$ monolayer appears to have an IEP at this pH. Recent streaming current measurements show a similar value for the IEP of these methyl-terminated alkanethiol films [11,12], thus confirming this assignment.

For the symmetric C_{16}/C_{16} system displayed in Figure 5.11d there are two such distinctive pH-values. The lower one is similar to the value determined for EG_3/C_{16}. In addition, the force also vanishes at a higher pH-value of around 8. At pH 9.5 a strong dependence of the repulsive force on the ionic strength was found in Figure 5.5. This typical DLVO-type behaviour indicates the main contribution to the interaction to be of electrostatic nature under these conditions in contrast to pH ~6 where hydrophobic attraction dominates over any electrostatic component.

If pH 4 corresponds to the IEP of the methyl-terminated film then at pH 8 there must be a finite negative charge density present, which counterbalances and then overcomes the hydrophobic attraction. Consequently, the charging mechanism is not symmetric. This is reflected by the ζ-potentials of these films determined by streaming current measurements [11,12] and those of drops of hexadecane and dodecane in aqueous solutions [21].

The overall force at pH ~8 would be simply a linear superposition of attractive hydrophobic and repulsive electrostatic forces if both are competing and independent. What seems more plausible, however, is a more complex and nonlinear relation where the charge established at the surface can be viewed as a kind of chemical modification, which alters the nature of the surface as well as its hydrophobic properties. Therefore, it is difficult to extract a detailed picture at this pH without additional information.

5.2.3 Mechanism of Charge Establishment

One of the main questions that arises from the observed DLVO-like interaction behaviour concerns the origin of the electric surface potential at the organic/liquid interfaces and the mechanism of the charge establishment on the synthetic organic films. Several scenarios that describe the emerging of the negative surface charges can be imagined. It was reported that hydrophobic oil droplets from hexadecane also acquire a negative surface charge in aqueous solutions [21]. Similar arguments can be applied in our context:

First, the negative charge could be due to the depletion of hydronium ions at the organic/liquid interface leading to an excess of (negative) hydroxyl ions close to the organic surface. Second, a preferential orientation of water molecules and their corresponding dipoles induced by the strong interaction with the EG entities at the top of the SAM could result in a dipolar field in the close vicinity of the organic surface as described in the previous chapter and third, the adsorption of hydroxyl ions at the interface could be responsible for a negative

surface charge density, while the adsorption of ions other than hydroxyl or hydronium can be ruled out, based on the study with different ions from the Hofmeister series presented in Chapter 4 [2].

The depletion of (positively charged) hydronium ions is not realistic. A measured ζ-potential of approximately -50 mV and -70 mV at pH ~6 for C$_{16}$ and EG$_3$, respectively [11,12,22], corresponds to an excess ionic surface density on the order of 4×10^{-9} mol/m^2 and 7×10^{-9} mol/m^2 based on the Grahame equation (5.2) [23], assuming that the excess charges are solely due to OH$^-$ and that the surface potential, Ψ$_S$, is equal to the ζ-potential

$$\sigma = \sqrt{8\varepsilon\varepsilon_0 kTC_{El}} \sinh\left(\frac{ze\Psi_S}{2kT}\right) \tag{5.2}$$

The latter assumption is satisfactory for low and moderate electrolyte concentrations [24]. C_{El} is the total bulk ion concentration. A simple estimation of the thickness, δ, of the depletion layers for the hydronium [21] then results in $\delta = 4$ μm and $\delta = 7$ μm, respectively. Similarly, a potential of -80 mV at pH 8 for both EG$_3$ and C$_{16}$ monolayer films in 1mM solutions [11,12,22] results in a thickness of the depletion layer of 1 cm. From a physical point of view, however, δ should not exceed the Debye screening length, which is about 10 nm for 1 mM solutions [23]. This underlines that depletion can effectively be ruled out.

A long-range structured water interface was proposed earlier in this work in order to explain the observed long-range repulsion and the negative surface charge density [19,25]. A long-range directional ordering of water molecules occurring at the boundary to a non-polar organic surface is associated with a loss in entropy. The close approach of two such surfaces would lead to the expulsion of some amount of the oriented molecules into the bulk water phase, which is an entropically favoured process [23]. If such a long-range parallel ordering of water molecules takes place, it should lead to the appearance of a potential difference, Ψ, between bulk water and interfacial water. In addition, different ions from the Hofmeister series should have a different effect on such a structured water interface and hence the resulting range and surface charge density. The force-distance analysis presented in the previous chapter, however, did not show any systematic trend for different ions [2]. Therefore, this model is also not very likely.

The measured strong pH-dependence of the interaction forces involving EG$_3$-containing films suggests that the adsorption of hydroxyl ions at the organic/liquid interface is the most probable mechanism for the negative interfacial charging. It is known, however, that the close approach of an ion to the boundary between water and another phase of low dielectric constant is an energetically unfavourable process from an electrostatic point of view [26]. In consequence, ion adsorption can take place only if it is strongly favoured by some specific (not long-ranged electrostatic) interaction of the ion with the interface. This could be created either by the specific interaction of the ions with the organic molecules or by the particular structure of the water molecules at the interface. The latter hypothesis is supported by the fact that the boundary water molecules are highly ordered at the interface with hydrocarbon phases [23]. Theoretical considerations of the boundary between water and non-polar fluids have shown that the interfacial water molecules are preferentially oriented with the oxygen atoms towards the hydrophobic phase [27,28]. The adsorption of hydroxyl ions could then be explained with strong dipole or hydrogen bonding of the OH$^-$ ions with the hydrogen atoms of the interfacial water molecules.

The hydrogen bond between OH$^-$ ions and water molecules is usually classified as 'strong' with an energy of almost 60 kT per bond [29]. In the bulk aqueous phase, fractions of the hydrogen bonds between the water molecules are broken due to Brownian motion. Therefore, the specific adsorption could result from the restricted mobility of water molecules in the interfacial layer allowing more pronounced hydrogen bonding of the OH$^-$ ion and the neighbouring water molecules accompanied by a corresponding free energy gain.

5.2.4 Difference between EG$_3$ and C$_{16}$ Films

The most striking difference between EG$_3$-OMe, EG3-OH and methyl-terminated C$_{16}$ films is the fact that the EG$_3$ SAMs do not change sign of surface charge density over the whole pH-range investigated. The fact that the potentials for EG$_3$ and C$_{16}$ are similar at pH 8 [11,12,22] can be interpreted as an indicator for a similar mechanism of charge establishment in both systems. A possible reason for the different behaviour might then be found in the strength of the hydrogen bond of interfacial water to the synthetic surfaces. While weakly hydrogen-bonded water molecules in the interfacial region of the hydrocarbon/water system are stressed by Richmond and coworkers [7], who found changes in pH to cause a flip in orientation of water molecules and hence a reorientation of molecular dipoles, several other

studies emphasise the strong interaction of water with the oxygen atoms of ethylene glycol entities, which act as hydrogen bond acceptors [8-10]. It has been suggested that this particular influence of 'strong' hydrogen bonds over neutral 'weak' hydrogen bonds on the interaction forces in electrolyte solutions close to organic model surfaces is due to a reduction of the local dielectric constant of the solvent [30]. Such a strong hydrogen bond at the EG-terminated SAM surface would explain the persistent orientation of the water molecules at the EG$_3$-OMe surface over the broad pH-range investigated in the force-distance analysis presented above.

In a study that is concerned with pH-dependent adsorption of polyions on structured COOH/EG$_3$-OMe terminated gold surfaces [31] it was found that at low pH conditions, strong hydrogen-bonding at the ether and alcohol oxygens of the EG sites give rise to an enhanced adsorption of polyions, offering hydrogen bond donor sites. In addition, hydrophobic interactions of the ethylene groups in the EG repeat units with polyions having hydrophobic backbones are proposed to further support the adsorption. The strong tendency of the EG entities for hydrogen bonding, in particular at low pH, supports the interpretation of a strong association of water molecules with the EG$_3$-OMe SAM via hydrogen bonds. Theoretical studies on the EG$_3$-OMe/water interface discuss the high surface density of hydrogen bonds between EG units and water molecules as the critical parameter leading to the remarkable resistance to protein adsorption of these films [1,32,33]. It is suggested that water molecules are able to penetrate the SAM in such a way, that the topmost ethylene and the alcoholic oxygens are particularly involved in hydrogen-bonding with water molecules [1,3].

While from an electrostatic point of view both organic films EG$_3$-OMe and C$_{16}$ appear experimentally similar with comparable negative surface potentials for certain pH-values [11,12,22], the stability of the established charge could play a decisive role. A stronger interaction of water with the EG entities could be responsible for the robustness of the interfacial charges of the OEG films towards changes in pH. In contrast, more weakly bonded water at the C$_{16}$ interface would lead to a breakdown of the water interface itself and the surface charges resulting in a change of sign when varying the pH. A prerequisite for the charges that are due to hydroxyl ions is a stagnant water layer associated with the organic film. Such layers are found on rough and smooth charged surfaces and it has been speculated that they also persist on uncharged surfaces [34].

Finally, the fact that PEG polymers do not show long-range electrostatic forces in electrolyte solutions could be due to the size of 'typical structures', i.e., the local density of ethylene glycol units and the distance between them. The concept of hydrophobicity is closely related to hydrogen-bonded networks of water and the ability of water molecules to establish local networks [35]. The extended EG structures of the monolayer films do not allow the same water arrangement as do the polymer chains. The extended, two-dimensional structure created at surface of the densely packed SA films depletes the number of hydrogen bonds that can be established between neighbouring water molecules, while hydrogen-bonding can simply go around the free PEG polymer chains. As a result, OH^- association does not occur or is very weak in the latter case. This might well account for the difference. If the OEG structure, however, is too densely packed as in case of the EG_3-OMe SAM on silver, a hydrophobic behaviour similar to C_{16} films is measured [19,36] accompanied by a loss of protein resistance [36]. Therefore, film density also has to be considered a crucial parameter for the establishment of the stagnant water layer and the subsequent adsorption of hydroxyl ions.

The force measurements on the partially covered PEG films discussed in Chapter 3 can also be interpreted in this picture. The PEG films with 25% and 50% of relative film density comprise film thicknesses that are comparable to that of OEG SAMs. Therefore, single chains are not extended into solution but remain in close vicinity to the gold surface, most likely due to van der Waals attraction. This leads to a restricted access of the EG entities for water molecules preventing the establishment of a hydrogen-bonded network all around the chains. As a consequence, a similar templating effect of interfacial water as observed for OEG SAMs might also account for the interaction behaviour of the incompletely covered PEG films.

The differences observed for the polymer PEG and SAMs of EG_3-OMe and C_{16} might well be closely related to the 'two faces of water', which play an important role in hydrophobic interactions and protein folding processes and were recently described by Chandler [37]. The transition form oligmer to polymer behaviour occurs at nanometer length scales, when the local concentration of ethylene glycol units is sufficiently high, or when the accessible apolar surface is sufficiently large.

5.3 Conclusions

Chemical force spectroscopy on tri(ethylene glycol)-containing and methyl-terminated self-assembled monolayers under liquids with differently functionalised tips was employed to mimic the interaction between proteins and model organic surfaces. The crucial parameters were tip functionalisation as well as pH-value and ionic strength of the electrolyte solution. Force-distance measurements performed with hydrophobically functionalised as well as positively and negatively charged AFM probes reveal a difference in the forces observed on the organic films. In particular, the change in sign of the interaction force with change in sign of the probe's surface charge in combination with theoretical curve fits provides a strong indication for an effective negative surface charge at the SAM/water interface.

The establishment of a negative surface charge on both monolayer films can conclusively be assigned to the adsorption of hydroxyl ions from solution. Crucial for the stability of the surface charge appears to be interfacial water that is associated with the organic films forming a strongly hydrogen-bonded two-dimensional network, and which acts as a template for hydroxyl adsorption. While charges on C$_{16}$ show a dependence on the pH, its influence on those associated to EG$_3$-OMe was found to be minor. The measurements suggest that the template for OH$^-$ adsorption created by the immobilised interfacial water is more stable in the case of the OEG interface compared to hydrophobic methyl groups.

A further crucial parameter appears to be the size of 'typical' structures which determines the networks that can be established by water molecules. This might well account for the different behaviour observed for PEG films and OEG SAMs.

5.4 Literature

[1] Pertsin, A. J.; Grunze, M. *Langmuir* **2000**, *16*, 8829

[2] Dicke, C.; Hähner, G, *J. Phys. Chem. B* **2001**, *106*, 4450

[3] Zolk, M.; Eisert, F.; Pipper, J.; Herrwerth, S.; Eck, W.; Buck, M.; Grunze, M *Langmuir* **2000**, *16*, 5849

[4] Du, Q.; Freysz, E.; Shen, Y.R. *Phys. Rev. Lett.* **1994**, *72*, 238

[5] Kim, J.; Cremer, P.S. *J. Am. Chem. Soc.* **2000**, *122*, 12371

[6] Kim, J.; Kim, G.; Cremer, P.S. *Langmuir* **2001**, *17*, 7255

[7] Scatena, L. F.; Brown, M. G.; Richmond, G. L. *Science* **2001**, *292*, 908

[8] Dreesen, L.; Humbert, C.; Hollander, P.; Mani, A. A.; Ataka, K.; Thiry, P. A.; Peremans, A. *Chem. Phys. Lett.* **2001**, *333*, 327

[9] Huang, L.; Nishinari, K. *J. Polym. Sci. B* **2001**, *39*, 496

[10] Ide, M.; Yoshikawa, D.; Maeda, Y.; Kitano, H *Langmuir* **1999**, *15*, 926

[11] Schweiss, R.; Welzel, P. B.; Werner, C.; Knoll, W. *Langmuir* **2001**, *17*, 4304

[12] Schweiss, R.; Welzel, P. B.; Werner, C.; Knoll, W. *Colloid and Surf. A* **2001**, *195*, 97

[13] Lin, X.; Creuzet, F.; Arribart, H. *J. Phys. Chem.* **1993**, *97*, 7272

[14] Parks, G. A. *Chem. Rev.* **1965**, *65*, 177

[15] Marti, A. PhD Thesis, ETH Zürich, Diss. No. 12320, **1997**

[16] Kokkoli, E.; Zukovski, C. F. *Langmuir* **2000**, *16*, 6029

[17] Sposito, G. *The Environmental Chemistry of Aluminium*, 2nd Ed., CRC Press: Boca Raton, Florida, **1995**

[18] Yopps, J. A.; Fuerstenau, D. W. *J. Colloid Sci.* **1964**, *19*, 61

[19] Feldman, K.; Hähner, G.; Spencer, N. D.; Harder, P.; Grunze. M. *J. Am. Chem. Soc.* **1999**, *121*, 10134

[20] Butt, H.-J. *Biophys. J.* **1991**, *60*, 777

[21] Marinova, K. G.; Alargova, R. G.; Denkov, N. D.; Velov, O. D.; Petsev, D. N.; Ivanov, I. B.; Borwankar, R. P. *Langmuir* **1996**, *12*, 2045

[22] Grunze, M.; Chan, M. *private communication*

[23] Israelachvili, J. N. *Intermolecular and Surface Forces,* 2nd Ed., Academic Press: London, **1992**

[24] Hunter, R. J. *Zeta Potential in Colloid Science: Principles and Applications;* Academic Press: New York, **1981**

[25] Wang, R. L. C.; Kreuzer, H. J.; Grunze, M. *J. Phys. Chem. B* **1997**, *101*, 9767

[26] Landau, L. D, Lifshitz, E. M. *Electrodynamics of Continuous Media,* 2nd ed.; Pergamon Press: Oxford, **1984**

[27] Conway, B. E. *Adv. Colloid Interface Sci.* **1977**, *8*, 91

[28] Dubrovich, N. A. *Kolloidn. Z.* **1995**, *57*, 275

[29] Spangler, D.; Christoffersen, R.E. *Int. J. Quant. Chem.* **1980**, *17*, 1075

[30] Smith, D. A.; Wallwork, M. L.; Zhang, J.; Kirkham, J.; Robinson, C.; Marsh, A.; Wong, M *J. Phys. Chem.* B **2000**, *104*, 8862

[31] Clark, S. L.; Hammond, P. T. *Langmuir* **2000**, *16*, 10206

[32] Wang, L. C.; Kreuzer, H. J.; Grunze, M. *Phys. Chem. Chem. Phys.* **2000**, *2*, 3613

[33] Pertsin, A. J.; Hayashi, T.; Grunze, M. *Phys. Chem. Chem. Phys.* **2001**, *3*, 1598

[34] Lyklema, J.; Rovillard, S.; De Coninck, J. *Langmuir* **1998**, *14*, 5659

[35] Lum, K.; Chandler, D.; Weeks, J. D. *J. Phys. Chem. B* **1999**, *103,* 4570

[36] Harder P.; Grunze, M.; Dahint, R.; Whitesides, G. M.; Laibinis P. E. *J. Phys. Chem. B* **1998**, *102*, 426

[37] Chandler, D. *Nature* **2002**, *417*, 491

Chapter 6

Force Spectroscopy on derivated Tri(Ethylene Glycol)-containing Self-Assembled Monolayers

Continuing studies on the influence of different solution properties on the interfacial water structure discussed in the previous chapters this chapter focuses on the influence of varying hydrophobic end groups terminating tri(ethylene glycol)-containing SAM films. Experimental parameters covering length of EG-tail, type of dissolved ions as well as salt concentration and pH-value of the electrolyte solution have been subject to intense investigation in this work during the previous sections. From all results discussed so far, the force between a hydrophobic C_{16}-probe and EG_3 monolayers appears to be electrostatically promoted [1-4]. Intense effort has been spent on the question for the origin of this electrostatic character of the interaction in several studies [5-10], but an appropriate model to describe the observed forces and therefore the ability of these films to resist non-specific protein adsorption, however, could not be finally elucidated so far. In the previous chapter, the adsorption of hydroxyl ions has been stressed to account for the establishment of the negative surface charge density. Furthermore, a thin layer of interfacial water has been proposed to act as stabilising template for the hydroxyl adsorption [4].

In another recent study some attention has been spent on the interface of EG functional groups and a hydrophobic backbone under water for PEG modified with alkane chains [11]. A very low hydration of the PEG units near the PEG/hydrocarbon interface was found, which increased towards the outer region of the PEG tail. In combination with a SAM film such a terminal hydrophobic functionalisation might represent a suitable tool to tune the

hydration of the EG entities, and therefore to subsequently modify the capability of the film to resist protein adsorption.

In order to gain more information on the protein resistant properties of the oligo(ethylene glycol)-containing self-assembled monolayers, a series of new derivates of tri(ethylene glycol)-containing alkanethiols with varying lengths of alkyl tail (EG$_3$-OR; R = H, Me, Et, Pr and Bu) has been prepared on polycrystalline gold surfaces. These SAMs have been studied with respect to the relevant interaction forces discussed in the previous chapters. Prior to force-distance analysis, X-ray photoelectron spectroscopy and contact angle measurements have been performed for film characterisation of the novel alkanethiols [12]. Additionally, quantitative protein adsorption data have been recorded on the different EG$_3$-OR SAM films using infrared spectroscopy.

6.1 Results

6.1.1 Film Characterisation by XPS and Contact Angle Measurements

X-ray photoelectron spectroscopy has been employed by S. Herrwerth at University of Heidelberg in order to characterise the monolayer films of the novel EG$_3$ derivates and to ensure film quality and cover density [12].

SAM	Relative Density [%]
EG$_3$-OH	81 ± 4
EG$_3$-OMe	79 ± 4
EG$_3$-OEt	79 ± 4
EG$_3$-OPr	81 ± 4
EG$_3$-OBu	82 ± 4

Table 6.1: *Relative density of the differently terminated tri(ethylene glycol) SAMs (measured by S. Herrwerth) [12].*

The relative coverage of the differently terminated tri(ethylene glycol) SAMs were determined according to literature [6]. A reference system of four alkanethiols on gold with

12, 16, 18 or 20 carbon atoms was used. Table 6.1 displays the relative densities of the differently terminated tri(ethylene glycol) SAMs [12]. Cover rates of the different EG$_3$-derivates appear to be in very good agreement within the experimental error for all SAMs. Within the experimental error, all monolayers exhibit around 80% of the density determined for a hexadecanethiol SAM.

In addition, contact angle measurements have been performed by S. Herrwerth in order to determine stability and hydrophilicity/hydrophobicity of the SA films. The different values obtained for the advancing water contact angles are listed in Table 6.2 [12].

SAM	Contact angle [°]
EG$_3$-OH	34 ± 3
EG$_3$-OMe	65 ± 3
EG$_3$-OEt	84 ± 3
EG$_3$-OPr	94 ± 3
EG$_3$-OBu	107 ± 3

Table 6.2: *Advancing contact angle measurements on the differently terminated tri(ethylene glycol) SAM surfaces (measured by S. Herrwerth) [12].*

The EG$_3$-OH sample features the lowest contact angle with 34°. This is due to the terminating hydroxyl group at the top of the SAM film. With increasing length of the alkyl tail the water contact angles of the monolayer surfaces increase, subsequently. Finally, the EG$_3$-OBu SAM shows a high contact angle of 107° that is comparable to that of a hexadecanethiol SAM indicating a strong hydrophobicity. The successive increase in the contact angle reflects the strong influence of the terminal groups on the ethylene glycol moieties with respect to hydrophilicity/hydrophilicity of the monolayer films.

6.1.2 Force Spectroscopy Analysis

Hydrophobically functionalised SFM probes were used for force spectroscopy measurements on the different EG$_3$-containing samples under electrolyte solutions at varying ionic strengths and constant neutral pH-value. Again, aqueous KNO$_3$ solution was chosen as 'standard electrolyte' for force-distance analysis.
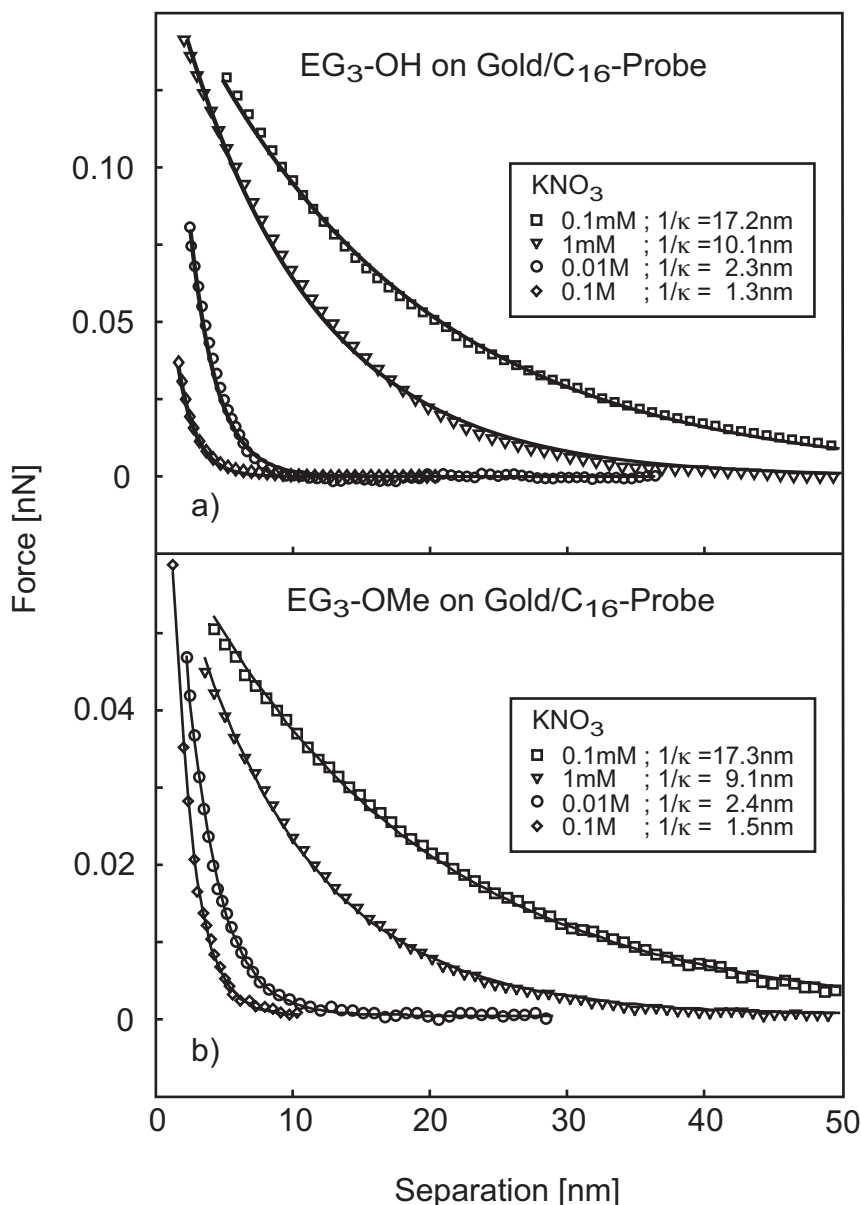
Figure 6.1: *Advancing force-versus-distance curves (averaged) measured with a hydrophobic C₃-probe on a) an EG₃-OH SAM and b) an EG₃-OMe SAM on gold in aqueous KNO₃ solution of different concentration (◇ - 0.1M; ○ - 0.01M; ▽ - 1mM; □ - 0.1mM).*

The interaction between the hydrophobic probe and the EG₃-OH sample displayed in Figure 6.1a shows an exponentially decaying repulsive force for low ionic strength. At a salt concentration of 0.1 mM, a decay length of 17.2 nm was observed. Increasing the ion concentration resulted in smaller values. An exponential decay length of 10.1 nm was found for 1 mM and for 0.01 M solutions 2.3 nm could be calculated. Finally, for the highest ion concentration (0.1 M) investigated, a value of 1.3 nm was observed. Figure 6.1b displays the interaction forces between the EG₃-OMe sample and a hydrophobic probe at different salt

concentrations. Solution with lowest ionic strength (0.1 mM) was introduced first again. A repulsive force with an exponential decay length of 17.3 nm can be observed. Subsequently, the ionic strength of the solution was increased. This resulted in a decrease in decay length of the repulsion. The interaction pattern is very similar to the EG₃-OH SAM. Force-distance curves show repulsive forces with decay lengths strongly depending on the salt concentration. As discussed in the previous chapters this is a typical DLVO-like behaviour [1-4].
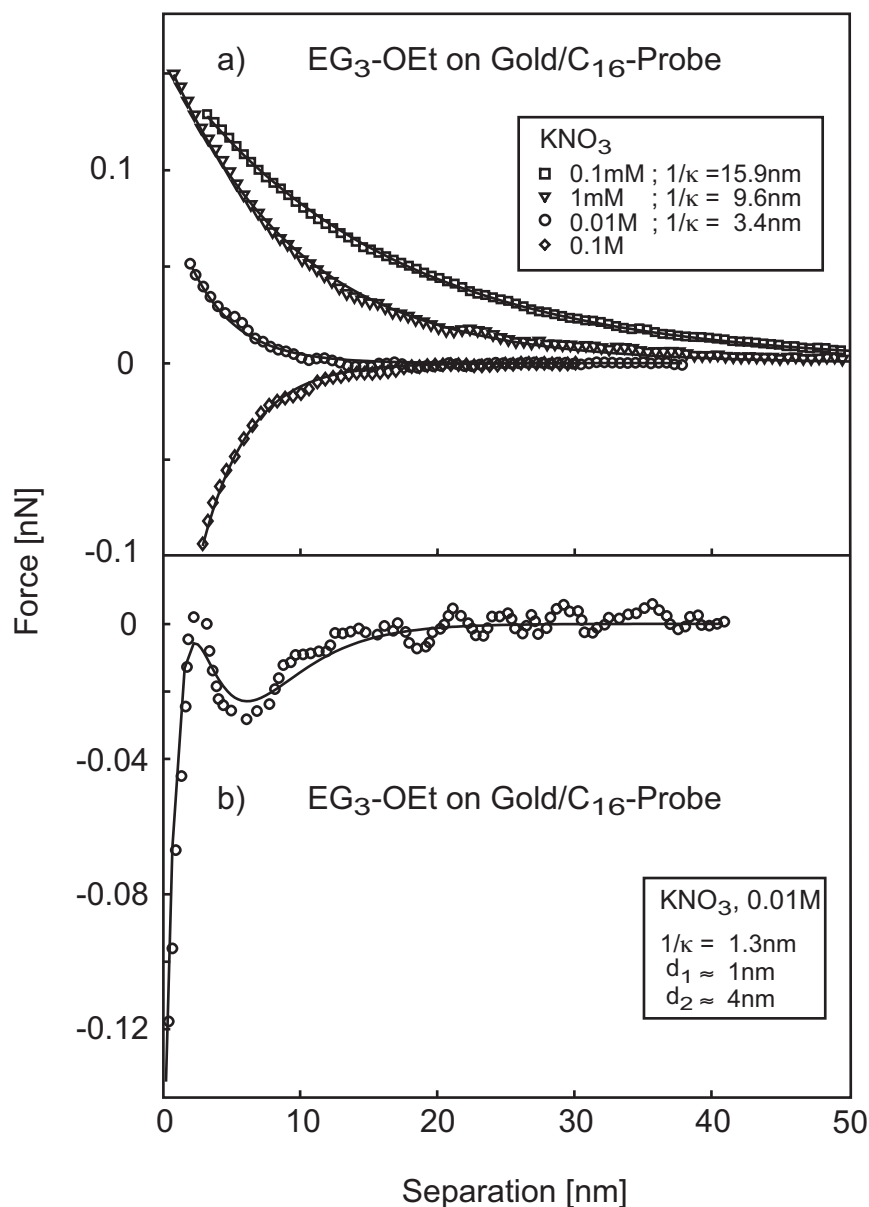

Figure 6.2: a) Advancing force-versus-distance curves (averaged) measured with a hydrophobic C_{16}-probe on an EG_3-OEt SAM on gold in aqueous KNO_3 solution of different concentration (◇ - 0.1M; ○ - 0.01M; ▽ - 1mM; □ - 0.1mM); b) advancing force-distance curve (selected f-c curves averaged) at 0.1M with secondary minimum.

Force-distance measurements on an ethoxy-terminated EG$_3$ SAM reveal slight changes in the interaction behaviour towards the hydrophobic probe. For low concentrations again long-range repulsive forces are observable in Figure 6.2a. At a salt concentration of 0.1 mM the exponential decay length can be calculated to 16.1 nm. With increasing ionic strength the decay length of this repulsion decreases subsequently. Decay lengths of 9.6 nm for 1 mM and 3.4 nm for 0.01 M solutions were found. In contrast to the measurements described above the interaction between the EG$_3$-OEt sample and the C$_{16}$-probe shows an additional attractive contribution to the interaction force at a concentration of 0.1 M, which interferes with the purely repulsive interaction observed for EG$_3$-OH and EG$_3$-OMe samples.

Figure 6.2b shows the averaged force-distance curve at the highest introduced concentration of 0.1 M in more detail. There is a weak secondary minimum observable at a distance of around 6nm above the sample surface. This behaviour is not detectable in all force curves collected at this concentration but appears at times with reasonable reproducibility. In other force-distance curves the probe tends to jump into contact earlier and thus the small barrier cannot be resolved here. Therefore, the above displayed force-distance curve is averaged over selected single curves, which represent approximately a third of the total number of collected curves.

The total interaction force can be expressed in terms of a superposition of DLVO-like forces and hydrophobic forces [13,14]:

$$F_t = F_e + F_h \tag{6.1}$$

where F_t is the total force between probe and sample surface, F_e is the DLVO-type force and F_h is the hydrophobic force.

The DLVO-like force F_e between a sphere (SFM tip) and a flat sample surface is usually given as (compare Equation 3.1) [1]

$$F_e = a\exp(-\kappa s) \tag{6.2}$$

where κ^{-1} is the decay length of the force, s is the separation between tip and sample and a is a parameter accounting for the strength of the force primarily covering the two surface charge densities and the radius of the sphere.

Attractive forces between hydrophobic surfaces in water have been measured for different systems over the last twenty years [15-18]. There have been many theories suggested to explain the observed forces [19-21]. Most commonly, these hydrophobic forces are described by the following empirical law [13,14]

$$F_h = c_1\exp(-s/d_1) + c_2\exp(-s/d_2) \tag{6.3}$$

in which d_1 and d_2 represent the decay lengths of the short- and long-range attractive force, respectively, and c_1 and c_2 are the respective strengths of the force contributions.

Using Equation 6.1 to fit the force-distance curve as shown in Figure 6.2b reveals a decay length of the short-range repulsive force F_e of 1.3 nm, which is in good agreement with the other measurements at this concentration (compare Figure 6.1) and though slightly above the experimental error also in the range of the value of around 1 nm for the Debye length predicted by DLVO theory.

For the decay lengths of the hydrophobic contributions, values of around 1 nm for the short-range contribution d_1 and 4 nm for the long-range contribution d_2 can be fitted. In particular, the value of the long-range decay length d_2 is in good agreement with force-distance measurements at pure hydrophobic hexadecanethiol terminated surfaces [3,4].

The ratio of the strengths of the different contributions a / c_1 / c_2 is found to be approximately 0.7 / 0.6 / 0.3.

Figure 6.3a illustrates the effect of increasing hydrophobicity of the film by further extension of the alkyl tail by another alkyl group. The interaction of the hydrophobic C$_{16}$-probe and an EG$_3$-OPr SAM at low ionic strength is again repulsive and of long range. Decay lengths of 24.8 nm and 8.7 nm can be observed for 0.1 mM and 1 mM solutions, respectively. At a salt concentration of 0.01 M the repulsion vanishes and at the highest introduced concentration of 0.1 M the interaction becomes clearly attractive.

The trend observed above is further enhanced by addition of another alkyl group to the EG$_3$-tail of the SAM. Figure 6.3b displays the interaction between the hydrophobic C$_{16}$-probe and an EG$_3$-OBu SAM. Force-distance curves acquired at low concentrations again show a long-range repulsion with exponential decay lengths of 17,6 nm for 0.1 mM and 9.5 nm for 1 mM, respectively. After introduction of solutions with higher salt concentrations into the

liquid cell the repulsive interaction is completely suppressed and the interaction force becomes clearly attractive.
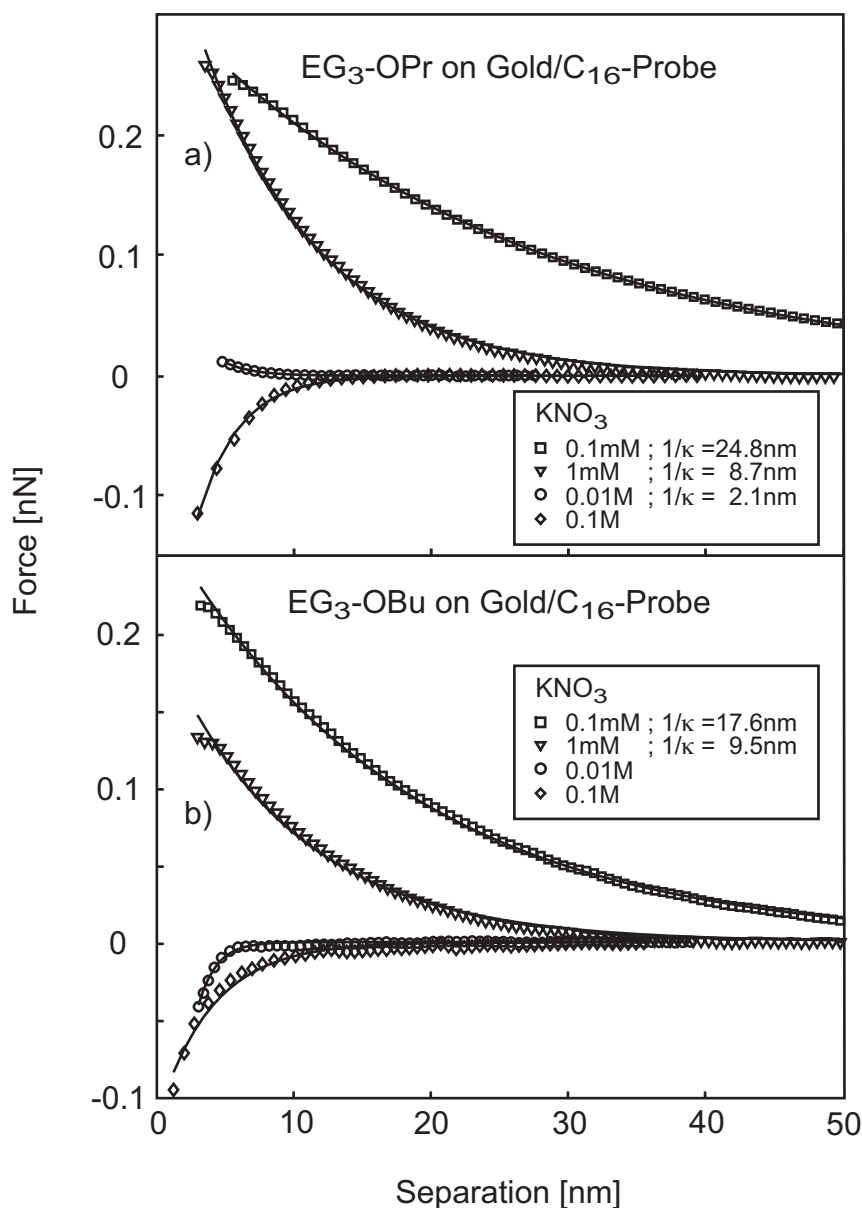
Figure 6.3: *Advancing force-versus-distance curves (averaged) measured with a hydrophobic C_{16}-probe on a) an EG_3-OPr SAM and b) an EG_3-OBu SAM on gold in aqueous KNO_3 solution of different concentration ($\diamondsuit$ - 0.1M; $\bigcirc$ - 0.01M; $\bigtriangledown$ - 1mM; $\square$ - 0.1mM).*

Retracting parts for all force-versus-distance curves are not shown in detail in this study, but they show a strong tendency for higher adhesion forces with increasing number of terminal alkyl groups at the top of the EG_3 SAM. Individual force curves showing not only the approaching but also the retracting parts for an EG_3-OMe and an EG_3-OBu sample under

0.1 M KNO$_3$ solution and perfluorodecalin, respectively, are displayed exemplarily in Figure 6.4. All measurements were performed with the same hydrophobic C$_{16}$-probe and unchanged laser position on the cantilever to ensure good comparability in the entire set of data, although tip shape and cantilever force constant were not determined explicitly.

Figure 6.4: *Representative force-versus-distance curves measured with a hydrophobic C$_{16}$-probe on a) an EG$_3$-OMe SAM and b) an EG$_3$-OBu SAM in aqueous 0.1 M KNO$_3$ solution.*

Figures 6.4a and 6.4b display the different interaction behaviour in the approaching parts of the force-distance curves known from Figures 6.1b and 6.3b. They exhibit a shrot-range repulsive interaction for the EG$_3$-OMe sample (Figure 6.4a) and an attractive interaction

for the EG$_3$-OBu sample (Figure 6.4b). Distinct differences in the retracting parts of the force-distance curves concerning the pull-off forces are also clearly detectable. The hysteresis in the force-distance curves for the EG$_3$-OBu sample is noticeably enhanced. Figures 6.5a and 6.5b, in contrast to measurements under aqueous salt solution, show an attractive behaviour for both EG$_3$-OMe (Figure 6.5a) and EG$_3$-OBu (Figure 6.5b) samples when approaching the tip to the sample surface under perfluorodecalin. The retracting parts display no differences in pull-off forces, which is also a remarkable difference to force-distance measurements under aqueous solution (compare Figures 6.4a and 6.4b).
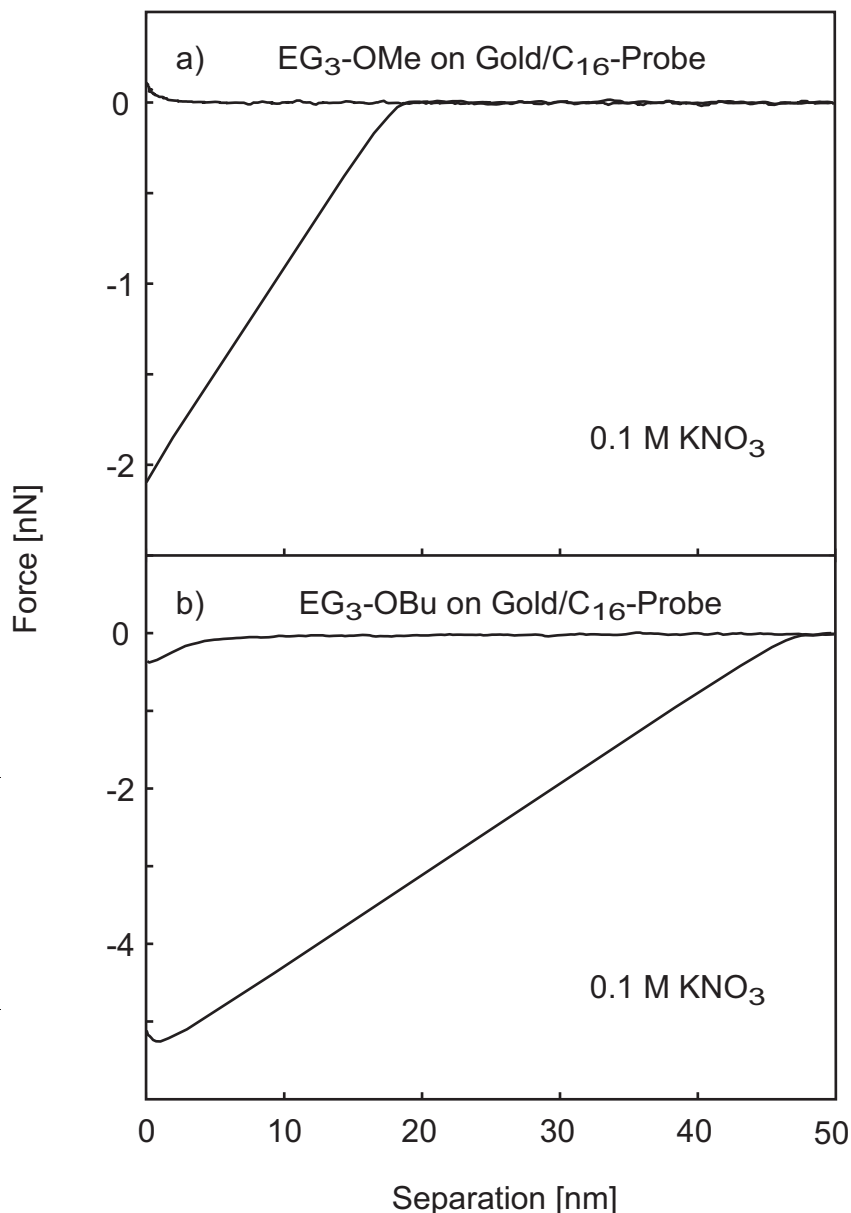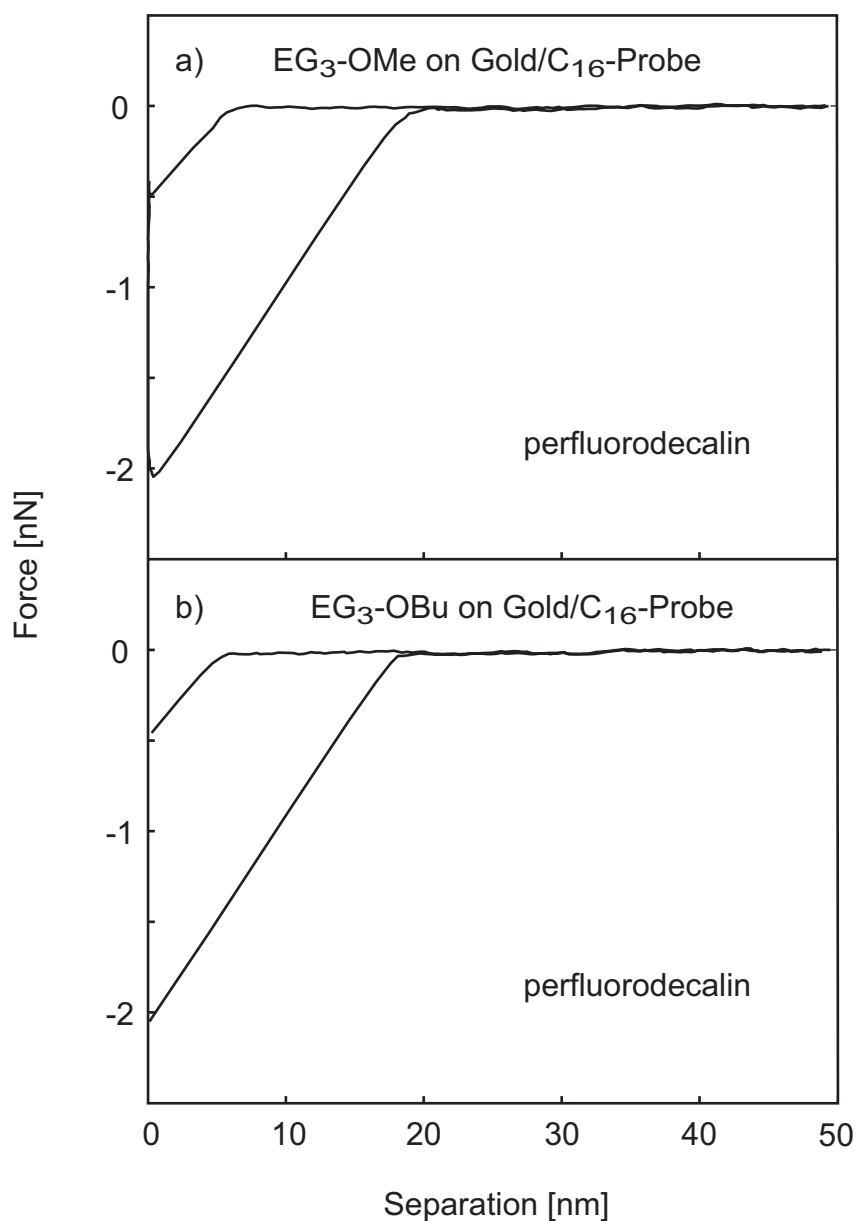

Figure 6.5: *Representative force-versus-distance curves measured with a hydrophobic C$_{16}$-probe on a) an EG$_3$-OMe SAM and b) an EG$_3$-OBu SAM in perfluorodecalin.*

It has been shown in an earlier study that force-distance measurements on synthetic organic surfaces, utilising hydrophobic C$_{16}$-probes to mimic proteins approaching the sample, strongly correlate with the capabilities of these surfaces to resist protein adsorption [1]. Therefore, resistance to protein adsorption of the differently terminated tri(ethylene glycol) SAMs has also been subject to investigation. Samples of freshly prepared SAMs have been immersed into PBS solution containing fibrinogen for approximately 30 minutes at a typical concentration of 1mg/ml. Table 6.3 lists the ratios of protein adsorption onto the different EG$_3$ SAMs derived from IR measurements by S. Herrwerth [12]. The amount of adsorbed proteins was quantified by integration of the amide I (1667cm^{-1}) and amide II (1545 cm^{-1}) bands and was normalised to the amount of protein adsorption on a hexadecanethiole monolayer on gold according to a procedure described in literature [10,22].

SAM	Protein Adsorption [%]
EG$_3$-OH	0 ± 8
EG$_3$-OMe	0 ± 8
EG$_3$-OEt	62 ± 8
EG$_3$-OPr	73 ± 8
EG$_3$-OBu	70 ± 8

Table 6.3: *Amount of fibrinogen adsorbing onto the different terminated tri(ethylene glycol) SAMs (measured by S. Herrwerth) [12].*

From Table 6.3 the differently terminated EG$_3$ SAMs can definitely be distinguished into protein resistant and non-resistant SAMs. The -OH as well as the -OMe terminated SAMs show a distinct resistance to protein adsorption, whereas the SAMs of -OEt, -OPr and -OBu clearly adsorb fibrinogen out of 0.15 M buffer solution. This result exactly matches the interaction pattern observed for the different functionalised SAMs with hydrophobically functionalised SFM probes at similar salt concentrations described above. The -OH as well as the -OMe terminated monolayer films show short-range repulsive forces at 0.1 M, whereas the measurements on the SAMs of -OEt, -OPr and -OBu display attractive forces.

6.1.3 SFM image analysis

Samples with distinct areas consisting of EG_3-OMe and EG_3-OBu SAMs were generated on a polycrystalline gold surface applying the µCP technique. SFM images were taken with hydrophobic C_{16}-probes in constant force and lateral force mode simultaneously. Additionally, different liquid environments were chosen.
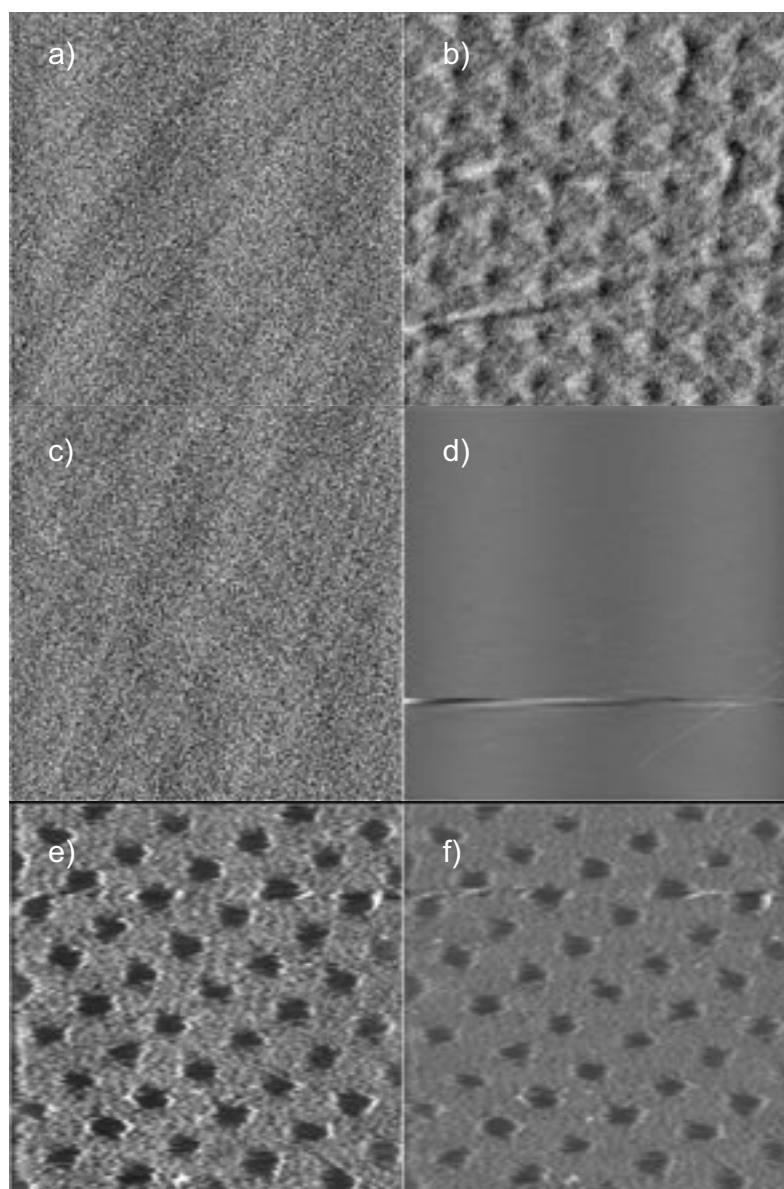
Figure 6.6: *EG_3-OMe/EG_3-OBu µ-patterned surface - topography and lateral force images (15 µm × 15 µm) under a)+b) aqueous KNO_3 0.1 M solution, under c)+d) perfluorodecalin and e)+f) after protein adsorption under 0.15 M phosphate buffer solution. Z range for topography images is 2 nm for a)+c) and 10 nm for and e). Z range for lateral force images is 0.1 V for b)+d) and 0.2 V for f).*

Figures 6.6a and 6.6b show SFM images under 0.1 M aqueous KNO$_3$ solution. The topography image (see Figure 6.6a) does not reveal any information about the spatial distribution of the different functionalised areas. In contrast, the lateral force image plotted in Figure 6.6b clearly resolves the patterned surface chemistry resembling the differently functionalised SAM regions.

Images of the same sample region were taken after exchange of liquids. Perfluorodecalin, a highly apolar liquid with low refractive index, was introduced into the liquid cell and again topography as well as friction images were acquired. Neither the topography image (Figure 6.6c) nor the lateral force image (Figure 6.6d) reveal any information about the spatial distribution of the different surface functionalisation. Note, that the friction contrast observable in Figure 6.6b vanishes completely when the polar electrolyte solution is substituted by the apolar perfluorodecalin.

In a final step, the surface was rinsed with pure ethanol and dried with nitrogen before immersion into a 0.15 M PBS solution containing 1 mg/ml fibrinogen for 30 minutes. The sample was taken out of the solution rinsed thoroughly with pure buffer solution before SFM images were recorded under PBS solution. Figures 6.6e and 6.6f show the corresponding topography and friction force images. In the topography image (Figure 6.6e) a distinct height difference of around 3 nm step size according to adsorbed proteins onto the EG$_3$-OBu functionalised regions is visible. The observed pattern corresponds well to the format shown in Figure 6.6b. The friction force image (Figure 6.6f) displays the same pattern.

6.2 Discussion

6.2.1 Force Spectroscopy Analysis

The force-distance measurements described above were performed in order to explore the influence of varying length of the SAM's terminal alkyl group on the repulsive interaction between hydrophobic probes and EG$_3$ containing monolayers. The -OH and -OMe terminated monolayers show a persistent repulsive behaviour depending on the ionic strength of the electrolyte solution (Figure 6.1). The exponential decay lengths at various salt concentrations are in good agreement with theoretical values predicted by DLVO-theory. In previous chapters this interaction behaviour has been assigned to an effective negative surface charge

due to oriented water molecules and/or the interaction with hydroxyl and hydronium ions from solution at the top of the EG_3 containing SAM [3,4].

Apart from the highest introduced salt concentration, where an additional attractive contribution to the total interaction force (Figure 6.2) can be observed, the interaction behaviour for the -OEt terminated monolayers is similar to that of the -OH and -OMe monolayers. The increasing influence of the observed additional attractive component can be traced very easily in the force-distance measurements of the -OPr and -OBu terminated films (Figure 6.3), where it is even detectable at the more moderate concentration of 0.01 M.

Film characterisation with XPS has revealed similar densities of coverage for all EG_3 monolayers (see Table 6.1) suggesting comparable film properties concerning structure, defect sites, etc. Therefore, the observed differences in the interaction behaviour can be strictly attributed to the varying lengths of the alkyl tails at the top of the EG_3 monolayers.

As already discussed in earlier studies water plays a central role for the observed long-range repulsive interaction [1-4]. Measurements of the water contact angles feature a significant increase in hydrophobicity of the films with increasing length of the alkyl tail (see Table 6.2). This leads to an increasing additional hydrophobic interaction contributing to the total interaction force between the EG_3 monolayers and the hydrophobic C_{16}-probe. At high concentrations, where the DLVO-type repulsive force exhibits very short decay lengths the influence of the hydrophobic interaction is clearly observable. The attractive hydrophobic interaction starts to dominate the short-range repulsive force at 0.1 M in the case of the -OEt films and even at 0.01 M in the case of the -OPr and the -OBu films.

The force-distance curve shown in Figure 6.2b for the -OEt films at 0.1 M gives clear evidence for the competition between the DLVO-like short-range repulsive force and the attractive hydrophobic interaction.

In the previous chapters, however, it has been suggested that the electrostatic repulsion derives from a strong interaction of water molecules with the EG units of the monolayer and a subsequent adsorption of hydroxyl ions leading to a negative surface charge density [3,4]. According to a theoretical study by Pertsin et al. a possible preferential association of the water molecules to the SAM has been stressed [7]. In addition, strong hydrogen bonds as emphasised by Smith et al. are supposed to promote the establishment of an interfacial water layer [23]. This, in turn, stabilises the adsorption of negatively charged hydroxyl ions and hence explains the observed DLVO-like behaviour. Introduction of additional alkyl groups at

the top of the SAM gives rise to the increase in the attractive hydrophobic contribution. In a simple model both interactions can be thought to independently contribute to the total interaction force. This leads to a superposition of the two forces as described by Equation 6.1.

The competition between both contributions is displayed in evidence in Figure 6.2b. The abundantly clear consistency of analytical fit, employing Equation 6.1, and experimental data affirms the additive superposition of repulsive electrostatic and attractive hydrophobic forces. For the repulsive force described by Equation 6.2, a decay length of 1.3 nm is found, which is in good agreement with the value predicted by DLVO theory. The two contributions to the attractive force following Equation 6.3 exhibit decay lengths of around 1 nm for the short range and approximately 4 nm for the long range hydrophobic interaction, respectively. Although the latter is of rather short range compared with values discussed in literature [13,14,24,25], it is in good agreement with values that have been observed in Chapters 4 and 5 on bare hexadecanethiol SAMs adsorbed on polycrystalline gold [3,4].

Another reason for the interaction observed above might be the suppressed hydration of the EG units due to the longer terminating alkyl tails. In a recent study it has been shown that the hydration of the ethylene glycol entities is very low near the EG/hydrocarbon interface and increases towards the outer region of the EG chain [11]. If the conformation of the EG₃ tails in connection with water is responsible for the repulsive interaction in case of the -OH and -OMe SAMs, it might be possible, however, that the requisite hydration of the EG entities is impeded by the enhanced terminating hydrophobic tail. In fact, it has been shown, that at the top of the EG SAM the alkyl tails tend to organise with increasing length in a similar way to the alkyl backbone below the EG strands [26-28]. This result perfectly supports the picture of a hindering barrier.

At low salt concentrations corresponding to longer decay lengths, however, the interfering influence of the enhanced alkyl tails cannot be observed directly. The order of magnitude of the hydrophobic interaction is generally treated to be rather independent from the salt concentration [3,4]. Thus, assuming similar decay lengths for the attractive contributions as observed in Figure 6.2b results in vanishing strength of the attractive contribution. With this the interaction at low salt concentrations can almost exclusively be described by the repulsive electrostatic contribution (compare Equation 6.2). Therefore, from the results described above it can be concluded that the hydration of the EG entities remains rather unhindered despite the increasing length of the alkyl tail. Consequently, the preferential

association of water molecules to the EG entities due to strong hydrogen bonds as stressed in Chapter 5 is hypothesised to take place *within* the EG layer and not exclusively at the SAM/electrolyte interface. The interfacial water layer, which is suggested to serve as a template for hydroxyl ion adsorption as proposed for the EG3-OMe films previously, is therefore not hampered seriously by the enhanced hydrophobic tails.

Furthermore, the clear tendency for the diminution of the repulsive interaction at the highest introduced concentration of the electrolyte solution in the force-distance data can be discussed from another point of view. The vanishing resistance to protein adsorption with increasing alkyl tail at the top of the EG_3 SAM listed in Table 6.3 correlates strongly with the force-distance measurements at a salt concentration of 0.1 M presented above. All films, that have proven resistance to protein adsorption (-OH and -OMe), feature repulsive interaction forces, whereas the other films (-OEt, -OPr and -OBu) display attractive forces at comparable salt concentrations. As a consequence, force spectroscopy in this particular setup is able to predict protein resistance of the films [1].

6.2.2 SFM Image Analysis

The different capabilities of the EG_3-OMe and EG_3-OBu monolayers to resist protein adsorption can be distinguished very well from the μC-printed pattern in Figures 6.6e and 6.6f. A dense protein film with a thickness of around 3 nm is formed on the μC-printed -OBu film, whereas no protein adsorption can be traced on the solution-grown -OMe film. The thickness of the protein layer on the EG_3-OBu terminated surface areas is in good agreement with ellipsometry measurements (not explicitly shown) taken on the normally prepared solution-grown EG_3-OBu SAM.

The characteristic pattern generated by the μCP technique is also visible for the bare films, but only in the lateral force image (Figure 6.6b). Despite the difference in length of 3 alkyl groups no height difference is displayed in the topography image (Figure 6.6a). The different friction forces established between the hydrophobic C_{16}-probe and the EG_3-OMe and EG_3-OBu films, respectively, can be explained by the significant difference in adhesion forces found in the force-distance measurements (Figures 6.4a and 6.4b).

In the case of good comparability of chemical composition and structure of the films conclusions about the friction behaviour can be deduced from the adhesion forces [29-31].

Taking Figures 6.4a and 6.4b and the displayed pronounced difference in the pull-off forces into account, it is not astonishing that the lateral force image in Figure 6.6b taken under 0.1 M KNO$_3$ illustrates the µC-printed pattern clearly. Another reason for the different friction properties displayed in this image might be due to the different process of deposition. While the -OBu terminated areas of the film were achieved employing the µCP technique, the -OMe areas simply formed due to immersion into the corresponding solution. This has been shown to lead to morphological and conformational differences in the film composure resulting in differing friction properties [32-34]. To reduce or even exclude this influence images were recorded under highly apolar perfluorodecalin, where force-distance curves have proven almost identical interaction behaviour between hydrophobic probes and the SAM surfaces (Figures 6.5a and 6.5b). Here, no differences in either topography (Figure 6.6c) or friction (Figure 6.6d) can be distinguished. Therefore, possible disparities in morphological or conformational film properties can be judged to have only a minor influence on the friction force under aqueous KNO$_3$ solution compared to the different chemical composition of the terminal group. In an aqueous environment, however, both films establish different surface properties due to the hydration of the EG entities and the unequal hydrophobic interaction. This results in different interaction behaviour towards hydrophobic probes, which can also be proven from the corresponding force-distance curves (Figures 6.4 and 6.5).

6.3 Conclusions

A series of new tri(ethylene glycol)-containing alkanethiols exhibiting alkyl tails of different lengths has been studied. Force-versus-distance curves between these EG$_3$-containing SAMs and hydrophobic C$_{16}$-probes were recorded under aqueous KNO$_3$ solutions of varying ionic strength. The force curves show a strong dependence on the length of the terminating alkyl group at the SAM surface. It appears that a significant electrostatic component is involved in the repulsive force observed, which becomes suppressed subsequently by an increasing attractive hydrophobic component with increasing alkyl tail. The origin of an effective negative surface charge established on the OEG SAMs was suggested to be due to a preferentially oriented layer of water molecules and/or the interaction with hydroxyl ions from solution in the previous chapters. Given the enhanced terminating

alkyl strands, the preferential orientation of water molecules at the SAM/water interface seems unlikely so that the concept of a thin layer of interfacial water providing a template for hydroxyl ion adsorption as proposed in Chapter 5 is supported strongly by the measurements described above. This interfacial water layer does not appear to be influenced strongly by the enhanced alkyl tail at the top of the EG_3 SAM and is therefore stressed to form *within* the EG layer instead of emerging exclusively at the organic/liquid interface. The alkyl tail rather seems to enhance the hydrophobic component to the interfacial force independently.

The total interaction can thus be described as an additive superposition of an electrostatic repulsion and an attractive hydrophobic interaction. Additional force-versus-distance measurements performed under perfluorodecalin underline the significance of water for the interaction. SFM image analysis further supports the force-distance data and illustrates the different capabilities to protein resistance of these chemically very similar SAM surfaces. Finally, protein adsorption measurements and force-distance measurements on the EG_3-OR samples utilizing hydrophobic C_{16}-probes proved to be in very good agreement.

6.4 Literature

[1] Feldman, K.; Hähner, G.; Spencer, N. D.; Harder, P.; Grunze, M. *J. Am. Chem. Soc.* **1999**, *121*, 10134

[2] Dicke, C.; Feldman, K.; Eck, W.; Herrwerth, S.; Hähner, G. *Pol. Prep.* **2000**, *41*, 1444

[3] Dicke, C.; Hähner, G, *J. Phys. Chem. B* **2001**, *106*, 4450

[4] Dicke, C.; Hähner, G, *J. Am. Chem. Soc.* **2002**, *124,* 12619

[5] Prime, K. L.; Whitesides, G. M. *J. Am. Chem. Soc.* **1993**, *115*, 10714

[6] Harder P.; Grunze, M.; Dahint, R.; Whitesides, G. M.; Laibinis P. E. *J. Phys. Chem. B* **1998**, *102*, 426

[7] Pertsin, A. J.; Grunze, M. *Langmuir* **2000**,*16*, 8829

[8] Zolk, M.; Eisert, F.; Pipper, J.; Herrwerth, S.; Eck, W.; Buck, M.; Grunze, M *Langmuir* **2000**, 16, 5849

[9] Taunton, H. J.; Toprakcioglu, C.; Fetters, L. J.; Klein, J. *Nature* **1988**, 712

[10] Schwendel, D.; Dahint, R.; Herrwerth, S.; Schloerholz, M.; Eck, W.; Grunze, M. *Langmuir* **2001**, *17*, 5717

[11] Caldararu, H.; Caragheorheopol, A.; Schlick, S. *Bull. Pol. Acad. Sc. Chem.* **2000**, *48*, 367

[12] Herrwerth, S. *private communication*

[13] Rabinovich, Y. I.; Yoon, R.-H. *Colloids and Surfaces A* **1994**, *93*, 263

[14] Yoon, R.-H.; Flinn, D. H.; Rabinovich, Y. I. *J. Colloid Interf. Sc.* **1997**, *185*, 363

[15] Israelachvili, J. N.; Pashley, R. M. *Nature* **1982**, *300*, 341

[16] Pashley, R. M.; McGuiggan, P. M.; Ninham, B. W.; Evans, D. F. *Science* **1985**, *98*, 500

[17] Claesson, P. M.; Christenson, H. K. *J. Phys. Chem.* **1988**, *92*, 1650

[18] Herder, P. C. *J. Colloid. Interface Sci.* **1991**, *143*, 573

[19] Parker, J. L.; Claesson, P. M. *Langmuir* **1994**, *10*, 635

[20] Podgornik, R. *J. Chem. Phys.* **1991**, *154*, 477

[21] Rabinovich, Y. I.; Yoon, R.-H. *Langmuir* **1994**, *10*, 1903

[22] Liedberg, B.; Ivarson, B.; Lundstroem, I. *J. Biochem. Biophys. Methods* **1984**, *9*, 233

[23] Smith, D. A.; Wallwork, M. L.; Zhang, J.; Kirkham, J.; Robinson, C.; Marsh, A.; Wong, M *J. Phys. Chem.* B **2000**, *104*, 8862

[24] Ederth, T.; Claesson, P.; Liedberg, B. *Langmuir* **1998**, *14*, 4782

[25] Hato, M. *J. Phys. Chem.* **1996**, *100*, 18530

[26] Vanderah, D. J.; Meuse, C. W.; Silin, V.; Plant, A. L. *Langmuir* **1998**, *14*, 6916

[27] Vanderah, D. J.; Pham, C. P.; Springer, S. K.; Silin, V.; Meuse, C. W. *Langmuir* **2000**, *16*, 6527

[28] Zwahlen, M. *private communication*

[29] Carpick, R. W.; Salmeron, M. *Chem. Rev.* **1997**, *97*, 1163

[30] Green, J.-B. D.; McDermott, M. T.; Porter, M. D. *J. Phys Chem.* **1995**, *99*, 10960

[31] Frisbie, C. D.; Rosznyai, L. F.; Noy, A.; Wrighton, M. S.; Lieber, C. M. *Science* **1994**, *265*, 2071

[32] Eberhardt, A. S.; Nyquist, R. M.; Parikh, A. N.; Zawodzinski, T. A.; Swanson, B. I. *Langmuir*, **1999**, *15*, 1595

[33] Fischer, D.; Marti, A.; Hähner, G. *J. Vac. Sci. Technol. A.* **1997**, *15*, 2173

[34] Bar, G.; Rubin, S.; Parikh, A. N.; Swanson, B. I.; Zawodzinski, T. A., Jr.; Whangbo, M.-H. *Langmuir*, **1997**, *13*, 373

Chapter 7

Force Spectroscopy on derivated Hexa(Ethylene Glycol)-containing Self-Assembled Monolayers

In the previous chapter it has been shown that additional aliphatic end groups exert a crucial influence on the protein-resistance properties of EG_3-containing monolayers. A competition between electrostatic repulsion and attractive hydrophobic interaction has accounted for the complete vanishing of the repulsive forces with longer terminating alkyl groups. An enhancement in the number of EG units on the other hand might reinforce the repulsive component to the total interaction force. In fact, EG_6-containing SAMs have been found to feature better protein-resistant capabilities than EG_3-containing monolayers [1,2]. Schwendel et al. have studied the temperature-dependence of the protein resistance of poly- and oligo(ethylene glycol)-terminated alkanethiolate SAMs. It has been found that EG_3-OMe monolayers prepared on polycrystalline gold adsorb a significant amount of proteins below 20° C, whereas EG_6 SAMs remain protein resistant for temperatures ranging from 0° to 85° C [2]. In addition, unlike EG_3-terminated monolayers, SAMs prepared from EG_6 alkanthiolates have proven a high degree of variability in conformation ranging from a crystalline, helical phase to an amorphous phase [3], which is characteristic of PEG chain conformations in the liquid state [4].

Vanderah and coworkers, as well as Liedberg and coworkers have also found stable helical structures for similar EG_6-containing SAMs [5-8]. An additional amide group at the junction of alkyl backbone and EG units has been shown to even improve film structure and stabilise the helical conformation of the EG units [7,8]. Inverted SAM structures, where the EG units are directly attached to the surface active thiolate group followed by the alkane

chain, have been found to adopt helical conformation in the EG region, whereas the terminating alkane chains consisting of 10 or even 18 carbon atoms have proven a similar all-trans conformation with even a comparable tilt angle towards the surface as already known from 'regular' OEG SAMs used in this study [5,6].

In order to study the influence of increasing hydrophobic end groups on the protein resistance properties of these synthetic surfaces in more detail, a series of novel hexa(ethylene glycol)-containing (EG_6-OR; R = H, Me, Et, Pr and COOH) alkanethiols was prepared on polycrystalline gold surfaces. X-ray photoelectron spectroscopy and contact angle measurements have been performed for film characterisation of the afore newly synthesised alkanethiols prior to force-distance analysis [9].

7.1 Results

7.1.1 Film Characterisation by XPS and Contact Angle Measurements

X-ray photoelectron spectroscopy was used by S. Herrwerth at University of Heidelberg to ensure quality and coverage of the EG_6-OR-containing films prepared by self-assembly, while contact angle measurements were performed in order to quantify film wettability [9].

The relative density and thus the coverage of the monolayers displayed in Table 7.1 were determined according to literature [3].

SAM	Relative Density [%]
EG_6-OH	74 ± 4
EG_6-OMe	71 ± 4
EG_6-OEt	71 ± 4
EG_6-OPr	71 ± 4
EG_6-OCOOH	70 ± 4

Table 7.1: *Relative density of the differently terminated hexa(ethylene glycol) SAMs (measured by S. Herrwerth) [9].*

The differently terminated EG$_6$ SAMs show relative coverages of around 70% of that of a hexadecanethiol SAM. All films appear to exhibit a similar coverage within the experimental error. These values are slightly lower than for the derivated EG$_3$ SAMs described in the previous chapter.

From Table 7.2 the varying wettabilities of the different terminated EG$_6$ films can clearly be observed. The advancing water contact angles display a strong dependency on the terminating functional group [9].

SAM	Contact angle [°]
EG$_6$-OCOOH	15 ± 3
EG$_6$-OH	32 ± 3
EG$_6$-OMe	67 ± 3
EG$_6$-OEt	87 ± 3
EG$_6$-OPr	97 ± 3

Table 7.2: *Advancing contact angle measurements at the different terminated tri(ethylene glycol) SAM surfaces (measured by S. Herrwerth) [9].*

The lowest contact angle of 15° was found for the carboxyl-functionalised EG$_6$ SAM. This low value indicating a highly hydrophilic surface is due to the terminating -OCOOH group. For the -OH terminated SAM a value of 32° was determined. This value increases subsequently with increasing alkyl tail. A value of 67° was found for the -OMe SAM, while the -OEt SAM showed a contact angle of 87°. Finally, the -OPr SAM exhibits the highest value for the contact angle of 97° indicating a strong hydrophobicity. The stepwise increase of the advancing water contact angles with increasing alkyl tail reflects the strong influence of the terminating groups on the ethylene glycol strands with respect to the wettability of the self-assembled structure.

7.1.2 Force Spectroscopy Analysis

Force-versus-distance measurements have been performed with hydrophobically functionalised C$_{16}$-probes under electrolyte solution at room temperature. Aqueous KNO$_3$ solution at varying ionic strength and constant neutral pH-value was chosen as 'standard

electrolyte' according to earlier studies [10-13]. As described in Chapter 2, at least 64 force curves over an area of 2 μm × 2 μm were recorded per sample. The resulting averaged force-distance curves are displayed below.
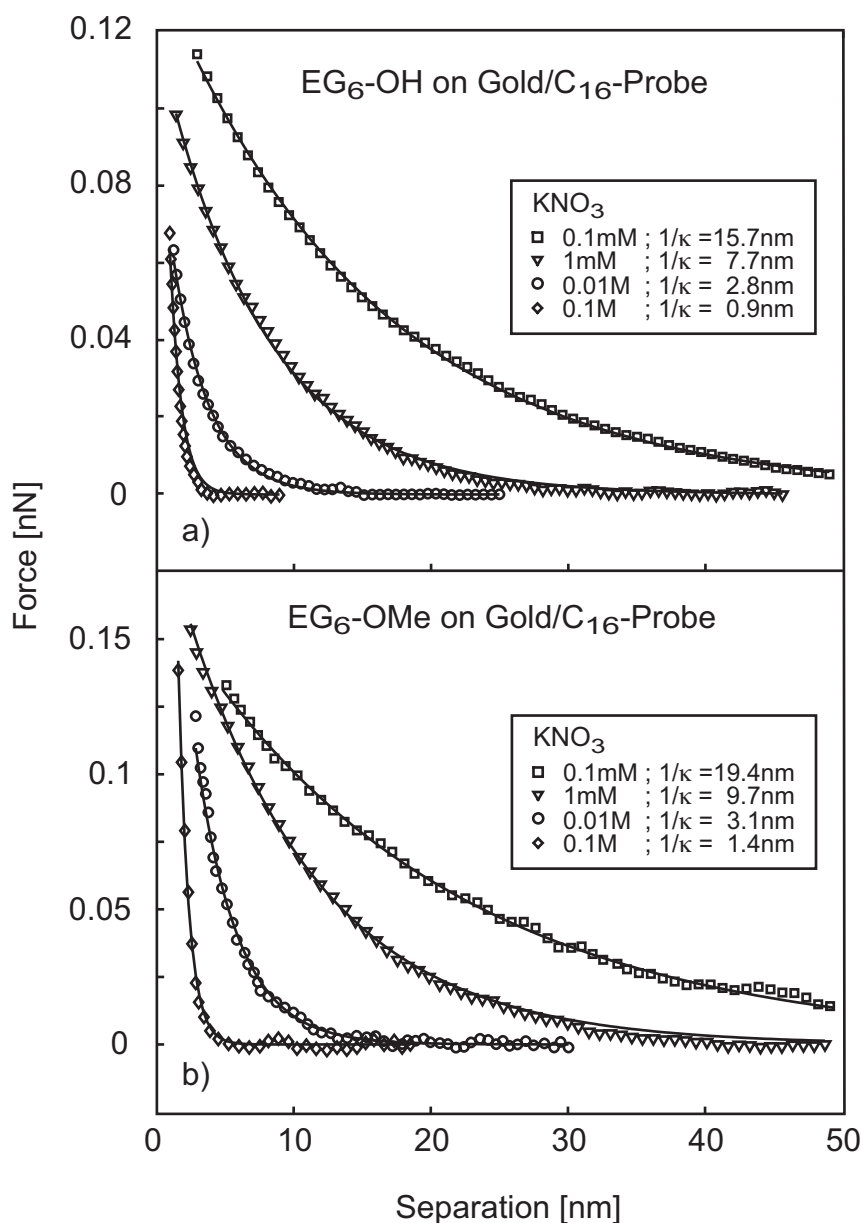

Figure 7.1: *Advancing force-versus-distance curves (averaged) measured with a hydrophobic C_{16}-probe on a) an EG_6-OH SAM and b) an EG_6-OMe SAM on gold in aqueous KNO_3 solution at different concentrations (◇ - 0.1M; ○ - 0.01M; ▽ - 1mM; □ - 0.1mM).*

Figure 7.1 shows advancing force-distance curves recorded on an EG_6-OH SAM (Figure 7.1a) and an EG_6-OMe SAM (Figure 7.1b), respectively. Both measurements display a similar interaction pattern towards the hydrophobic probe. For the lowest introduced salt

concentration of 0.1 mM an exponentially decaying repulsive force of long range can be observed. Increasing the salt concentration by factors of ten, subsequently, results in a stepwise reduction of the decay length of the repulsive force. At the highest introduced concentration of 0.1 M the repulsive force is of very short range. A strong dependency of the repulsive force upon the ionic strength of the solution known from the previous chapters can be observed.

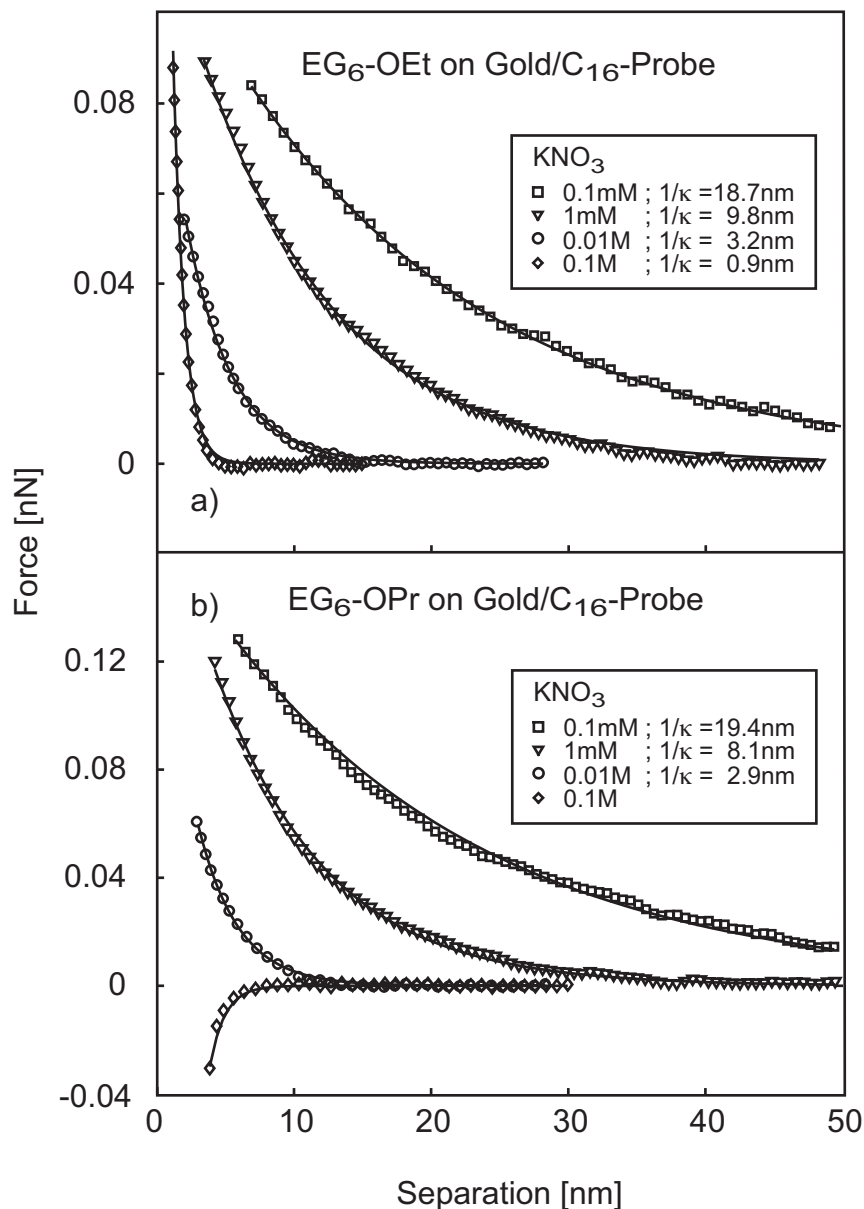***Figure 7.2:*** *Advancing force-versus-distance curves (averaged) measured with a hydrophobic C_{16}-probe on a) an EG_6-OEt SAM and b) an EG_6-OPr SAM on gold in aqueous KNO_3 solution at different concentrations (◇ - 0.1M; ○ - 0.01M; ▽ - 1mM; □ - 0.1mM).*

In Figure 7.2, force-distance curves for EG$_6$ SAMs with slightly enhanced alkyl tails and therefore more hydrophobic end groups (compare Table 7.2) are displayed. The observed interaction force between the hydrophobic probe and both an EG$_6$-OEt SAM as well as an EG$_6$-OPr SAM, appears to be very similar to the force-curves shown in Figure 7.1. A subsequent decrease in the exponentially decaying repulsive force originates from increasing the salt concentration of the aqueous solution. Only the force-distance curves recorded at the highest ionic strength in the case of the EG$_6$-OPr SAM shows a significant difference to the other measurements at this concentration. Instead of a short-range repulsive force, an attractive force is detectable, which illustrates the effect of increasing hydrophobicity of the film by further extension of the alkyl tail by another alkyl group.
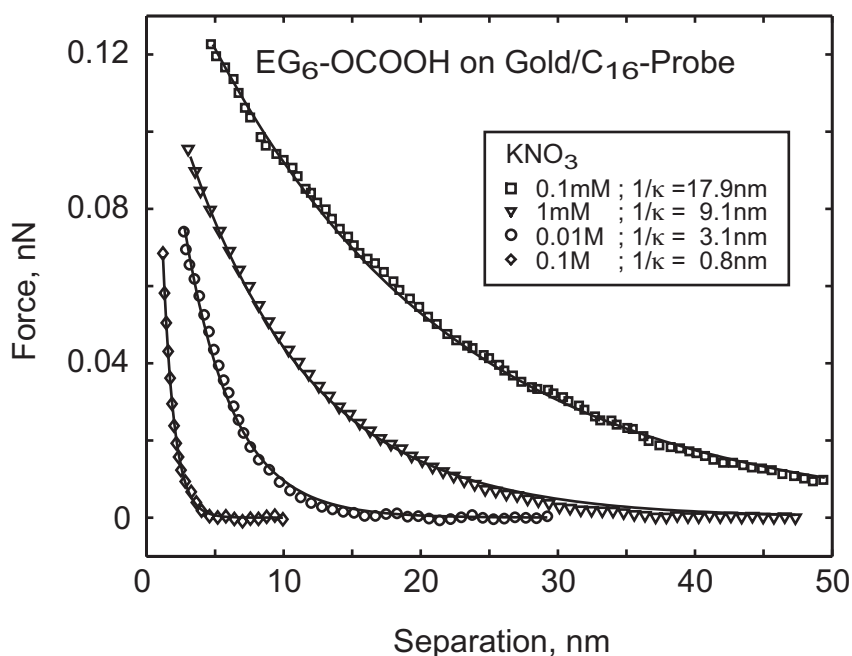

Figure 7.3: *Advancing force-versus-distance curves (averaged) measured with a hydrophobic C$_{16}$-probe on an EG$_6$-OCOOH SAM on gold in aqueous KNO$_3$ solution at different concentrations (◇ - 0.1M; ◯ - 0.01M; ▽ - 1mM; □ - 0.1mM).*

Force-distance curves at varying ionic strengths recorded on an EG$_6$-OCOOH SAM are shown in Figure 7.3. At neutral pH-values the carboxyl group at the top of the SAM is deprotonated, what from a net negative surface charge density originates. The resulting repulsive interaction force between the model organic surface and the hydrophobically functionalised SFM probe again shows a clear dependence upon the salt concentration of the KNO$_3$ solution. The exponential decay length of the repulsive force decreases subsequently with increasing ionic strength.

7.2 Discussion

7.2.1 Film Characterisation by XPS and Contact Angle Measurements

The relative densities of the differently terminated hexa(ethylene glycol)-containing monolayers show very similar values within the experimental error. Compared to a hexadecanethiol film, the cover rates are around 70%. These values are slightly lower than the values of the correspondent tri(ethylene glycol)-containing monolayers discussed in the previous chapter, where values around 80% have been found [9,12]. According to the good agreement in terms of monolayer coverage within the experimental errors comparable film properties concerning structure, defect sites, etc. can be assumed.

In addition, advancing water contact angle measurements have been performed to study the wettability of the different EG$_6$ SAMs. Depending on the terminating group the hydrophilicity/hydrophobicity of the EG$_6$ monolayers shows a similar behaviour as already observed for the shorter EG$_3$ SAMs earlier [12]. With increasing alkyl tail the contact angle measurements feature a significant increase in film hydrophibicity on the one hand, whereas the terminating hydroxyl and carboxyl groups on the other hand are responsible for very low hydrophilic values. Within the experimental error the single values for the different terminating alkyl tail lengths are in very good agreement for both the EG$_3$ and the EG$_6$ SAMs.

Due to the enhanced hydrophobic character of the SAMs with increasing alkyl tail a pronounced contribution of the hydrophobic interaction could be also observed in force spectroscopy measurements for the shorter EG$_3$ SAMs [12]. Correspondingly, a comparably important role of the hydrophobic interaction because of the similar film properties can be expected for the EG$_6$ SAMs.

7.2.2 Force Spectroscopy Analysis

Force-distance measurements on the differently terminated hexa(ethylene glycol)-containing monolayers have been acquired with hydrophobic probes in order to study the influence of increasing hydrophobic alkyl tails at the top of EG$_6$ SAMs on the interaction force. All force-distance curves display a strong dependency of the repulsive force on the ionic strength of the salt solution. Additionally, at higher concentrations the interaction of the

hydrophobic probe and the EG_6-OPr SAM displays an attractive force, whereas all other SAMs with shorter alkyl tails do not. This particular concentration-dependent interaction behaviour has been observed for other oligo(ethylene glycol)-containing SAMs in the previous chapters [10-13]. The fact that the exponential decay lengths of the repulsive forces scale with values predicted by DLVO theory (compare Table 4.3), leads to the suggestion that surface charges are involved in the interaction, although the surfaces of probe and sample are intrinsically uncharged. It has been discussed in the previous chapters that the charges associated with the synthetic organic films might, for example, be due to the adsorption of hydroxyl ions onto the EG interface mediated by an interfacial water film associated with the OEG tail [11]. It is conceivable that the establishment of a water interface directly associated to the EG strands at the top of the SAM surface via hydrogen bonds can be disturbed or even destroyed by introducing a hindering barrier such as additional alkyl tails. Such alkyl tails terminating an EG polymer chain have been shown to hinder the hydration of the EG entities dramatically [14].

A similar study emphasising this concept has already been performed on similarly alkyl terminated EG_3 SAMs as described in Chapter 6 [12]. The effect of additional alkyl tails on the interaction force has been interpreted as the preferentially oriented association of water molecules or ions to the EG strands taking place *in* the utmost layers of the SAM rather than exclusively in a pronounced layer at the very top of the SAM surface. This suggestion is in good agreement with theoretical studies of Pertsin et al., who studied the spatial distribution of water at the SAM/water interface of such OEG films [15]. Basically, the interaction behaviour observed in Chapter 6 is similar to the interaction between the hydrophobic C_{16}-probe and the differently terminated EG_6-derivates reported here. The striking difference between both studies is the critical length of the hydrophobic alkyl tail, from which point the hydrophobic interaction becomes more important and the repulsive DLVO-like interaction vanishes. Comparing both studies, it is important to note that in case of the EG_6 SAMs one more alkyl group is necessary to tune the interaction force from repulsive to attractive at a salt concentration of 0.1 M. For the EG_6-OPr SAM thus the force-versus-distance dependence displays the same interaction behaviour as was observed for the EG_3-OEt SAM in Chapter 6.

This result is somewhat consistent with investigations of the 'strength' of the protein resistance of such films [1,2]. Over a temperature range from 0° to 85° C EG_6 monolayers

have been proven to resist the non-specific adsorption of proteins, whereas EG$_3$ SAMs have been found to adsorb proteins at lower temperatures up to 20° C. A thin layer of interfacial water associated to the EG strands via hydrogen bonds as emphasised in Chapter 5 will be strongly affected by the temperature of the aqueous solution and therewith the thermal motion of the water molecules [11]. Taking into account the energy of solvation of the EG entities, however, a complete dehydration appears to be unlikely [16]. In fact, a more pronounced EG structure as provided by the EG$_6$ SAMs might be able to 'trap' water molecules better than less enhanced EG layers as present at the top of EG$_3$ SAMs.

Of course, film properties have to be comparable to draw a final conclusion on this phenomenon. The relative densities of EG$_6$ monolayers (Table 7.1) for example are found to be slightly lower than observed for EG$_3$ SAMs (compare Table 6.1). This might lead to a better accessibility of the EG units in case of the EG$_6$ films, so that water molecules or ions can diffuse easier into the topmost layer of the SAM. Contact angle measurements on the other hand reveal almost identical values for both series suggesting very similar conformations of the terminating alkyl groups at the top of the SAMs. In fact, NEXAFS studies have shown that the relative order of the SAMs increases with increasing number of alkyl groups, suggesting a well-defined conformation in the terminating alkyl tail similar to that in the alkyl backbone of the SAM [17].

According to Caldararu et al., the hydrophobic alkyl groups hinder the hydration of the EG units close to the junction [14]. In this picture, the results presented above can be interpreted in a way, that the 'longer', less densely packed EG strands at the top of the EG$_6$ SAM surface might be able to overcome the hindering influence of the added alkyl tails. As a result the hydration of the ethylene glycol units is more stable and a more enhanced alkyl termination of the SAM is needed to hamper the water association to the EG strands. This further supports the idea of a reaction of the EG entities with water molecules or ions, respectively, *in* the topmost layers of the SAM instead of a pronounced oriented water layer. Comparing the results for the EG$_3$ and EG$_6$ monolayer films, the interfacial water layer associated to the EG moieties of the SAM as proposed in Chapter 5 appears to be more stable against addition of hydrophobic tail groups with increasing number of EG units.

Another approach has been investigated by substituting the alkyl end groups with a reactive carboxyl group. At neutral pH-values, the -OCOOH group is deprotonated and this leads to the establishment of a negative surface charge density at the SAM. Thus, the corresponding force-distance curves display concentration-dependent repulsive forces with exponential decay lengths comparable to the theoretical values predicted for the Debey length. This DLVO-like interaction behaviour has already been observed for the -OH and -OMe SAMs, although these SAM films are immanently uncharged. The almost identical interaction behaviour of the -OCOOH SAM further supports the earlier suggestion, that the interaction of oligo(ethylene glycol)-terminated surfaces and hydrophobic probes generally can be treated as electrostatically mediated.

The good comparability in film structure proven by XPS measurements as well as in the interaction behaviour towards hydrophobic probes of these monolayers suggests similar properties concerning protein resistance. The strong hydrophilic -OCOOH terminated SAMs, however, adsorb proteins intrinsically due to the charge established at its surface after deprotonation. Nevertheless, interesting applications in the field of biosensors can be derived from this observation. For example, mixed SAM films consisting of -OMe and low fractions (<0.10) of -OCOOH can offer the possibility to tailor ultrathin homogeneous surface layers to be protein resistant with distinct islands offering adsorption sites, which can be activated utilising the reactive -OCOOH group [18,19]. A similar approach utilising short chain PEG has been reported by Herrwerth et al. [20]. Carboxyl-terminated EG_{33} films have been found to suppress non-specific adsorption and to provide specific linkage sites simultaneously. By activating the terminal carboxyl-groups antibodies can be covalently attached to the films following a general procedure [21], with the films still featuring resistance to non-specific adsorption. Due to specific antigen-antibody recognition it was possible to adsorb antigens to the films specifically without interfering effects due to non-specific interactions of proteins with the film. This way, the central problem in sensor technology [22], the discrimination between specific and non-specific signals, could effectively be solved.

In contrast to polymer films, end-functionalised self-assembled monolayers provide much thinner and better-defined surfaces. Therefore, the approach using EG_6-SAMs promises better suitability for future applications such as biosensor materials, where miniaturisation

plays a major role. The smaller a component becomes, the better defined and controlled its structure has to be.

7.3 Conclusions

A series of novel hexa(ethylene glycol)-containing alkanethiols self-assembled on polycrystalline gold surfaces has been analysed by means of chemical force spectroscopy. Force-versus-distance analysis utilising hydrophobic C$_{16}$-probes revealed the strong DLVO-like character of the interaction force, which becomes suppressed at higher salt concentrations by the addition of enhanced alkyl tails to the functional end group. The difference between EG$_3$ and EG$_6$ SAMs in number of hydrophobic alkyl groups necessary to dominate the interaction represents a strong hint for the preferential hydration of the EG units and the subsequent adsorption of hydroxyl ions to the EG strands *in* the utmost layers of the SAM. Depending on the length of alkyl tail and EG unit the competition between electrostatic repulsion and hydrophobic attraction can be altered. This further supports the picture of a preferential association of water molecules to the EG moieties of the SAM penetrating the topmost layers of the same and underlines the importance of its stability, because the so generated interfacial water layer has been suggested earlier to provide a template for the consecutive adsorption of hydroxyl ions establishing a net negative surface charge density [11].

Furthermore, EG$_6$ SAMs with a terminal carboxylic group have been studied. Due to the deprotonation these SAMs carry a total negative surface charge density at neutral pH-values, which is responsible for the clearly DLVO-like interaction observed in Figure 7.3. Because the carboxyl group can easily be addressed via a chemical reaction, intrinsically protein resistant EG$_6$-OMe SAMs containing low fractions of -COOH promise highly interesting applications in the field of applied biosensors.

7.4 Literature

[1] Prime, K. L.; Whitesides, G. M. *J. Am. Chem. Soc.* **1993**, *115*, 10714

[2] Schwendel, D.; Dahint, R.; Herrwerth, S.; Schloerholz, M.; Eck, W.; Grunze, M. *Langmuir* **2001**, *17*, 5717

[3] Harder, P.; Grunze, M.; Dahint, R,; Whitesides, G. M.; Laibinis, P. E. *J. Phys. Chem. B* **1998**, *102*, 426

[4] Harris, J. M. *Poly(Ethylene Glycol) Chemistry*, Plenum Press, New York, **1992**

[5] Vanderah, D. J.; Meuse, C. W.; Silin, V.; Plant, A. L. *Langmuir* **1998**, *14*, 6916

[6] Vanderah, D. J.; Pham, C. P.; Springer, S. K.; Silin, V.; Meuse, C. W. *Langmuir* **2000**, *16*, 6527

[7] Valiokas, R.; Svedhelm, S.; Svensson, S. C. T.; Liedberg, B. *Langmuir* **1999**, *15*, 3390

[8] Valiokas, R.; Svedhelm, S.; Ostblom, M.; Svensson, S. C. T.; Liedberg, B. *J. Phys. Chem. B* **2001**, *105*, 5459

[9] Herrwert, S. *private communcication*

[10] Dicke, C.; Hähner, G. *J. Phys. Chem. B* **2002**, *106*, 4450

[11] Dicke, C.; Hähner, G. *J. Am. Chem. Soc.* **2002**, *124,* 12619

[12] Dicke, C.; Hähner, G.; Herrwerth, S.; Eck, W.; Grunze, M. *in preparation*

[13] Feldman, K.; Hähner, G.; Spencer, N. D.; Harder, P.; Grunze, M. *J. Am. Chem. Soc.* **1999**, *121*, 10134

[14] Caldararu, H.; Caragheorheopol, A.; Schlick, S. *Bull. Pol. Acad. Sc. Chem.* **2000**, *48*, 367

[15] Pertsin, A. J.; Grunze, M. *Langmuir* **2000**, *16*, 8829

[16] Wang, R. L. C.; Kreuzer, H. J.; Grunze, M. *Phys. Chem. Chem. Phys.* **2000**, *2* 3613

[17] Zwahlen, M. *private communication*

[18] Lahiri, J.; Ostuni, E.; Whitesides, G. M. *Langmuir* **1999**, *15*, 2055

[19] Lahiri, J.; Isaacs, L.; Tien, J.; Whitesides, G. M. *Anal. Chem.* **1999**, *71*, 777

[20] Herrwerth, S. Dissertation, Ruprecht-Karls-Universität Heidelberg, **2002**

[21] Vaughan, R. D.; O'Sullivan, C. K.; Guilbault, G. G. *Fres. J. Anal. Chem.* **1999**, *364*, 54

[22] Göpel, W.; Jones, T. A., Kleitz, M.; Lundström, I.; Seiyama, T. *Chemical and Biochemical Sensors*, Weinheim, VCH, **1991**

Chapter 8

Conclusions and Outlook

This thesis is concerned with surface coatings for modern technological applications, in particular biomaterials. Ultrathin films with specifically tailored properties represent a highly promising class of such modern surface coatings. Therefore, particular focus has been spent on self-assembled monolayers as model systems for synthetic organic surfaces. SAMs have become of great interest over the last twenty years because of their well-defined structural and chemical properties, long-term stability and therefore their significant technological potential for various applications.

In this work, extensive effort has been spent on SAMs of oligo(ethylene glycol)-containing alkanethiols adsorbed on polycrystalline gold surfaces to explore the driving forces responsible for protein resistance. Atomic force microscopy equipped with a liquid cell and specifically functionalised probes has been employed in order to mimic proteins approaching the synthetic model surfaces in a typical natural environment. Prior to force-distance analysis, X-ray photoelectron spectroscopy as well as contact angle measurements have been performed to characterise film properties and ensure monolayer quality.

Force-versus-distance curves between different OEG-containing SAMs and hydrophobic probes have been recorded under different electrolyte solutions and for varying ionic strength. From these measurements it appears that a significant electrostatic component is involved in the observed repulsive force. In another series of experiments, in which the influence of differently charged probes and varying pH-values has been subject to exploration, it could be proven that an effective negative surface charge is established at the SAM/water interface.

A model has been proposed that assigns the establishment of this net negative surface charge density to a thin layer of interfacial water and the consecutive adsorption of hydroxyl ions from solution. This seems particularly likely since the specific affinity of some of the ions dissolved in the electrolyte solution to the ethylene glycol interface could be excluded by additional XPS and ToF-SIMS analysis.

By varying the number of hydrophobic tail groups at tri- and hexa(ethylene glycol)-containing monolayers the ability of these films to resist non-specific adsorption of proteins could be sensitively tuned. It emerges that the addition of single methylene units is a crucial parameter in the interaction with the hydrophobic probe. With an increasing number of alkyl groups, the aliphatic terminal groups appear to establish a barrier for the water molecules or ions to diffuse into the film, which, in turn, causes a loss in resistance to the adsorption of proteins. Thus, the concept of a preferential association of water with the EG moieties involves penetration *into* the topmost layers of the SAM rather than occuring exclusively at the SAM/electrolyte interface. This layer of interfacial water is suggested as being crucial for the stability of charge establishment and ultimately the decisive factor for the protein resistance of these films.

Furthermore, a model related to the 'two faces of water' has been introduced, which explains the differences observed for polymer (PEG) and oligomer (OEG) films. It is speculated that the extended EG moieties of the monolayer films do not allow the same water arrangement as the polymer chains. While water molecules can surround the free polymer chains completely in a hydrogen-bonded network, the number of hydrogen bonds that can be established between neighbouring water molecules is restricted in the densely packed SAM. Here, the immobilised water molecules seem to form a two-dimensional interfacial layer acting as a template for a successive hydroxyl ion association, resulting in the observed negative surface charge density of these SA structures.

Nonetheless, further investigation of the organic/liquid interface with *in-situ* techniques is still required in order to gain a final understanding of the underlying mechanism responsible for the protein resistance of these synthetic surfaces.

Temperature-dependent force-distance analysis under liquids presents a potential extension of this work in order to probe the effect of Brownian motion of water molecules in the vicinity of the organic surface. An increase in the environmental temperature would

dramatically affect a potentially immobilised layer of interfacial water and thus provide further information about the molecular conformation of the interface. In addition, recently developed Interfacial Force Microscopy (an AFM derivative employing an oscillating probe in close vicinity to the interface with adjustable spring constant to avoid the jump-into-contact) shows great promise for investigating the organic/liquid interface in depth.

An experimental setup probing the structure of the topmost layers of the SAM under electrolyte solution with high local sensitivity/resolution is required to determine the conformation of water molecules or ions at the SAM/water interface conclusively. A technique showing great promise for future studies is *in-situ* InfraRed-Visible Sum Frequency Generation (IR-Vis SFG) because of its intrinsically high interface sensitivity and the specific probing of molecular vibrations. In this way, the proposed layer of interfacial water molecules associated with the EG strands could be proven directly. Another technique that provides information about the orientation of molecules at surfaces is Near-Edge X-ray Adsorption Spectroscopy (NEXAFS). Unfortunately, this technique is presently limited mainly to vacuum conditions, although some effort is being spent on the transfer to ambient and even liquid environments.

The oligo(ethylene glycol)-containing alkanethiols investigated in this work, when used in mixed SAMs consisting of alkanethiols that present other functional groups (e.g. terminal carboxyl groups), isolate the *specific* biomolecular interactions of interest from *non-specific* effects. Therefore, they allow selective adsorption of proteins onto the specifically addressable linkage sites embedded within a protein-resistant matrix, which simplifies fundamental studies on protein adsorption and ultimately represents a highly promising technology for biosensor arrays. Additional investigations that give further insight into the attachment and spreading of cells on surfaces, can even extend the scope of potential technological applications to sophisticated microrobotic devices for drug delivery or in-situ tissue manipulation.

Appendix A

Surface Inorganic Chemistry: The Reaction of Hydroxyl-Terminated Alkanethiols on Gold with a Zirconium Coordination Compound[*]

Unlike the investigations discussed in the previous chapters the study presented in the following is not concerned with resistance to protein adsorption of synthetic organic surfaces but with another interesting application for such self-assembling monolayers.

The recent years have seen a steady increase in work on reactions of ω-functionalised thiol self-assembled monolayers (SAMs) with organic reagents ranging from 'small' molecules to polymers [1-3]. For example, hydroxyl-terminated thiols may act as immobilised alcohols in esterification reactions [4] or react with diisocyanates, which themselves act as linkers to firmly attach other reagents to the surface [5]. Corresponding interfacial chemical reactions with inorganic partners have so far largely been restricted to ion-exchange reactions in aqueous solution, using SAMs bearing anionic functionalities such as the carboxylato, phosphonate or sulfato group for the electrostatic attachment of metal cations [6-10]. More recently, gas-phase growth of metal multilayers on functionalised SAMs [11-13] and the deposition of both oxide thick films and nanocrystallites on $-SO_3H$ and $-COOH$-terminated SAMs from aqueous solutions [14-18] have been reported.

To achieve controlled molecular architecture with inorganic compounds, one possibility is to try to incorporate functionalities with a high surface affinity such as the thiol,

disulfide or silane groups into the ligand sphere and then let these tailored compounds self-assemble on the desired surface. Although the viability of this approach has been demonstrated in one case [19], substantial synthetic effort is required for each individual metal-ligand system and the spectrum of possible target complexes will be limited for chemical stability reasons.

We have preferred an approach where, in a first step, a well-defined reactive surface is created by conventional organic self-assembly. In a second step, the reactive terminal groups of this organic film are then exposed to the dilute solution or vapor of a coordination compound. Depending on the chosen system, the reaction will lead to either electrostatic or covalent bonding of the metal to the surface. This new approach has the advantage of a high flexibility, as there is a broader choice of reactive terminal groups than of ligands suitable for self-assembly. Any existing self-assembly technology, such as thiol, silane, or phosphonate chemistry, can be employed, as long as it provides films that carry the required reactive endgroups. Thus, a broad variety of substrate materials becomes accessible without any need to modify the inorganic reagent. As an additional benefit, a well-defined hybrid organic–inorganic bilayer can be created, where the organic and inorganic component can be chosen independently to match the desired application. The goal of the present study was to demonstrate the potential of this new approach, by developing a methodology for covalent adsorption from solution and characterising the properties of a first model film system.

A.1 Results

Materials

The two thiols used in this study, 11-mercapto-1-undecanol ($>97\,\%$ purity) and 1-dodecanethiol ($98.6\,\%$), were purchased from Aldrich Chemical Co., MI, USA and used without further purification. The hydroxyl- and methyl-terminated SAMs have been prepared according to the procedures described in chapter 2. The advancing water contact angles of the obtained SAMs ($<15°$ for the hydroxyl-terminated thiol SAMs and $>110°$ for the methyl-terminated) conformed to standard values reported in the literature [23].

Bis(acetylacetonato)bis(1,1,1,3,3,3-hexafluoroisopropanolato)zirconium (abbreviated as Zr(acac)$_2$(hfip)$_2$ or **1.**, Figure A.1) was synthesised as described elsewhere and purified by short-path vacuum distillation immediately prior to use [20]. Solutions of **1.** (2.0 mM) in either dry hexane or isooctane (Fluka Chemicals, Switzerland, for analysis grades) were prepared under inert conditions, filled into Schott-bottles and stored in a glove box until use.

Tetrakis(acetylacetonato)zirconium (abbreviated as Zr(acac)$_4$, **2.**, Figure A.1) ($> 98\%$ pure), a reference compound for the assignment of XPS binding energies, was purchased from Fluka Chemicals, Switzerland and further purified by vacuum sublimation.
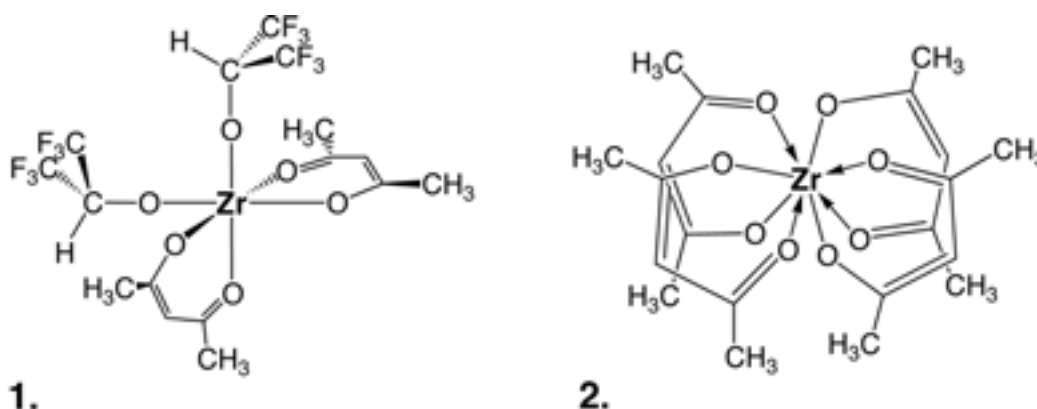

Figure A.1: *Schematic of the zirconium reagent Zr(acac)$_2$(hfip)$_2$ (**1**) and the reference compound Zr(acac)$_4$ (**2**)*

Prior to measurements, the thiolate SAM-coated wafers were, inside a glove-box (< 1 ppm O$_2$ and H$_2$O), placed in the dilute Zr(acac)$_2$(hfip)$_2$ solution for different periods of time (5 s - 10 h). The samples were then removed from solution, thoroughly washed with the corresponding hydrocarbon, stored under the same solvent for another 10 minutes, blown dry with argon and immediately transferred to UHV for analysis.

Contact Angle Measurements

As listed in Table A.1, the initially very low advancing water contact angle of less than 15 degrees for the non-reacted OH-terminated film on gold increases to 66 degrees after several hours of functionalisation with the zirconium reagent. Very similar values have been reported for 1,4-phenylenediisocyanate-functionalised C$_{11}$-OH-SAMs [5] and both hydroxyl- and COOH-terminated thiol SAMs after esterification or dosing of amines [4,24]. As evident

from the data shown in Table A.1 there is a rather large hysteresis between the advancing and the receding water-contact-angle value.

sample	H_2O, adv. [°]	H_2O, rec. [°]	HD, adv. [°]	HD, rec. [°]
Zr-modified	66 ± 2	11 ± 1	12 ± 1	7 ± 1
C_{11}-OH	14 ± 1	9 ± 1	8 ± 1	9 ± 1
C_{11}-OH (lit. [b])	< 15	—	< 10	—

Table A.1: *Dynamic contact angles of native and functionalised OH-terminated thiol SAMs on polycrstalline gold [a]*

[a]   *C_{11}-OH after 26 h, Zr-SAMs after 16 h immersion into the corresponding solution; HD = n-hexadecane.*
[b]   *Data from ref. [23]*

The contact angles measured using hexadecane (HD) are all very low and do not appear to be strongly sensitive to changes in this particular surface chemistry. Pictures of the droplets of water or hexadecane were taken during the dynamic contact angle measurements, and Figure A.2 illustrates examples the quantitative values given in Table A.1 exemplarily.
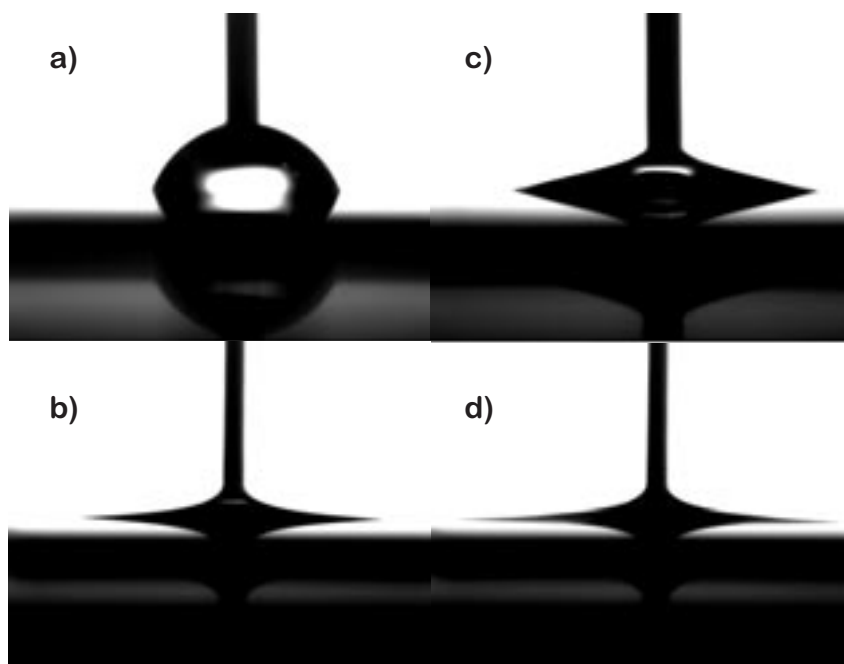

Figure A.2: *Advancing contact angle images taken for water on a) a Zr-SAM and b) a C_{11}-OH SAM and for n-hexadecane on c) a Zr-SAM and d) a C_{11}-OH SAM.*

X-ray Photoelectron Spectroscopy

XPS was used as a chemical probe to follow the course of the functionalisation reaction. As a reference for C 1s and O 1s peak assignments, firstly XP spectra of the untreated hydroxyl-terminated SAM, of the zirconium reagent and $Zr(acac)_4$ as a standard for a Zr-bound acac ligand were measured.
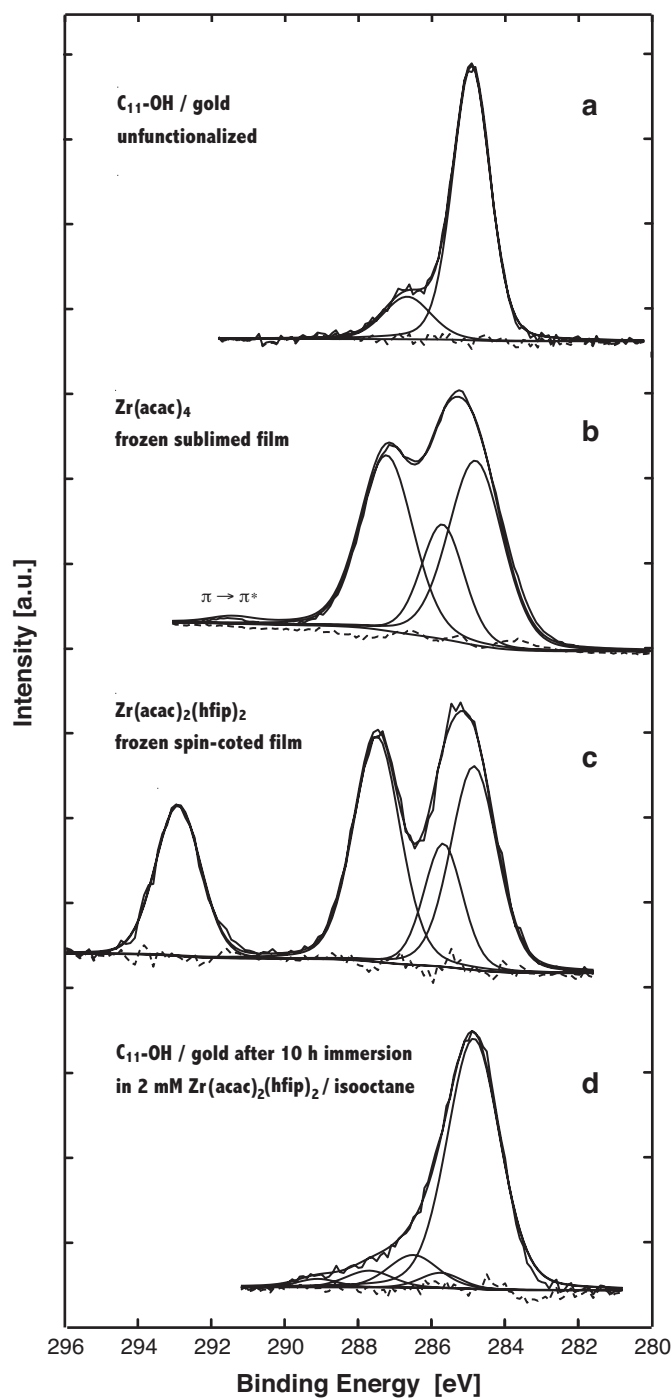

Figure A.3: *Carbon 1s X-ray photoelectron detail spectra of a) untreated hydroxyl-terminated C11-OH SAM on gold, b) neat $Zr(acac)_4$, c) neat $Zr(acac)_2(hfip)_2$ and d) a Zr-functionalised C_{11}-OH SAM.*

Figures A.3a and A.4a display detail spectra of a self-assembled monolayer formed by 11-mercapto-1-undecanol (C$_{11}$-OH) on a polycrystalline gold substrate *before* reaction with the zirconium complex.
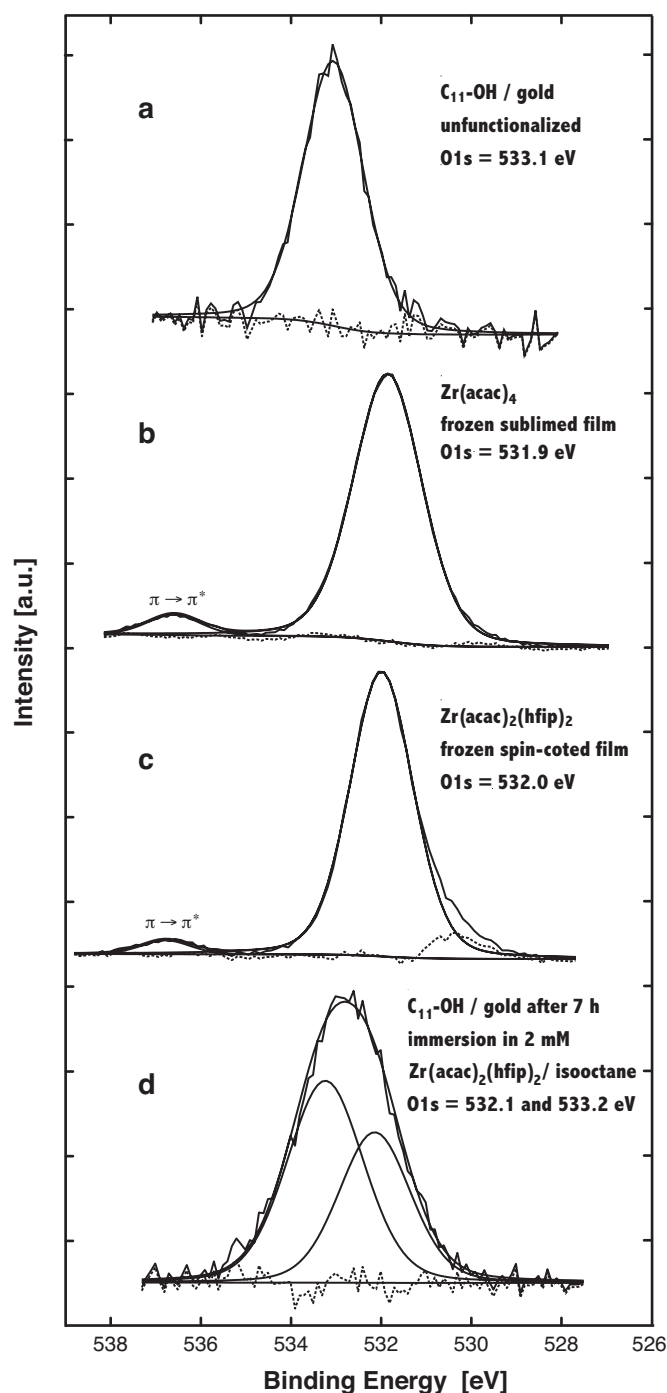

Figure A.4: *Oxygen X-ray photoelectron detail spectra of a) untreated hydroxyl-terminated C$_{11}$-OH SAM on gold, b) neat Zr(acac)$_4$, c) neat Zr(acac)$_2$(hfip)$_2$ and d) a Zr-functionalised C$_{11}$-OH SAM.*

The main C 1s peak is centered at a binding energy of 284.9 eV and shows a shoulder towards higher energies at 286.7 eV (Fig. A.3a). The peak positions agree nicely with the data of Bain et al. for C_{11}-OH [21], who observed these signals at 284.9 and 286.8 eV, respectively. As listed in Table A.2 the corresponding full widths at half maximum (fwhm) of the fitted peaks are 1.2 and 1.3 eV. We assign the low-binding energy species to the alkane chain methylene carbons, while the other signal corresponds to the terminal, oxygen-bonded carbon. The observed peak area ratio of $\approx 6 : 1$ (aliphatic to C-O) agrees well with that earlier reported by other groups using similar measurement conditions [21].

The oxygen region consists of a single symmetric peak centered at 533.0 eV with a fwhm of 1.6 eV (Figure A.4a). Quantification yields a C/O ratio of ~7:1, a value lower than the theoretical elemental ratio for a bulk sample of 11:1.

Carbon and oxygen 1s detail spectra of the reference compound $Zr(acac)_4$ are shown in Figures A.3b and A.4b. The Zr 3d region (not shown) displayed a single 3:2 doublet of a fwhm of 1.7 eV, the main peak located at 183.2 eV (3d $\frac{5}{2}$) and a separation of 2.4 eV. The carbon region (Fig. A.3b) is composed of three species with binding energies of 284.8, 285.7 and 287.2 eV, respectively, and fwhm of 1.7 eV. The peaks can be assigned to the methyl groups (C-$\underline{C}H_3$), to the central methine carbon of the acetylacetonato ligand (H_3C-OC-$\underline{C}$-CO-CH_3), and to the keto carbon (C_2-$\underline{C}$=O), respectively. Their experimentally determined ratio of 41:20:39 is close to the expected theoretical value of 40:20:40 (Table A.2). The oxygen region shows one main symmetric peak at 531.5 eV with a fwhm of 1.8 eV. A second, low-intensity feature at 536.3 eV is attributed to a $\pi \rightarrow \pi^*$ shake-up structure of the same oxygen species. Similar O1s $\pi \rightarrow \pi^*$ transitions have already been observed for other metal acetylacetonates, both by optical spectroscopy [25] and XPS [26-28]. The satellite separation of 4.8 eV found here fits nicely into the range of 4.0 to 4.8 eV reported for anionic acac [26]. The XPS quantification results of $Zr(acac)_4$ agree well with the calculated values, as expected for a bulk-like sample.

The spectra of the pure bulk inorganic reagent that was used as second reference compound, $Zr(acac)_2(hfip)_2$, are also shown in Figures A.3 and A.4. The main differences to the XP spectrum of $Zr(acac)_4$ are related to the presence of the CF_3 groups of the additional hfip (1,1,1,3,3,3-hexafluoroisopropanolato) ligand.

XPS region	Film and species	Expected position	Observed position	Expected abundancy	Observed abundancy
C 1s	**C$_{11}$-OH/gold**				
	-CH$_2$-	284.9[b]	284.9	91	85
	-CH$_2$-OH	286.8	286.8	9	15
	Zr(acac)$_4$				
	-CH$_3$	284.9	284.8	40	41
	H$_3$C-C-**C**-C-CH$_3$		285.7	20	20
	C$_2$-**C**=O		287.2 (291.4)	40	39
	Zr(acac)$_2$(hfip)$_2$				
	CH$_3$	284.9	284.8	25	30
	H$_3$C-C-**C**-C-CH$_3$		285.7	12.5	15
	C$_2$**C**=O +		287.5	37.5	34
	Zr-O-**C**(CF$_3$)$_2$				
	CF$_3$	292.7-8[c,d]	292.9	25	21
O 1s	**C$_{11}$-OH/gold**				
	C-**O**-H		533.1		
	Zr(acac)$_4$				
	Zr-**O**-C	532.0±0.2[e]	531.9 (536.6)		
	Zr(acac)$_2$(hfip)$_2$				
	Zr-**O**-C [c]		532.0 (536.8)		
F 1s	**Zr(acac)$_2$(hfip)$_2$**				
	C**F$_3$**	688.6[c]	688.6		

Table A.2: *XPS peak positions and assignments for reference compounds* [a]

[a] *Binding energies relative to Au 4f 7/2 = 84.0 eV. Values in brackets identify $\pi \to \pi^*$ shake-up satellites of the corresponding core-level peak.*

[b] *ref. [21]*

[c] *ref. [29,30]*

[d] *convoluted peak of both ligand types*

[e] *value for the acetylacetonato (acac⁻) ligand in various d transition metal acetylacetonates, averaged from data in refs. [26,27].*

An intense additional signal in the carbon region can, by virtue of its unusually high BE of 292.9 eV, easily be identified as CF$_3$ carbon [29,30]; the corresponding trifluoromethyl F 1s signal being observed at 688.6 eV (Table A.2). The fwhm is 1.4 eV for all carbon species

and 1.9 eV for the fluorine peak. The relative ratio of the chemically different carbons differs slightly from what is expected for the intact compound, in that we found a slightly higher amount of aliphatic carbon. This might be due to traces of contaminants that have been introduced during sample preparation or cooling of the XPS chamber. The CF_3 carbon signal, however, is slightly less intense than expected. The oxygen region looks similar to that measured for $Zr(acac)_4$, including the presence of a small shake-up structure located at 536.8 eV. The signals of the different zirconium-bound oxygens from the alcoholato (OR^-) and acetylacetonato ($acac^-$) ligands are energetically very close and were treated as one peak during the later spectral fitting procedure.

The information gained from the above-described reference measurements was used for XPS signal assignment of the films obtained by functionalisation of OH-terminated thiol SAMs with dilute $Zr(acac)_2(hfip)_2$ solution in isooctane. The first indication of successful surface-attachment of the reagent was the detection of a well-resolved Zr 3d signal at 183.2 eV, which could neither removed by washing nor by long-term immersion in hexane or isooctane. Another piece of information that could immediately be extracted from the XPS data is the absence of the F 1s signal, indicating that both hfip groups had been eliminated during the course of the reaction. Correspondingly, the CF_3 carbon signal was also missing. This observation is made independent of the time of immersion. Figures A.3d and A.4d show the oxygen and carbon XPS regions, respectively, after 10 hours reaction of a hydroxyl-terminated thiol monolayer on gold with the Zr solution.

After functionalisation, the oxygen region is principally composed of three chemically different species: one is due to the inorganic compound and two are due to the thiol. The latter are those that had reacted with the inorganic reagent as well as those that did not react. We have, however, fit to only two peaks, one at 533.1 ± 0.1 eV and one at 531.8 ± 0.3 eV with fwhm around 1.8 eV. The former stems from the non-reacted thiol, while the latter is due to the Zr-bound oxygens both of the acac ligand and the reacted thiol, i.e. $-CH_2OZr$. The energetic difference between the 1s electrons of the latter O atoms is expected to be very small, as also found in the case of $Zr(acac)_2(hfip)_2$. The fitted intensity ratio of O(H) to O(Zr) obtained for longer immersion time periods ranged between 1:1 and 2:1 for the different experimental series. Under the assumption that all oxygen atoms are nearly within the same depth of the layered structure, i.e., the attenuation of the 1s electrons is similar for all of them, one can deduce the relative ratio of Zr atoms to thiol molecules present at the surface. One

has, however, to account for the fact that two thirds of the observed O(Zr) signal intensity is introduced by the four oxygens of the two acetylacetonato ligands per attached complex, while only one third stems from the two reacted thiol alcoholato groups. For an O(H) to O(Zr) peak area ratio of 1:1 this means that 25 % of the thiol molecules have reacted with the inorganic compound. Under the assumption that the complex is bound via two Zr-O-C bonds to the thiol chain, which is supported by the elimination of both hfip groups observed in XPS, the total ratio of Zr to thiol molecules amounts to 1:8. For smaller O(Zr) to O(H) ratios, the coverage is correspondingly lower.

Species	C1s (1)	C1s (2)	C1s (3)	C1s (4)	C1s (5)	O1s (1)	O1s (2)	Zr3d 5/2
thiol	CH$_2$	–	CH$_2$OH	–	–	C-**O**-Zr	CH$_2$**O**H	**Zr**-O
acac	CH$_3$	CH	–	C$_2$C=O	–	C-**O**-Zr	–	**Zr**-O
BE [eV]	284.9	285.8	286.5	287.7	289.1	531.8±0.3	533.1±0.1	183.2
Fwhm [eV]	1.7	1.3	1.6	1.5	1.3	1.75-2.0	1.7-1.9	1.4
at. ratio[%]	80	3	10	5	2	50-66	50-34	100

Table A.3: *Film-originating XPS signals detected in Zr-functionalised SAMs.*

For the carbon region of a Zr-functionalised thiol, at least four different species are expected, on the basis of the reference measurements. These are the aliphatic methylene and methyl carbons at 284.9 eV, the CH$_2$OX carbon of both the unreacted and the reacted thiol end groups (286.5 eV), and the carbonyl (287.7 eV) and the methine (285.8 eV) carbon of acetylacetone. Deconvolution of the C1s region, where the ratio of the acetylacetone-originating signals **C**H to C$_2$**C**=O was fixed at 1:2, showed the presence of the above-listed peaks and an additional unassigned species at 289.1 eV, which may be the result of partial hydrolytic decomposition. Since the quality of the fit was not satisfactory, we modified the carbonyl to methine ratio slightly to ~1.7. Note, however, that the absolute intensities of these signals are small and should therefore not be overinterpreted. Table A.3 summarises the obtained electron binding energies and percentage of the chemically different species originating from the Zr-functionalised SAMs.

The carbonyl (5 %) and the methine carbon species (3 %) are both indicative of the inorganic compound. These deconvoluted signals provide, in addition to the O1s method, an

alternative route to determine the amount of the inorganic reagent relative to the thiol present at the surface. After 10h of immersion, both species together contribute around 8 % to the overall observed carbon signal. An amount similar to the carbonyl signal, i.e. 5 %, is expected from the methyl groups of the Zr compound to contribute to the aliphatic signal. The ratio of the C that originates from the Zr compound to the C that originates from the thiol can then be determined to be (8+5) % / (80-5) % =13/75 ~1:6. Since 10 carbon atoms contribute to both parts, the ratio of Zr compound relative to thiol is 1:6, a ratio only slightly larger than the value derived from oxygen. A similar value is also obtained solely based on the aliphatic signal. The latter is composed of the inorganic compound and the thiol, and their ratio amounts to 5 / (80-5) = 5/75 = 1/15. Since, however, only 4 C contribute per Zr compound but 10 per thiol molecule, the Zr / thiol ratio is 1/15 x 10/4 = 1:6, which is consistent with the value deduced above.

As a common result of both the O1s and the C1s XPS peak deconvolution methods, the number of Zr compounds adsorbed on the surface is estimated to be approximately one order of magnitude lower than the number of thiol molecules. The packing density of thiols on a Au(111) surface corresponds to 5×10^{14} molecules/cm^2 [31]. From this value the final coverage of the Zr compound can be estimated to be on the order of 5×10^{13} molecules/cm^2, i.e., 200 Å^2 per molecule.

Time-dependent Data

We also recorded spectra for thiol-covered samples that had been treated for various periods of time (5 s – 24 h) with the Zr compound in solution. The carbon signal at 285.4 eV as well as the decomposition of the O1s region into the different contributing species allow a rate constant of adsorption, λ, to be deduced for the reaction of the Zr compound with the SAM.

Figure A.5 shows the oxygen peak-area ratios as a function of reaction time. We have modeled the data with simple Langmuir-type kinetics according to $\theta(t) = 1 - e^{-\lambda \cdot c \cdot t}$ and determined λ by a least squares fit routine. The resulting adsorption constant was derived for a solution concentration of 2 mM and amounts to $7 \pm 3.5 \times 10^3$ cm^{3}mol^{-1}s^{-1}. For comparison, the rate constant of adsorption found for alkanethiols on gold is three orders of magnitude higher [32].
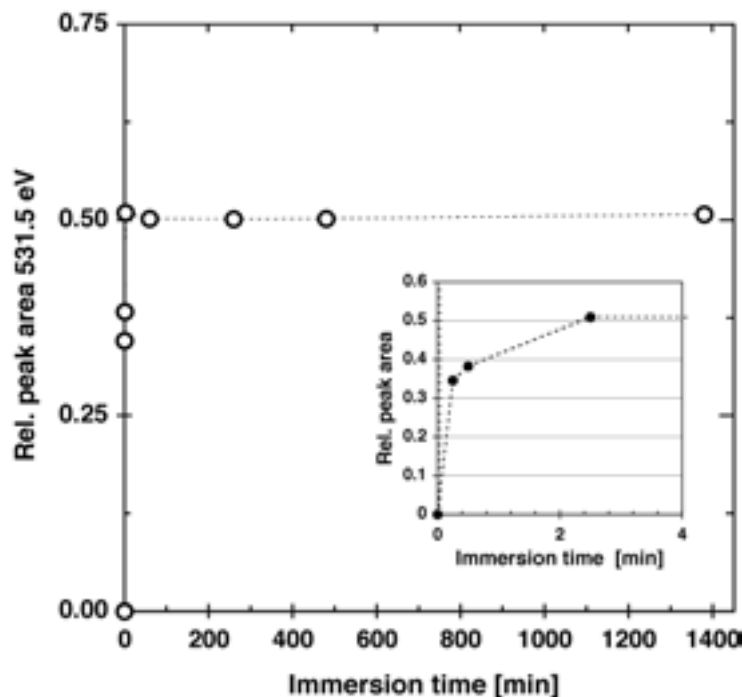
Figure A.5: Oxygen 1s XPS peak area ratio of O-Zr (531.8 eV) to O-H as a function of the immersion time.

Time-of-Flight Secondary Ion Mass Spectrometry

All spectra were recorded for a sample that had been modified with the Zr compound for 4 h. The relative intensities of the most prominent secondary ion masses, both positively and negatively charged, can be found in Appendix B.

Figure A.6 shows a sample spectrum of the observed positively charged ions in the range of 121.5 to 130.5 amu, where the main peak (m/z 124, note the excellent agreement between calculated and observed exact mass) has been identified as $^{90}ZrO_2H^+$. The observed characteristic zirconium isotope pattern ($^{90}Zr - 51.45\%$; $^{91}Zr - 11.22\%$; $^{92}Zr - 17.15\%$; $^{94}Zr - 17.38\%$; $^{96}Zr - 2.80\%$) was also used to identify other fragments stemming from the inorganic reagent. The main signal is superimposed by two additional fragments, ZrO_2^+ (122 amu for the main Zr isotope) and $ZrO_2H_2^+$ (124 amu for the main Zr isotope). Despite their weak intensity compared to the ZrO_2H signal, the characteristic Zr isotope pattern is again observed with only minor deviations.
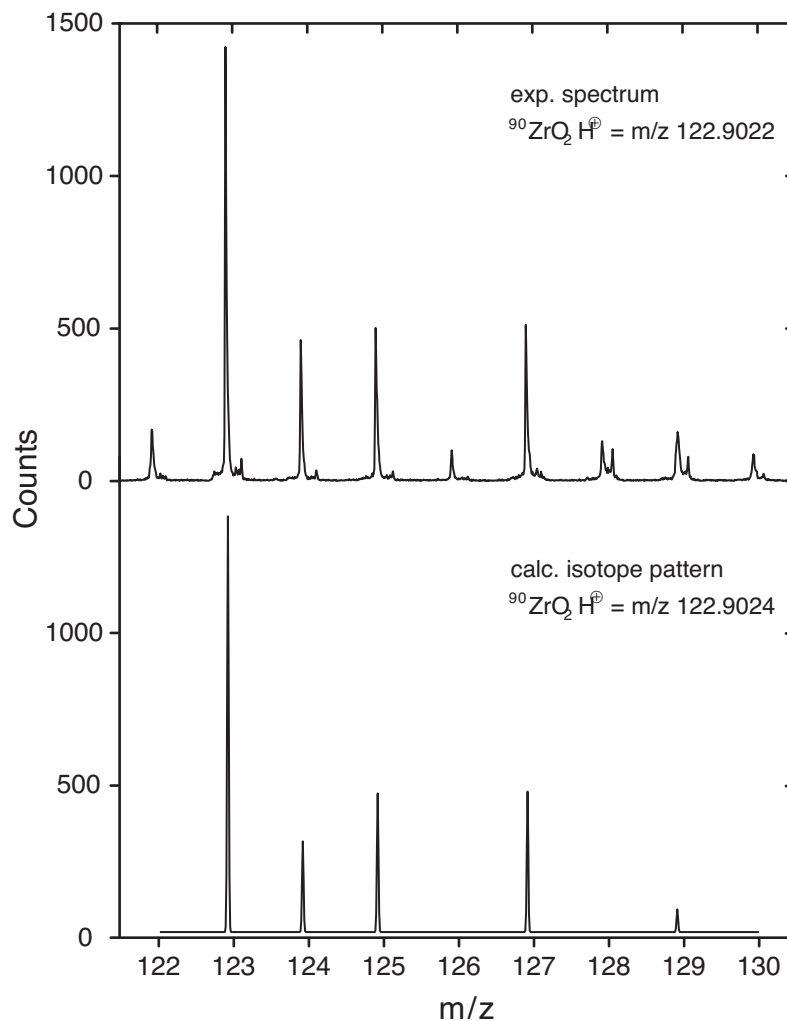
Figure A.6: *Detail of the high-resolution Cs^+-ToF-SIMS spectrum of a Zr-functionalised C_{11}-OH SAM.*

While the positively charged ions mainly originate from the organic/inorganic hybrid SAM, the negatively charged ions display some variety and comprise also fragments of the substrate including Au and S-Au. In addition to the latter, different alkyl chain fragments with the OH-endgroup of the SAM still attached, and fractions of the acac-ring and the Zr compound are observed. Moreover, they exhibit traces of fluorine-containing ions, indicating small amounts of either non-reacted or chemisorbed (as hfipOH) CF_3 ($m_i = 19, 69, 167$), which were not detected by XPS. Masses indicative of the complete acac ligand $C_5H_7O_2$ ($m_j = 99.205$) were also found, which means that these structures detach intact from the surface and no decomposition had occurred during the surface-reaction of the Zr reagent with the thiol hydroxyl group. Despite the fact that many more fragments are detectable, coinciding mass values and a decreasing signal-to-noise ratio made it more difficult to assign characteristic Zr-containing fragments in the high mass range.

Selectivity of the Reaction

In order to determine the selectivity of the reaction, we also treated methyl-terminated thiols with the Zr solution for extended periods (up to two days). The XPS spectra of such substrates, however, showed no indication whatsoever of Zr attachment.
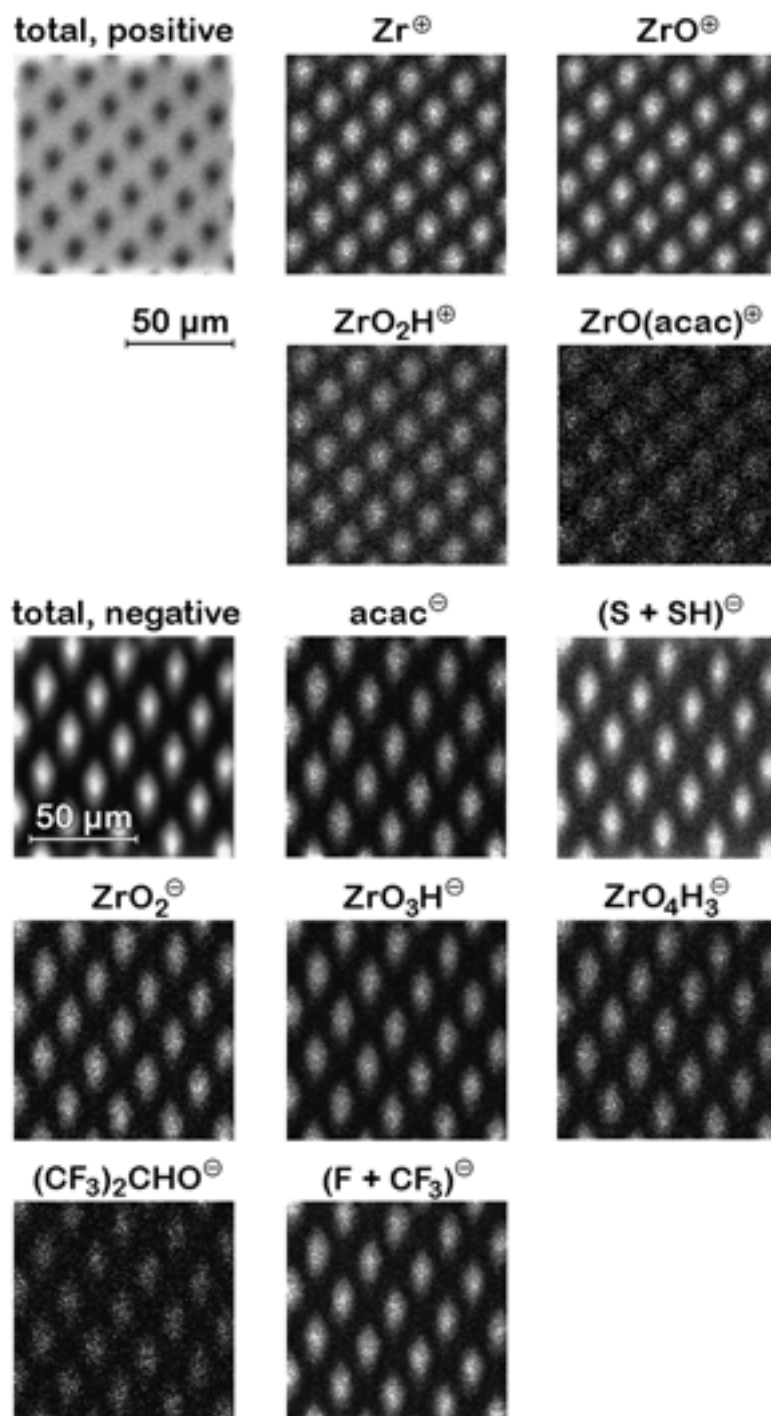

Figure A.7: *ToF-SIMS images (In$^+$) of a chemically patterned surface after functionalisation with dilute Zr(acac)$_2$(hfip)$_2$ solution. Bright regions represent high count intensity, grid = C$_{11}$-CH$_3$, dots = C$_{11}$-OH thiol SAMs on gold.*

To corroborate our finding, a surface was chemically structured by the microcontact printing (μCP) technique. We first printed a structure of methyl-terminated thiols and subsequently immersed the substrate into an ethanolic solution containing hydroxyl-terminated thiols. This procedure yielded a chemically well-defined organic surface, chemically patterned with a pitch in the $10 * 10$ μm² region. This sample was subsequently treated with the Zr solution for 16 hours and imaged by ToF-SIMS. By optical inspection of the images of total positive and total negative ion yield shown in Figure A.7, it becomes evident that positively charged ions predominantly originate from the methyl-terminated areas, whereas negatively charged ions detach preferentially from the hydroxyl-terminated areas.
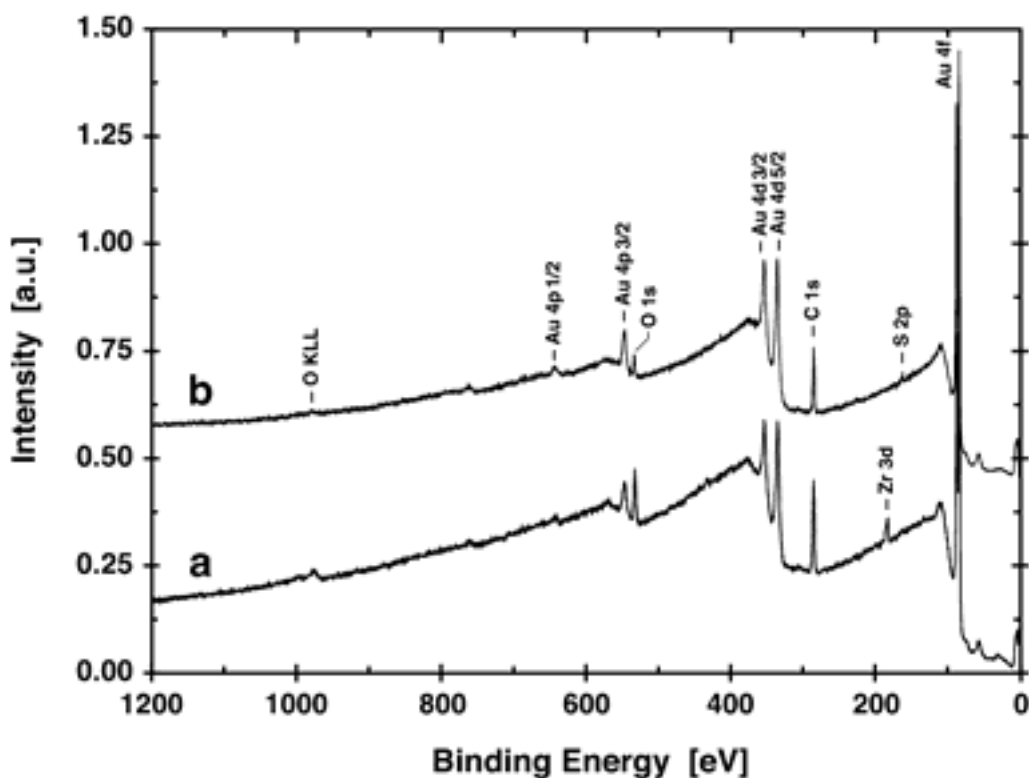

Figure A.8: *XPS survey spectra of a Zr-functionalised SAM a) before and b) after treatment with dry ethanol for 4 hours. Note the complete reversibility of the Zr attachment reaction.*

We have grouped fragments indicative of the Zr compound and displayed them together. Fragments of the inorganic reactant give rise to both positive and negative ions (Appendix B). The inorganic reagent reacts exclusively with the hydroxyl-terminated thiols, while the methyl groups appear to be completely inert to it. Again, fingerprints of the complete acac-pattern can be found (acac + ZrOacac), underlining the presence of the intact

Zr(acac)$_n$ subgroups. There are also some fluorine-containing traces (F, CF$_3$, (CF$_3$)$_2$CHOH) visible, which also appear to stem exclusively from the hydroxyl-terminated areas.

In order to check the reversibility of the reaction, we treated a sample consisting of a hydroxyl-terminated thiol layer after reaction with the Zr reagent with ethanol. In contrast to the stability of the bi-layer system under hexane and isooctane the reaction of the Zr compound with the thiol was found to be completely reversible in this case. After this treatment, no traces of the Zr(acac)$_2$ moiety could be detected, instead the spectra of an intact hydroxyl-terminated thiol monolayer were observed by XPS (Figure A.8).

A.2 Discussion

Wettability

Contact angle measurements confirm that the quality of the hydroxyl-terminated thiol films on gold are similar to those prepared by other groups [23]. The observed increase of the advancing water contact angle from 14 degrees for the pure hydroxyl-terminated alkanethiol on gold to 66 degrees for the saturated Zr-covered films indicates that during the derivatisation reaction, at least part of the polar endgroups of our system have been replaced by nonpolar ones. This indicates the formation of a more hydrophobic layer on top of the underlying SAM.

The fact that the receding contact angle of the reacted thiol film is, within the experimental error, indistinguishable from that of a native C$_{11}$-OH film can be explained by the sensitivity of Zr-O-bonds to protic reagents, such as water or alcohols. Most likely the complex has been partially hydrolysed by the water drop so that upon drop shrinkage during the receding contact-angle measurement, previously wetted surface gets exposed, which predominantly consists of restored OH-terminated thiolato molecules.

Photoelectron Spectroscopy

The XP spectra of the pure thiol layer correspond to the chemical composition expected for an intact film. The deviation of the ratio of aliphatic carbon to oxygen-bound

carbon from the expected theoretical value of 10:1 is due to the ordering of the film, which leads to an attenuation of the near-substrate carbon photoelectrons by the topmost atomic layers and was also reported by other groups [21]. The same argument applies to the observed lower ratio of carbon to oxygen, which is also a consequence of the ordering of the film.

The signals we recorded for the reference compound Zr(acac)$_4$ are in good agreement with values for related compounds taken from the literature [26-28]. The comparatively low binding energy of the acetylacetonato oxygens in this material is probably due to an electron density donation by the Zr atom. The XP spectra recorded for a neat sample of the reagent Zr(acac)$_2$(hfip)$_2$ showed small amounts of aliphatic contaminants and a slightly smaller CF$_3$ signal than expected, otherwise agreement was good. The deviations can be explained by partial cleavage of the fluorinated alcohol by hydrolysis during sample preparation, followed by evaporation before or during the measurement.

The binding energies of the carbon and oxygen species found for the Zr compound after reaction with the organic monolayer resemble those of the non-reacted model substances. There is a deviation, however, for the carbonyls, which were observed at 287.7 eV and thus display a higher binding energy compared to the reference samples (287.2, 287.5). This could reflect a weak charging of the inorganic overlayer, relative to the remote gold surface used as binding energy reference. A similar effect in the oxygen region may possibly be hidden by a slight broadening of the peak.

The relative ratio of Zr reagent to thiol was independently derived from both the oxygen and the carbon region. The results, about 1:8 based on the oxygen signal and about 1:6 from the C1s signal, agree within the experimental error. Additional signals of zirconium and of the newly introduced acac ligands were observed both in the XPS and ToF-SIMS spectra. The spectroscopic results are in agreement with a structure as illustrated in the middle part of Figure A.9, where the acac ligands form the upper shell of the organic-inorganic double layer. In connection with the contact-angle results a picture emerges where the 'aliphatic' side of the acac ligands forms the outermost layer of the functionalised film and is predominantly exposed to the environment. The acetylacetonato 'wings' are substantially shielding both the underlying polar metal-oxygen bonds and the remaining, unreacted hydroxyls.
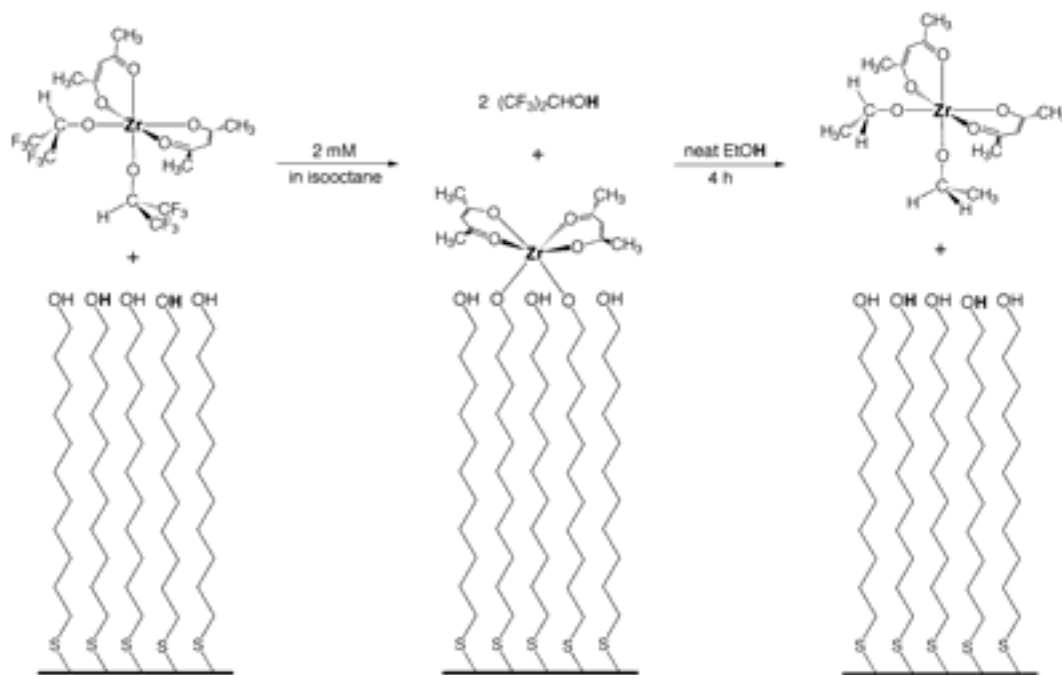
Figure A.9: *Schematic of the reaction and retro-reaction of Zr(acac)₂(hfip)₂ with a hydroxyl-terminated alkanethiol film and the resulting organic/inorganic architecture.*

The determined area of about 200 A^2 per molecule is about twice that of the projected area of the compound, which is estimated to be 100 A^2. However, the accessibility of the OH groups will be affected and reduced by the presence of neighboring Zr compounds, and maximum coverage will be regulated by the configuration of inorganic compounds already present.

The fact that, unlike in solution chemistry [33,34], a mono-exchanged product is never observed raises the question of the reason for such selectivity. The answer lies undoubtedly in the specific geometric situation of an interfacial reaction. Once the complex has been immobilised on the surface by the first exchange step, exchange of the second hfip ligand will be fast due to the high probability of meeting one of the proximate terminal OH groups. Looking secondly at the retroreaction, it is less clear why the equilibrium shown in Equation A.1 would be that clearly shifted in the favour of the thiol rather than the free alcoholato ligands.

$$Zr(acac)_2(hfip)_2 + 2HO - R \overrightarrow{}\overleftarrow{} Zr(acac)_2(OR)_2 + 2H - hfip \qquad (A.1)$$
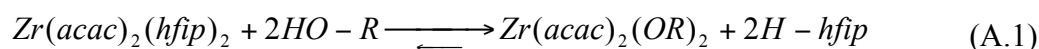
The key factor here is that the small absolute number of eliminated hexafluoroisopropanol molecules is practically infinitely diluted by the supernatant solvent, which makes the ligand exchange quasi-irreversible. Also, since each Zr is bound to two thiol oxygens, even in the unlikely case that one of the surface-bound alcoholato legs has been cleaved by reaction with a first hexafluoroisopropanol molecule, it would take the coinciding collision with yet *another* alcohol to detach the entire molecule from the surface. Because of the very low concentration of these species in solution, this is highly unlikely to occur before the first hexafluoroisopropanol is eliminated by the retroreaction. However, as we have demonstrated by the reaction of the functionalised film with neat ethanol, complete removal can be achieved given a sufficiently high alcohol concentration.

No multilayer formation takes place at prolonged reaction times. It is even observed that not all hydroxyl groups do react, although the inorganic reagent is nearly commensurate with the ideal thiol spacing. This is probably due to the large footprint of the bulky $Zr(acac)_2$ moiety. The zirconium can easily be removed by immersing the SAM in an excess of alcohol, thereby restoring the original, intact OH-terminated SAM.

Kinetics

The ligand metathesis runs at a speed approximately three orders of magnitude slower than that of alkanethiol adsorption on a gold surface [32]. About 90 % of the final coverage is achieved within several minutes at millimolar concentration. Both fluorinated alcoholato groups are replaced at once, as is evident from the absence of any fluorine or CF_3 carbon in the XP spectra. The rate constant of adsorption is determined both by the accessibility of the reaction sites at the surface and the possible retro reaction of the (semi-)attached reagent. Steric hindrance with increasing coverage should be of minor importance, although it might have a small effect. The more important factor is probably the reaction mechanism itself. It involves a ligand exchange process, which, due to the conformational changes required to reach the transition state can be expected to be much slower than the simple dissociative chemisorption of R-SH on gold. Also of importance could be the temporary adsorption of the reaction product $(CF_3)_2CHOH$ at the liquid/solid interface, which might lead to some degree of retro-reaction.

Mass Spectrometry

The observed preferential detachment of positive ions from the methyl-terminated areas and negatively charged fragments from the hydroxyl-terminated molecules can be explained by the strong electronegative character of oxygen, carrying a negative charge with high probability, while the alkyl chains coming from the methyl-terminated areas have high probability to carry positive charges.

The fluorine-containing fragments detected on the hydroxyl-patterned areas after treatment with the Zr reagent are most likely due to hexafluoroisopropanol that is hydrogen-bonded to residual hydroxyl endgroups. This interpretation, rather than the assumption of hfip ligands of a small number of semi-attached complexes, is consistent with the frequent observation that the amount of fluorine-related signals increased with increasing age of the reagent solution. In older solutions, a larger amount of free hexafluoroisopropanol has been formed by way of reagent hydrolysis. However, since a fluorine signal was never observed in XPS, the quantity of such species is below about 0.2 at.%.

Comparison with Gas-Phase Adsorption Studies

It is of interest to compare the results of this solution adsorption study to related investigations on the gas-phase adsorption of zirconium alcoholates, especially since $Zr(acac)_2(hfip)_2$ is used as a zirconia chemical vapor deposition (CVD) precursor [35]. Two recent studies demonstrate that at the vapor/solid interface, initial anchoring of the homoleptic zirconium alcoholate $Zr(OtBu)_4$ on inorganic OH-terminated surfaces takes place by elimination of the protonated alcohol and formation of (surface)-O-Zr bonds [36,37]. This low-activation energy reactive adsorption mechanism is in absolute agreement with our findings for the liquid/solid interface. It can thus be concluded that a) the adsorption mechanism is probably generally valid for dilute inert media and that b) surface-attachment of $Zr(acac)_2(hfip)_2$ in the CVD process will most likely occur via alcoholato elimination. The latter concept agrees nicely with the lower deposition temperatures accessible using this heteroleptic precursor in relation to zirconium acetylacetonates, which do not possess alcoholato anchoring sites.

We investigated the reaction of an inorganic Zr compound containing fluorinated alcohol groups with a hydroxyl-terminated alkanethiol. As derived from conventional solution

chemistry, out of the two ligand types present in Zr(acac)$_2$(hfip)$_2$, the alcoholato groups are more likely to react with other alcohols. In time-dependent measurements, we indeed found quick and selective exchange of the alcoholato ligands by the surface-immobilised hydroxyl groups while methyl groups displayed complete inertness. The inorganic compound established a monolayer on top of the organic film thus building an organic/inorganic bi-layer system. This approach provides basic insight in the reactive adsorption of alcoholato metal complexes on many polar surfaces and shows promise for the production of similar hybrid systems on various substrates and with different inorganic materials.

A.3 Conclusions

We investigated the reaction of an inorganic Zr compound containing fluorinated alcohol groups with a hydroxyl-terminated alkanethiol. As derived from conventional solution chemistry, out of the two ligand types present in Zr(acac)2(hfip)2, the alcoholato groups are more likely to react with other alcohols. In time-dependent measurements, we indeed found quick and selective exchange of the alcoholato ligands by the surface-immobilised hydroxyl groups while methyl groups displayed complete inertness. The inorganic compound established a monolayer on top of the organic film thus building an organic/inorganic bi-layer system. This approach provides basic insight in the reactive adsorption of alcoholato metal complexes on many polar surfaces and shows promise for the production of similar hybrid systems on various substrates and with different inorganic materials.

A.4 Literature

[1] Chechik, V.; Crooks, R. M.; Stirling, C. J. M. *Adv. Mater.* **2000**, *12*, 1161

[2] van der Boom, M. E.; Richter, A. G.; Malinsky, J. E.; Lee, P. A.; Armstrong, N. R.; Dutta, P.; Marks, T. J. *Chem. Mater.* **2001**, *13*, 15

[3] Dannenberger, O.; Weiss, K.; Wöll, C.; Buck, M. *Phys. Chem. Chem. Phys.* **2000**, *2*, 1509

[4] Sabapathy, R. C.; Crooks, R. M. *Langmuir* **2000**, *16*, 1777

[5] Persson, H. H. J.; Caseri, W. R.; Suter, U. W. *Langmuir* **2001**, *17*, 3643

[6] Evans, S. D.; Ulman, A.; Goppert-Berarducci, K. E.; Gerenser, L. J. *J. Am. Chem. Soc.* **1991**, *113*, 5866

[7] Venkataramanan, M.; Murty, K. V. G. K.; Pradeep, T.; Deepali, W.; Vijayamohanan, K. *Langmuir* **2000**, *16*, 7673

[8] Lee, H.; Kepley, L. J.; Hong, H.-G.; Mallouk, T. E. *J. Am. Chem. Soc.* **1988**, *110*, 618

[9] Ansell, M. A.; Zeppenfeld, A. C.; Yoshimoto, K.; Cogan, E. B.; Page, C. J. *Chem. Mater.* **1996**, *8*, 591

[10] Brust, M.; Blass, P. M.; Bard, A. J. *Langmuir* **1997**, *13*, 5602

[11] Weiß, J.; Himmel, H.-J.; Fischer, R. A.; Wöll, C. *Chem. Vap. Depos.* **1998**, *4*, 17

[12] Wohlfart, P.; Weiß, J.; Käshammer, J.; Kreiter, M.; Winter, C.; Fischer, R.; Mittler-Neher, S. *Chem. Vap. Depos.* **1999**, *5*, 165

[13] Fisher, G. L.; Hooper, A. E.; Opila, R. L.; Allara, D. L.; Winograd, N. *J. Phys. Chem. B* **2000**, *104*, 3267

[14] Katz, H. E. *Chem. Mater.* **1994**, *6*, 2227

[15] Fischer, A.; Jentoft, F.C.; Weinberg, G.; Schlögl, R.; Niesen, T. P.; Bill, J.; Aldinger, F.; De Guire, M. R.; Rühle M., *J. Mater. Res.* **1999**, *14*, 3725

[16] Bandyopadhyay, K.; Vijayamohanan, K. *Langmuir* **1998**, *14*, 6924

[17] Wang, Y.; Supothina, S.; De Guire, M. R.; Heuer, A. H.; Collins, R.; Sukenik, C.N. *Chem. Mater.* **1998**, *10*, 2135

[18] Koumoto, K.; Seo, S.; Sugiyama, T.; Seo, W. S.; Dressick, W .J. *Chem. Mater.* **1999**, *11*, 2305

[19] Haga, M.-A.; Hong, H.-G.; Shiozawa, Y.; Kawata, Y.; Monjushiro, H.; Kukuo, T.; Arakawa, R. *Inorg. Chem.* **2000**, *39*, 4566

[20] Morstein, M. *Inorg. Chem.* **1999**, *38*, 125

[21] Bain, C. D.; Troughton, E. B.; Tao, Y.-T.; Evall, J.; Whitesides, G. M.; Nuzzo, R. G. *J. Am. Chem. Soc.* **1989**, *111*, 321

[22] Nuzzo, R. G.; Dubois L. H.; Allara, D. L. *J. Am. Chem. Soc.* **1990**, *112*, 558

[23] Laibinis, P. E.; Whitesides, G. M. *J. Am. Chem. Soc.* **1992**, *114*, 1990

[24] Sabapathy R. C.; Crooks, R. M. *Langmuir* **2000**, *16*, 7783

[25] Schmidtke, H.-H.; Voets, U. *Inorg. Chem.* **1981**, *20*, 2766

[26] Srivastava, S.; Badrinarayanan S.; Mukhedkar, A.J. *Polyhedron* **1985**, *4*, 409

[27] Kishi, K. Ikeda, S. *Appl. Surf. Sci.* **1980**, *5*, 37

[28] Perera, J. S. H. Q.; Frost D. C.; McDowell, C. A. *J. Chem. Phys.* **1980**, *72*, 5151

[29] Jenneskens, L. W.; Mahy, J.; de Brabander-van den Berg, E. M. M.; van der Hoef, I.; Lugtenburg, J. *Recl. Trav. Chim. Pays-Bas.* **1995**, *114*, 97

[30] Frey, S.; Heister, K.; Zharnikov, M.; Grunze, M. *Phys. Chem. Chem. Phys.* **2000**, *2*, 1979

[31] Ulman, A. *An Introduction to Ultrathin Organic Films: From Langmuir-Blodgett to Self-Assembly*; Academic Press, New York **1991**

[32] Buck, M.; Eisert, F.; Fischer, J.; Grunze, M.; Träger, F. *Langmuir* **1991**, *53*, 552

[33] Wakeshima, I.; Ohta, K.; Kazama, Y.; Kijima, I. *Nippon Kagaku Kaishi* **1994**, *9*, 805

[34] Saxena, U. B.; Rai, A. K.; Mathur, V. K.; Mehrotra, R. C.; Radford, D. *J. Chem. Soc. A* **1970**, *6*, 904

[35] Morstein, M.; Pozsgai, I.; Spencer, N. D. *Chem. Vap. Depos.* **1999**, *5*, 151

[36] Lu, G.; Purvis, K. L.; Schwartz, J.; Bernasek, S. *Langmuir* **1997**, *13*, 5791

[37] Kukli, K.; Ritala, M.; Leskelä, M. *Chem. Vap. Depos.* **2000**, *6*, 297

164

Appendix B

Table B.1: Positive static ToF-SIMS spectrum of a Zr-modified C_{11}-OH SAM on gold at 4 hours treatment time (Cs^+, 8 keV, total ion dose = $1.6*10^{12}$, $m/\Delta m$ = 6345). Zr peak positions for ^{90}Zr, intensities are relative to Cs^+.

m/z nom.	m/z exp.	m/z calc.	Relative Intensity	Molecular Formula	Assignment
15	15.0236	15.0235	7.14	CH_3	CH_3-SAM + acac-Fragm.
27	27.0239	27.0235	35.79	C_2H_3	CH_3-SAM + acac-Fragm.
29	29.0391	29.0391	33.82	C_2H_5	CH_3-SAM
39	39.0247	39.0235	27.39	C_3H_3	CH_3-SAM + acac-Fragm.
41	41.0396	41.0313	59.52	C_3H_5	CH_3-SAM
43	43.0551	43.0548	44.32	C_3H_7	CH_3-SAM
55	55.0560	55.0548	33.29	C_4H_7	CH_3-SAM
57	57.0717	57.0704	24.51	C_4H_9	CH_3-SAM
67	67.0569	67.0548	9.67	C_5H_7	CH_3-SAM
69	69.0724	69.0704	13.80	C_5H_9	CH_3-SAM
71	71.0881	71.0861	7.02	C_5H_{11}	CH_3-SAM
81	81.0733	81.0704	5.19	C_6H_9	CH_3-SAM
83	83.0892	83.0861	3.19	C_6H_{11}	CH_3-SAM
90	89.9314	89.9047	5.56	Zr	Zr-Compound
95	95.0897	95.0861	1.62	C_7H_{11}	CH_3-SAM
106	105.9150	105.8996	7.72	ZrO	Zr-Compound
122	121.9073	121.8945	0.40	ZrO_2	Zr-Compound
123	122.9092	122.9024	2.95	ZrO_2H	Zr-Compound
133	132.9086	132.9054	100.00	Cs	Primary Ion
141	140.9198	140.9129	1.02	ZrO_3H_3	Zr-Compound
205	204.9547	204.9442	0.84	$ZrO_3C_5H_7$	Zr-Compound

Table B.2: Negative static ToF-SIMS spectrum of a Zr-modified C11-OH SAM on gold at 4 hours treatment time (Cs$^+$, 8 keV, total ion dose = 4.9*10^{12}, resolution = 3177). Intensities are relative to Au$^-$.

m/z nom.	m/z exp.	m/z calc.	Relative Intensity	Molecular Formula	Assignment
13	13.0068	13.0078	74.11	CH	Both SAMs + acac-Fragm.
16	15.9955	15.9949	98.74	O	OH-SAM + acac-Fragm.
17	17.0029	17.0027	78.74	OH	OH-SAM + acac-Fragm.
19	18.9992	18.9984	2.12	F	Alcohol contamination
25	25.0074	25.0078	55.35	C_2H	Both SAMs + acac-Fragm.
32	31.9734	31.9721	11.65	S	Both SAMs
33	32.9799	32.9799	19.23	SH	Both SAMs
41	41.0023	41.0027	9.16	C_2OH	OH-SAM + Acac-Fragm.
43	42.9990	43.0184	2.59	C_2H_3O	OH-SAM + Acac-Fragm.
57	57.0334	57.0340	1.52	C_3H_5O	OH-SAM + Acac-Fragm.
69	68.9959	68.9952	0.67	CF_3	Alcohol-Contamination
71	71.0132	71.0133	3.89	$C_3H_3O_2$	Acac-Fragm.
73	73.0273	73.0290	0.44	$C_3H_5O_2$	Acac-Fragm.
75	75.0244	75.0446	0.32	$C_3H_7O_2$	Acac-Fragm.
83	83.0142	83.0133	0.86	$C_4H_3O_2$	Acac-Fragm.
85	85.0296	85.0290	0.74	$C_4H_5O_2$	Acac-Fragm.
99	99.0453	99.0446	3.39	$C_5H_7O_2$	Complete Acac
106	105.9124	105.899	0.19	ZrO	Zr-Compound
122	121.8981	121.894	0.81	ZrO_2	Zr-Compound
123	122.9034	122.902	0.71	ZrO_2H	Zr-Compound
137	136.9206	136.918	0.16	ZrO_2CH_3	Zr-Compound
139	138.8992	138.897	1.45	ZrO_3H	Zr-Compound
147	146.9042	146.902	0.36	ZrO_2C_2H	Zr-Compound
157	156.9090	156.907	0.62	ZrO_4H_3	Zr-Compound
163	162.9003	162.897	0.31	ZrO_3C_2H	Zr-Compound
167	166.9965	166.993	0.06	C_3F_6OH	Alcohol-Contamination
169	168.9079	169.908	0.21	ZrO_4CH_3	Zr-Compound

181	180.9089	180.907	0.33	$ZrO_4C_2H_3$	Zr-Compound
187	186.9218	186.918	0.09	ZrO_5CH_5	Zr-Compound
197	196.9685	196.966	100.00	Au	Au
198	197.9802	197.974	11.33	AuH	Au
199	198.9873	198.982	14.90	AuH_2	Au
229	228.9432	228.938	8.50	AuS	Au
230	229.9505	229.946	8.13	AuSH	Au
262	261.9222	261.918	3.78	AuS_2H	Au
319	318.9714	318.867	0.23	$ZrO_6C_{11}H$	Zr-Compound
394	393.9448	393.944	9.57	Au_2	Au
395	394.9517	394.950	10.09	Au_2H	Au
426	425.9148	425.915	6.13	Au_2S	Au
427	426.9221	426.913	7.30	Au_2SH	Au
591	590.9178	590.899	4.28	Au_3	Au
623	622.8889	622.871	3.13	Au_3S	Au
788	787.8934	787.866	0.40	Au_4	Au
789	788.9002	788.874	0.34	Au_4H	Au
820	819.8655	819.838	0.50	Au_4S	Au
821	820.8708	820.846	0.61	Au_4SH	Au

List of Publications

1.   **Dicke, C.**; Hähner, G.; Herrwerth, S.; Eck, W.; Grunze, M. *in preparation*
     „Chemical Force Spectroscopy Study on Derivated Hexa(Ethylene Glycol)-Containing Self-Assembled Monolayers"

2.   **Dicke, C.**; Hähner, G.; Herrwerth, S.; Eck, W.; Grunze, M. *in preparation*
     „Chemical Force Spectroscopy Study on Derivated Tri(Ethylene Glycol)-Containing Self-Assembled Monolayers"

3 .   **Dicke, C.**; Hähner, G. *American Vacuum Society 49th International Symposium, Denver, Colorado, USA,* Nov 3-8, **2002**, oral presentation

4.   **Dicke, C.**; Hähner, G. *Journal of the American Chemical Society*, **2002**, *124*, 12619
     "pH-dependent Force Spectroscopy of Tri(Ethylene Glycol)- and Methyl-terminated Self-Assembled Monolayers Adsorbed on Gold"

5.   **Dicke, C.**; Hähner, G. *Journal of Physical Chemistry B*, **2002**, *106*, 4450
     "Interaction between a Hydrophobic Probe and Tri(Ethylene Glycol)-Containing Self-assembled Monolayers on Gold Studied with Force Spectroscopy in Aqueous Electrolyte Solution"

6.   **Dicke, C.**; Hähner, G. *General Conference of the Condensed Matter Division of the European Physical Society, Brighton, UK,* April 7-11, **2002**, oral presentation

7.   **Dicke, C.**; Morstein, M.; Hähner, G. *Langmuir*, **2002**, *18*, 336
     „Surface Inorganic Chemistry: The Reaction of Hydroxyl-Terminated Thiols on Gold With a Zirconium Coordination Compound"

8.   **Dicke, C.**; Hähner, G. *European Conference on Atomic and Molecular Physics, Berlin, Deutschland*, April 2-6, **2001**, oral presentation

9.   **Dicke, C.**; Feldman, K.; Eck, W.; Herrwerth, S.; Hähner, G. *Polymer Preprints* **2000**, *41*, 1444
     „Oligo(Ethylene Glycol)-Terminated Monolayers under Electrolyte Solution Studied with Scanning Force Microscopy"

Acknowledgements

Curriculum Vitae

The author of this thesis was born in Wickede/Wimbern, Germany, on September 30th, 1973. After finishing school in 1993, he accomplished a one-year mandatory military service in the German Army. In October1994, he started his studies of Physics at Westfälische Wilhems-Universität in Münster, Germany. After passing his intermediate diploma in 1996, he moved to Eidgenössische Technische Hochschule Zürich as a guest student in the Department of Physics in 1997. From 1998 to 1999 he worked on a project towards his diploma in the Department of Materials at ETH Zürich before finishing his studies at WWU Münster in September 1999. In January 2000 he returned to ETH Zürich to set work on his Ph.D. project being employed as Research Assistant at the Laboratory for Surface Science and Technology. In July 2001 he moved to London, UK, to carry on the work on his Ph.D. project as Research and Teaching Assistant in the Department of Physics and Astronomy at University College London until April 2002. From May to July 2002 he spent some time as Visiting Research Assistant in the School of Chemistry at University of St. Andrews, Scotland, UK.

Zürich, December 2002